GEOLOGIC AND GEOCHEMICAL ASSESSMENT OF ACID MINE DRAINAGE AND HEAVY METALS CONTAMINATION IN THE WEST RAND, WITWATERSRAND BASIN, SOUTH AFRICA

by

Abegunde Oluseyi Ayokunle (Blessed)

A thesis submitted in partial fulfilment of the requirements for the degree of Master of Science in Applied Geology in the Faculty of Natural Sciences, University of the Western Cape

Supervisor: Professor Charles Okujeni

Co Supervisor: Dr AM Siad

August 2014

Declaration

I therefore declare that this thesis report is my own, unaided work. It is being submitted for the degree of Masters of Science at the Department of Earth Science, Faculty of Natural Sciences, University of the Western Cape, Bellville. It has not been submitted before for any degree or examination in any other University.

……..

Student Signature

Abstract

Over the years, South Africa has produced over 468 million tons of mine waste yearly, in which gold mining waste accounted for 221 million tons (47%) of all mine waste produced, making it the largest, single source of waste and pollution. The exposure of these mine wastes such as tailings dams, waste rocks to oxidation and leaching has been the source of heavy metal release into the environment.

This study assessed the magnitude of possibly leachable metals, its distribution and associations and predicted the AMD load discharge over time, from Mogale's tailings dam into the environs in Randfontein area, Witwatersrand Basin, South Africa.

Fifty-one tailings dam samples were analysed for their mineral and multi-elements contents. Petrography studies was done by X-Ray Diffraction (XRD) technique to determine the mineralogical composition. X-ray fluorescence (XRF) and Inductively Coupled Plasma-Mass Spectrometry (ICP-MS) techniques were used to determine the multi-elements content in the tailings dam samples. The dataset were evaluated using multivariate statistics, Geographical Information Systems (GIS) and geochemical mass balance techniques.

From the results, the tailings dam lithology was grouped into four distinct layers. The uppermost oxidized layer is siliceous and contains the highest SiO_2 (87.32%) contents, which is with the lowest contents in Tot/S, U, As, Zn, Ni, Co, and Cu. A downward decrease in SiO_2 (76.39%) contents occurs, coupled by an increase in Fe_2O_3, Tot/S, U, As, Zn, Ni, Co, and Cu, reaching maximum contents in layer 3. Layer 4 is the least weathered horizon.

The cluster analysis grouped the samples into four sub-clusters based on the variation in SiO_2 and Al_2O_3 contents. Factor analysis (83.542% total data variance) related the four controlling factors of element distribution to the occurrence in ore elements (sulphides), silicates, mining additives and refractory minerals. Elements of the same origin show a similar concentration trend down hole in the GIS interpolation analysis. The geochemical mass balance showed variable gain and loss of oxides and trace elements within each layer. Based on the variation patterns of the Tot/S contents and other mobile elements, about 0.164kg/tonne/yr(±0.02) of the tailings materials are leached yearly. Layer 1 is the most altered.

This assessment and prediction study therefore gives an insight to the geochemical behaviour of an abandoned tailings dam, highlighting its extent of oxidation. However, the interaction

between the oxidized zone and transition zone should be given more attention, to determine the actual extent of damage

Keywords: Acid Mine Drainage; Assessment; Prediction; Weathering; Geochemical mass balance

Acknowledgement

First and Foremost, I would like to acknowledge the almighty God, the I am that I am, the all-sufficient God, the Alpha and Omega, and the everlasting God for seeing me through my Masters programme. No amount of words is sufficient to thank you.

I would like to thank my main supervisor, Prof Charles Okujeni, for his efforts day in and day out despite his tight schedule and other engagements, to scrutinise, peruse my thesis sheet by sheet, and see to the completion of this programme. May the lord bless you and grant you an everlasting joy. You made me a better person.

I acknowledge my co-supervisor, Dr AM Siad for grooming me into a GIS expert and putting me through the statistical analysis of this study. I also acknowledge all teaching and non-teaching staff of the department of Applied Geology, most especially Prof VB Donker, Ms. Davids, and Dr Opuwari for their support.

My sincere appreciation goes to my lovely parents Mr. H.I Abegunde and Chief Mrs E.O. Abegunde for all your efforts right from my cradle to this present time, for being the instrument God used to get me to the state I am. I also want to thank my brothers Mr Akindele Abegunde and Mr Rotimi Abegunde for your support. My thanks also go to my one and only blood sister for your financial support even when I was stuck in Nigeria. You people are blessings to me.

I would like to thank my lovely, wonderful and dearest wife, Mrs. Adeola Abegunde (Princess Adeola). Ever since you arrived in South Africa, my life has taken a great turn for good. Your smiles, encouragement, prayers and full support saw me through this study. I bless God for given you to me as an uncommon gift. I love you dear; the Lord will grant you the desires of your heart and keep us together.

I cannot but acknowledge my research partner Iris Wu for accepting me into this research and taking care of me like her brother. May God be with you and bless you abundantly in return. I also use this medium to appreciate my cousin and friend Mr Oluwasanmi Lawal for his support and encouragement. I will also want to thank my big brother Bro Ayo Adeoba for his financial support and Bro Sanya Omojola for being there. God bless you all.

I also want to thank all my colleagues in the Department of Applied Geology, most especially Monica Oghenekome, Chris Samakinde, Ayodele Oluwatoyin, Hakundwi Mandende and

Senza Ndum for their support. I will never forget to mention Mr Seun Fadipe for his words of encouragement. My thanks go to Ameh Emmanuel, Yohan Steve, Ademola Bode-Aluko, my pastor and brother, Dr O Fatoba and his family for their support ever since I arrived in South Africa. God used you to bring me here. The Lord will continually bless you. Also, I appreciate my Pastor at home, Pastor Dairo for his prayers and support.

Finally, I want to thank Inkaba and NRF for their financial support towards the completion of this study.

Table of Contents

List of Figures

List of Tables

List of Plates

Acronyms

AMD	Acid Mine Drainage
AP	Acidic Potential
CA	Cluster analysis
DDW	Deionised distilled water
FA	Factor analysis
FD	Fresh dump
GDP	Gross Domestic Product
GIS	Geographical Information System
GMB	Geochemical Mass Balance
GPS	Global Positioning System
ICP –MS	Inductive Coupled Plasma- Mass Spectroscopy
ICP OES	Inductive Coupled Plasma- Optical emission spectrometry
IDW	Inverse Distance Weight
LA	Laser Ablation
MPA	Maximum potential acidity
MT	Mogale tailings dam
ND	New dump
NP	Neutralisation Potential
OD	Old dump
PCA	Principal Component Analysis
QA/QC	Quality Assurance and Quality Control
REEs	Rare earth elements

SPSS	Statistical Package for Social Science
TDS	Total Dissolved Solids
USEPA	US Environmental Protection Agency
XRD	X-ray Diffraction
XRF	X-ray Fluorescence

CHAPTER ONE

1.0 Introduction

By 2004, South Africa has produced 50,055tons of gold and has massive gold ore reserve estimated to be 40,000 tons, in which, about 9,000 tons are economically feasible (Janisch, 1986). This entails major underground processes, reaching depths of over 3.8 km. These gold producing mines are found in the Witwatersrand Basin.

This Witwatersrand basin is an ancient placer deposit, containing gold-bearing conglomerates and grits. It stretches through an oval-shaped basin of around 400 km long and 150km wide in a northeast to southwest trending (Tutu, et al., 2008). The Witwatersrand extends over Free State, North West and Gauteng Provinces.

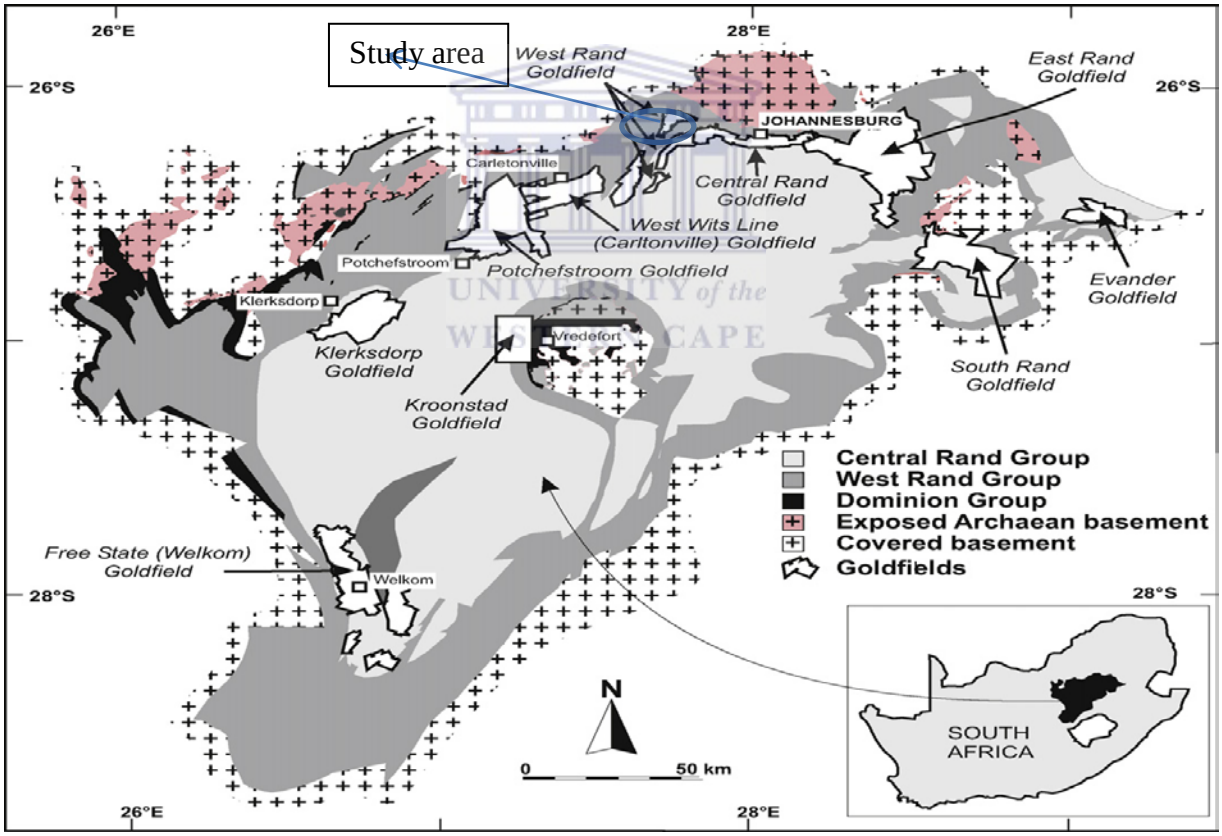

Figure 1: The Geological map of the Witwatersrand basin of various goldfields and general strata: Extracted from Dankert & Hein, (2009)

The Witwatersrand's gold mines are operated in seven major goldfields. They are the Free State goldfields, West Rand goldfields, Kosh goldfields, Far West Rand goldfields, East Rand goldfields and Central Rand goldfields, and Evander goldfields as shown in figure 1.

The gold-bearing conglomerate unearthed in the Witwatersrand reefs has a unique mineralogical composition. It contains quartz (70-90%), phyllosilicates (10–30%),other minor minerals including base metal sulfides (pyrite (3-5%) is the most prominent sulfide) and U-bearing minerals (Winde, et al., 2004; Tutu, et al., 2008).

In 1997, South Africa produced over 468 million tons of mine waste yearly, in which gold mining waste accounted for 221 million tons (47 %) of all mine waste produced. This made it the major, singular source of waste and pollution (Oelofse, et al., 2007). Despite this, the gold mining industry has contributed to the growth and strength of the South Africa economy, profiting from about 57% of all mining profits in the form of taxes and levies (Adler, et al., 2007).

More recently, the mining industry has become one of the sources of environmental problems for human health. This is because waste materials produced are of variable nature and extent. The mining industry is also a major source of revenue and creates a lots of job opportunities in South Africa. Mining procedures include raw material crushing, ore reprocessing and solid waste disposal, which can be causes of pollution within the ecosystem (Chunhacherdchai, et al., 2011). Therefore, these mining activities have exposed the Witwatersrand basin and environs to the threat of Acid Mine Drainage (AMD) pollution, creating mine wastes such as tailings dams, sand dump and waste rocks.

The main source and cause of this AMD is the oxidation of metal sulfides such as iron sulfide (FeS_2) 'known as pyrite or fool's gold' (Naicker, et al., 2003; Tutu, et al., 2008). Exposing mine wastes such as tailings, waste rocks to oxidation and leaching has been the source of heavy metal release into the environment. Acid drainage from mine tailings, waste rocks and mine edifices such as pits and underground workings is mainly a function of the mineralogy of the rock material and the accessibility of water and oxygen. The acidic solution produced from the oxidation of pyrite causes dissolution of the surrounding ore and rocks in the flooded part of the mine, rock piles, tailing dams and sand dumps, releasing those metals present. This may include aluminum, radium, uranium, manganese, iron, zinc, nickel, lead, cobalt, arsenic, copper and thorium (Naicker, et al., 2003; Durand, 2012). This results in contamination as the produced toxic and acidic water that was left untreated will have

detrimental effects on the ecosystem and lead into serious environmental liability in the mining industry.

Nonetheless, the tailing dams remain a major source of this acid mine drainage generation. This consists of crushed ore remnant, fine in grain size, disposed of through hydraulic pipes and mounted up in a dam (a specifically designated area of land). Most of the tailing dams in the Witwatersrand were formed over 30 years ago. There are over 270 tailing dams in the Witwatersrand covering 400km^2 of land space (Oelofse, et al., 2007).

Leachates caused by fluids (such as rainfall) coupled with oxidation, are product of the oxidation of the sulfides present. These leachates are transported away from the tailings surface and contaminate surrounding ecosystem.

Oxidation of sulfides depends on the water level, because the diffusion of oxygen in water is slow. Therefore, until the water level falls (occasionally or seasonally), the process of oxidation remains inhibited (USEPA, 1994).

The degree of mobility and toxicity of heavy metals in ecosystem and the drainage system is not only a function of their concentrations, but depend on both their associations and geochemical properties. They also depend on certain immediate environmental conditions such as redox potential, pH and biological effect of the roots and the production of chelates (Guillén, et al., 2012). Therefore, soil pollution cause by heavy metals and metalloids such as As, Cd, Cr, Cu, Ni, Pb and Zn, represents the source of a severe possible threat for the equilibrium of the ecosystem and well-being of humans and other living things (Guillén, et al., 2012).

For remediation of the ecosystem to be effective, the need for assessment and prediction is important because it evaluates the potential load and mass transfer of heavy metal pollutants, AMD produced and its mobilization. In addition, assessment and prediction of the ecosystem create a possible map on which remediation can be based on.

For a tailings dam, the tailings show likely susceptibility of a more even pollutant load, due to their uniform texture and mineralogy (USEPA, 1994). This indicates there will be similarities in the properties of tailings from the same dam. However, inconsistencies in the mineralogy and other factors contribute to the potential AMD loads in different tailings dams, and thus making the prediction the potential AMD load difficult, costly and of questionable reliability

(USEPA, 1994). Despite this, AMD prediction tests are gradually depended on, for the assessment of short-term and long-term potential of acid generation.

Numerous studies have focused on assessing the degree of pollution caused by previous mining activities (Rosner, 2000; Vermeulen, 2001; Naicker, et al., 2003; Nengovhela, et al., 2006; Oelofse, et al., 2007; Hobbs & Cobbing, 2007; Durand, 2012) and its remediation (Akcil & Koldas, 2006; Tutu, et al., 2008; Akpor & Muchie, 2010).

Little researchers have focused on prediction in the Witwatersrand (Nengovhela, et al., 2006; Bezuidenhout & Rousseau, 2006). Most of the studies focus on water and a few on leachates of mine waste. They have reported elevated concentration of both heavy, and trace metals. There is need for more studies to predict the potential volume of AMD loads, that can be generated from gold tailings as a requirement for a long-term and short-term prediction.

Within the Witwatersrand basin, the pollution load has been found to be greater at the end of wet season. This is largely because of rise in the water table and increased ground water seepage from the toe-ends of these slime dams (Tutu, et al., 2008). Pollution occurs in the form of low pH and high SO_4^{2-} concentrations in perennial streams, low pH and Eh, and high electrical conductivity in groundwater (Tutu, *et al*., 2008). While seepage is characterized by low pH values, high sulfates, as well as elevated concentration of toxic substances, including radionuclides (Naicker, et al., 2003).

Researchers have found that acidic water is contaminating the Witwatersrand's fresh ground water in the largely dolomitic aquifers underneath (Hobbs & Cobbing, 2007) and the natural environment is faced with AMD as time goes on. They also predicted that without active pumping, groundwater due to precipitation (e.g. rainfall) in the West Rand would fill mine void space and affect the dolomitic aquifer, which could lead to surface decanting.

Due to this imminent danger, decantation has started since certain mines were reopened, and rehabilitation processes commenced by treating the water and pumping it into the surrounding water pathway. This constant decantation of water has caused a higher AMD signature in the West Rand, such as a growth of a permanent water body in the Hippo Dam (Hobbs & Cobbing, 2007).

1.1 Extent of the level of AMD pollution of water supplies and risks posed in Witwatersrand basin

AMD leachates from abandoned mine waste materials are long-term threat to the environment. This directly pollutes surrounding streams, rivers, drinking and ground water, thereby, affecting wildlife habitat (as seen in Hippo dam) (Durand, 2012) and destroying the natural landscape. In that regards, mine waste materials (such as tailings, sand dumps), contain sulphidic materials that release heavy metals upon oxidation (leachates). This is because of the high mobility of the sulphide species and its affinity for acidic drainage generation.

According to facts about the Witwatersrand, the potential volume of AMD in its goldfields alone amounts to an estimated 350ml/day (Liefferink, 2012). This reflects the extent of threat posed by AMD. Therefore, the Witwatersrand basin is exposed to the surge of AMD, since the post-closure decantation of mines started (Hobbs & Cobbing, 2007). The threat posed could become worse if remediation activities are delayed or not implemented.

However, the extent of contamination is determined frequently to assess the extent of remediation success. This will help to determine the areas of much importance, which could lead to alleviating the risk posed. Besides, if remediation is implemented, its successes remain unknown unless there is constant monitoring and prediction evaluation.

1.2 Research Aim and Objectives

This study focuses on evaluating Mogale-Gold tailing dam in the Randfontein area, West Rand, Witwatersrand as a case study to assess the potential leachable metals and predict the AMD pollution load that could be generated.

To fulfil the aim of study above, the objectives of the study are highlighted below:

To evaluate the mineralogical and geochemical composition of the tailings dam to understand the geological characteristics of and link between each zone (oxidized, transition and un-oxidized).

To use multivariate statistical analysis tool assess the potential leachable heavy metals loads and the risk of heavy metals load present in the tailings dam, its associations and inter-relationships.

To map or model the distribution of elements based on the statistical analysis results using GIS spatial interpolation

To predict the possible AMD pollution loads that can be generated over the period of deposition of the tailing dam and its effect on the environment using geochemical mass balance and the economic value the tailings dam sampled will present.

1.3 Motivation for the Study

In lieu of a report by inter-ministerial committee on AMD in South Africa by a team of experts in 2010, limited expert investigations have been done to find out the status of the geo-hydrological system, the level of contamination, preferential channels and predictions on long-term transport of AMD (Expert Team of the Inter-Ministerial Committee , 2010).

The effect of gold mining activities introduces AMD into the environment. The tailing dams have been a major source of contamination and extensive studies has been made on the surface or top layer of the tailings (between 0 to 3.5m) of the oxidized zone. Few studies have been done on the interaction between the three zones (oxidized zone, transition zone and the un-oxidized zone) (Nengovhela, et al., 2006; Bezuidenhout & Rousseau, 2006). Besides, the geological characteristics of and link between these zones have not been extensively studied.

The impact of AMD on the natural environment in the Witwatersrand is obvious and visible. Across Witwatersrand gold basin, the West Rand is the smallest. Underground mining was stopped in the region in 1998 (Naicker, et al., 2003) due to extensive mining of gold over the years. Reclamation on tailing have recently started .The West Rand spreads from Randfontein in the west to Roodeport in the east and encompasses the town of Krugersdorp.

Despite the remediation put in place now, AMD heavy metals load in the West Rand still poses a great risk. Since the landowners and people around the area of study depend largely on ground water for domestic use, portable water, as well as business and agricultural use, this motivates this study. The physical impact of the AMD signature in the study area could show the environment is deemed to be in danger.

1.4 Research Questions

To achieve the aim and objectives of this study, the following questions will be considered:

- How do the physical characteristics of the tailings relates to its mineralogical and geochemical composition

- What is the link between the various zone present in the tailings because of its mineralogical and geochemical composition
- What are the various associations and interrelationships that can be highlighted by multivariate analysis
- Can the potential AMD heavy metals loads and potential acidity of tailings determined
- How are the elements distributed based on the factors determined using IDW interpolation and mass balance
- Can the source, AMD pollution load and extent of toxicity of heavy metals determined
- To what extent is the tailing dam oxidized and can a prediction model of oxidation generated

1.5 Thesis Structure

Chapter 2 (Literature review): This chapter highlights the history of gold in the Witwatersrand, extensive explanation of Acid Mine Drainage and related Issues, the effect of some heavy metals that are associated with AMD, statistical evaluation, and description of the study area and its climatic condition are discussed.

Chapter 3 (Geology): This explains the geology of the Witwatersrand and the local geology of the study area,

Chapter 4 (Methodology): This highlights the method of sample collection and preparation, instrumental analysis of XRD, XRF, ICP –MS and procedure, precision and accuracy, statistical analysis and geochemical mass balance.

Chapter 5 (Petrography): It describes of the tailing dam down depth in color, texture and mineralogy

Chapter 6 (Geochemistry): This covers the statistical summary and analysis of the geochemical data, GIS interpolations and geochemical mass balance analysis.

Chapter 7 (Discussion, Conclusion and Recommendation): This includes interpreting results and the possible solution to the problem identified.

UNIVERSITY of the
WESTERN CAPE

CHAPTER TWO: Literature Review

2.1 History of the Witwatersrand's Gold Mining

South Africa has one of the major gold reefs in world, sitting in the Witwatersrand Basin. Since the mining started, seven gold fields have been extensively mined for more than 100 years, thus, producing more than 41,000 tons of gold, according to South Africa mining reports. Gold mining remains to be an exceedingly significant economic activity in South Africa. South African gold mines now account for about 12% of global gold production yearly. However, in the mid-1990s, South Africa produced around 30% of the world's gold exportation (Durand, 2012). Despite the decline in gold production over the last decade, the nation is still home to a projected 50% of the world's gold reserves. Gold mining is a massive industry in South Africa and offers employment to a large percentage of the population. Nearly 500,000 of the populace are employed in South Africa's gold mines (Durand, 2012). Therefore, the gold industry accounts for around 18% of South Africa's annual Gross Domestic Product (GDP). In 2005, South Africa's gold exports were valued at $3.8 billion. South Africa is home to the two deepest gold mines in the world. These are East Rand Mine in Boksburg, and the TuaTona in Carletonville and are both nearly 3600 meters deep (Gold-Bullion-Pro, 2012). The mining areas at the depth are so hot and specialized cooling technology had to be put in place to safeguard the workers (Norman & whitfield, 2006).

However, the gold mining has started over a century ago, the Witwatersrand as remain active and a force to reckon with in gold economy. New gold mining industries have been founded and remain the financial block of South Africa. For the quantity of gold in its ore, 5 to 10 parts of gold are found and recovered for every million parts of rocks. Efficient and well-planned techniques are employed in South Africa, and have aided in making low quantity of gold to be economically viable from great depth. Gold extraction at first started with Hg Amalgam to extract gold from coarsely crushed ore and after extraction the tailings were disposed into huge dumps. As mining goes deeper, un-oxidized pyritic ore was encountered, making the Hg amalgam ineffective. This was replaced by cyanide extraction in 1915 and a finer milled tailings was produced (Tutu, et al., 2008) and discharged through hydraulic pipe, into a specially built disposal site known as slime dam. Cyanide extraction was efficient because it was selective of Au and Ag needing high pH, through adding lime (GDACE, 2007).

Now, the Witwatersrand is the largest gold and uranium deposit basin in the world with about 120 active mines. A record of 73000 tons of uranium has been extracted between the year 1953 and 1995 and over 43500 tons of gold, over the century. This basin covers an area of 1600km^2 containing some 400km^2 of mine tailings dams. It has the presence of about 6 billion tons of pyrite tailings of low grade Uranium (Chevrel, et al., 2003; Liefferink, 2012)

2.2 Acid Mine Drainage Issues

Since Gold mining started in the Witwatersrand basin, much AMD pollution load has been released into the ecosystem leading to increase in salinity, acidity and heavy metals concentration of the sediments, soils, surface and groundwater. After a while, AMD signatures become significant in the Witwatersrand and its environmental impacts have proved so costly because of the activities of the mining industry (Coetzee & Winde, 2006).

AMD, labelled as an environmental virus, since it negatively affects the ecosystem. If not monitored and remediated, may lead to chronic environmental epidemic. This is because of the release of some heavy and trace metals that can be dangerous to human health when it exceeded the limit of conduciveness to our environment. The footprint of these mining activities had been felt because of its reflectance on the surface and groundwater resources long after mining operations have stopped. Mostly, abandoned mine sites have been the major seat of AMD generation around the world today (Coetzee & Winde, 2006). Acid drainage produced from mine tailings, waste rock and mine structures such as pits and underground workings is determined by the mineralogy of the rock materials and water and oxygen (Price, 2009). Other human activities, such as road construction waste materials, tiling, and others (exposing them to oxygen and water) bring about Acidic drainage generation.

There is a general opinion that AMD is accountable for the most costly environmental and socio-economic effects. Oxidation of sulphur-rich tailings and other mine wastes in the presence of water (causing AMD), is one of the main environmental challenges facing the mining industry. AMD contains increased concentrations of ions of Arsenic, other heavy metals, and sulfates, which can affect the quality of surface water and groundwater in mining areas (Lee, et al., 2005). The dissolved As and other heavy metals can be immobilized by precipitation as insoluble or less soluble Fe-(oxy) hydroxides, oxides, and sulfates. In addition, they are adsorbed onto some materials such as clay minerals, oxides, and hydroxides (Lee, et al., 2005). This has created a great issue and threat that has remained an

uncontrollable release of AMD into the environment. While South Africa has made big progress in shifting policies to address mine water management and mine closure, mining industry reformed their practices to adapt to new rules. Susceptibilities in the current system remain (Oelofse, et al., 2007).

2.2.1.1 Previous studies and Cases

In a brief summary of previous studies on Witwatersrand basin's gold tailing dumps, the following authors have these findings.

According to Marsden, (1986), several studies are carried out to assess the degree of pollution caused by previous mining activities in the Witwatersrand. This is because, raised concentration of heavy and trace metal contaminate the water in the vicinity.

In addition, AMD generation usually but not only associated to iron sulfide– aggregated rocks only (USEPA, 1994).

According to Nengovhela, et al., (2006), secondary porosity (that is, cracks produced by roots on the dam surface) controls the inflowing of oxygen into the Witwatersrand tailings dams. Also, the time of formation of the tailings dam does not have a significant bearing on the level to which the oxidized zone developed. Later, AMD routes can develop and most of these routes take place within the first 3m of the tailings dams. However, the volume of rainfall plays a role in defining the extent to which an oxidized zone grows. The average oxidized zone in the five sites is 2.4m ranging from 2.2 to 3.5 meters (Nengovhela, et al., 2006).

Therefore, tailings dams with high porosity have high oxygen intake, increasing the chemical reaction rate through convection transport (Vermeulen, 2001). Water is the basic transport medium for contamination and it is a function of the control of water flow (Rosner, 2000; Bezuidenhout & Rousseau, 2006).

Akcil & Koldas, (2006) stressed on the increase in research and interest in AMD from all sector involved over the years, and asserting that through prevention of acid generating processes such as deployment of acid drainage migration measures (prediction) and treatment of effluent (remediation), the AMD problem can be alleviated or minimized.

The tailings dams in the Witwatersrand are mostly non-vegetated. Therefore, dust pollution is reduced by spraying water as a continuing management activity (Oelofse, et al., 2007). The

primary factors that control the rate of acid generation are pH, temperature, oxygen content of the gas phase (Rosner, 2000). Oxygen concentration of the water phase, degree of water saturation, surface area of expose metal sulphide: chemical activation energy required to initiate acid generation, bacterial activity, stating the importance of chemical, biological and physical and physical factors that controls the rate of acid generation (Rosner, 2000; Nengovhela, et al., 2006). Acidithiobacillus ferro-oxidans may hasten oxidation of sulphides of gallium, iron, antimony, molybellenum, copper, arsenic, cadmium, nickel, cobalt, zinc and lead at a favorable environmental condition such as pH less than 3.2 in water (Rosner, 2000).

Bezuidenhout & Rousseau, (2006) studied the depth and degree of weathering on some selected Witwatersrand gold tailings dams. The research shows that sulfide-containing fine-grained tailings dumps generate AMD through the diffusion of oxygen into unsaturated zone pore spaces. That is, the rate in which oxygen diffuse into tailing dam is a function of the oxygen-concentration gradient that exists between the transition layer and the surface of the tailings dam. These oxygen-concentrations gradient is controlled by the rate at which sulphides of heavy metals are oxidized. Therefore, since oxygen is being consumed at depth, the concentrations of gaseous oxygen decrease with depth, thus resulting in an oxidized outer cap, which will on the long run, produce AMD as it gets oxidised down depth.

Winde, et al., (2004) said the gold tailings dam in the Witwatersrand are the source of Uranium, often containing high levels of radioactive and chemically toxic heavy metals. From seepage produced, dissolved uranium and other heavy metals migrate from tailing deposit through ground surface water into neighboring fluvial systems and biosphere. Uranium is produce as a by-product of gold to subsidize the mining cost in South Africa. About 6000 tons of U was reported to be annually disposed into slime dams through wastes generated from processing gold ore in South Africa. Most tailings dams (including some old slime dams that were later reprocessed to recover U) contain uranium in high concentration as found in mineral ore.

Naicker, et al., (2003) reported the results of a thorough site-study where acidic seepage from ground water goes into a stream and channels into the south-eastern environs of Johannesburg and the western part of the neighboring municipality of Germiston. The study was done to gain an understanding into chemical processes operational at the pollution source. In addition, the research defined the rate of decay of the pollution load along the down stream

Tutu, et al., (2008) examined water quality within the neighborhood of tailing dams in and around Johannesburg. Pollution load was detected to be greater at the end of the rainy season and shows as low pH (>2) and high (SO_4^{2-}) concentration greater than 7000mg/l. The most important source of pyrite is the tailing dam, and many researches have depend on widely scattered sampling sites. These do not expose the full impact of the environment problems that has risen from previous mining activities. Surface water quality was low around the mine dump but increases as it moves further downstream.

Therefore, AMD predictions tests are gradually depended on to find out the long-term potential of acid generation (USEPA, 1994). Tailing dams carry a more unvarying contaminant load due to their more even texture and mineralogy (USEPA, 1994; Afriyie-Debrah, 2009). It is pertinent to note that diffusion of oxygen in water is retarded and hence, oxidation of iron sulphide is prevented until the water level drops, which can occur periodically or seasonally in some cases (USEPA, 1994; Afriyie- Debrah, 2009).

2.2.2 Formation of Acid Mine Drainage

During the operational phase of mines, seepage from the tailing dams are said to be typically saline and neutral (even alkaline) but since decommissioning and closure phases began, AMD can take place (Bezuidenhout & Rousseau, 2006). AMD generation feasibility starts when the mineral deposits containing sulphides are exposed and extracted during mining processes: such as cavern strip, and sedimentary mining of numerous minerals and metals such as gold, coal, lead, zinc, uranium, copper, titanium, aluminium, iron-bearing minerals and silicates.

One or more of the following characterize AMD: low pH, high sulphates (SO_4), high Total Dissolved Solids (TDS), and high levels of heavy metals–particularly nickel, manganese, iron and/ or cobalt. Heavy metals mobilized at low pH and high salt levels can pose a risk to human health and quality of the aquatic ecosystems as well as having a significant negative economic impact (Akcil & Koldas, 2006; Gaikwad & Gupta, 2008; Akpor & Muchie, 2010). The main cause of these AMDs is metal sulphides in which iron sulphide known as pyrite or fools' gold posed the major threat. This is because of pyrite oxidation (most especially reacting with water and oxygen) leading to leaching, formation of acid, and (effectively) lowering the pH of the drainage, water pathway and other water bodies affected. Oxidation of the pyrite increases the acidity of the water infiltrating through the dumps, which then goes

into the ground water system beneath the dumps and this acidic water is believed to be entering streams along the Witwatersrand (Naicker, et al., 2003).

This acid formed causes leaching of the surface of rocks, mine tailings, waste dump by the action of oxygen and water (from rainfall). As the water moves down the drainage or pathway, the acidic solution dissolves some heavy metals.

During mining processes, waste rocks and tailings dams containing sulphides (such as FeS_2) are exposed to oxygen (in the air) and the water (surrounding the mine or used in mining process or precipitation). Pyrite may occur in both euhedral (less reactive) or framboidal (more reactive) forms in the Witwatersrand reefs, due to the presence of biogenic carbonaceous material in the Witwatersrand reefs, with the presence of hydrothermally precipitated pyrite grains (Nengovhela, et al., 2006). The pyrite reacts in a series of steps in which there is a rate-determining step, which is the second step. This acid moves into the subversive waterways and contaminates the area around the site for many kilometres.

The steps are as follows:

Oxidation of pyrite in water & oxygen

1. $Fe^{2+} + 1/2O_2 + H^+ \longrightarrow Fe^{3+} + 1/2H_2O$

Oxidation of Iron II to Iron III (The major cause of yellow boy)

2. $FeS_2 + 7/2\ O_2 + H_2O \longrightarrow 2SO_4^{2-} + Fe^{2+} + 2H^+$

Conversion of Ferric Iron to Ferric Hydroxide (yellow boy)

3. $Fe^{3+} + 3H_2O \longrightarrow Fe(OH)_3 + 3H^+$

Total combination to form sulphuric acid

4. $FeS_2 + 15/4O_2 + 7/2H_2O \longrightarrow 2H_2SO_4 + Fe(OH)_3$

(H+) ion is release, which in turn reduces the pH of the drainage or streams, posed great threat to all organisms that cannot suffer stronger acidity levels. The natural buffering system of the stream, due to the presence of carbonates, may neutralize the pH and reduce the harm posed. The water acidity neutralizes the carbonate and the bicarbonate ions resulting in the formation of carbonic acid (H_2CO_3), which weakens the natural buffering actions of the water. At a pH of 4.2, the buffering system becomes inadequate for neutralization. The water

way or drainage suddenly becomes acidic, and therefore posed a great damage that is too late to reverse. This leads to the precipitation out of yellow boy $Fe(OH)_3$ on the surface of the water, which is a thin yellowish layer.

2.2.3 Factors that determine AMD generation

The process of the oxidation of tailings dams, waste rocks and soils has been responsible for the release and mobilization of toxic heavy metals and radioactive substances. This has been the seat of the problem of AMD in the Witwatersrand. Several factors determine the rate of acid generation and these can be classified into primary, secondary and tertiary factors. Each factor has contributed in one way or the other to the formation of AMD.

2.2.3.1 Primary Factors

The primary factors are directly involved in the formation of acidity and cannot be over-looked. They are temperature, sulfides (mostly pyrite), oxygen, water and bacterial activity.

Temperature affects the rate of reaction, because it favours and creates a better environment for the bacteria activity, when it falls between 30- 35^{o}C. Since the Witwatersrand is a semi-arid region, the temperature is ideal for the formation process of AMD. This is related to the chemical activation energy required for the reaction to take place.

Sulfides, mostly pyrite, FeS_2, are main carrier of AMD as we have discussed earlier. After a sequence of oxidation reactions of sulfides, most of the sulfide first at about 2m-3m depth of the tailing dam, which lies in the oxidized zone, may have been oxidised. These result into the formation of secondary minerals such as jarosite, haematite, ferrihydrite e.t.c.

Oxygen remains an important part of the reaction, because it serves as the oxidizing agent. The oxygen content of the gas phase and oxygen concentration of the water phase in the tailing dam determines the rate of availability of oxygen for the reaction (Rosner, 2000; Akcil & Koldas, 2006). Therefore, at the upper layer of the tailing dams more oxidize than sulphides are found. Oxygen is derived from the atmosphere, and is constantly replenished. Dumps with high permeability have high oxygen ingress or intake increase chemical reaction rate through convection (Akcil & Koldas, 2006).

The activity of bacteria plays a major role in the formation of AMD. Certain bacteria are responsible for the speeding up of the oxidation reaction. The oxidation of sulfide can be abiotic or biotic, and remains a function of the pH within the tailing dam. Biotic oxidation

facilitated by the presence of certain bacteria and pH < 3.5 (Rosner, 2000; Akcil & Koldas, 2006). Bacteria such as Acidithiobacillus ferrooxidans may speed up the oxidation of sulphides of iron, molybellenum, antimony, arsenic, gallium, copper, cobalt, cadmium, lead, zinc and nickel at a favourable environmental condition such as pH less than 3.2 in water (Akcil & Koldas, 2006). The efficiency of such bacteria is favoured by temperature, optimal pH, and sufficient nutrients for the bacteria, large surface area and pathway of the drainage system (Akcil & Koldas, 2006).

Water is the basic transport medium for contamination and the control of water flow will help in alleviating the risk of transport. “Water acts as a reactant, a reaction medium and as a product transport medium in the AMD generation and transport process” (Rosner, 2000). The degree of water saturation determines the extent of tailing depth oxidized (the moisture content of the tailing dam) controlling the bacteriological activity. Therefore, water acts as a reactant, reaction medium and as the transporting medium in the formation of AMD.

2.4.3.2 Secondary factors

Secondary factors are determine the process of formation of AMD after the primary factors have initiated the reaction. The presence of buffer minerals such as dolomite and calcite is the most important secondary factor. As soon as this acidic seepage from pyrite-tailings oxidation saturates the soil, the hydrogen ions are incompletely neutralized by weathering of silicate minerals, by exchangeable bases, or more intensely, by carbonates that serve as buffers (Simon, et al., 2005). Neutralization reduces the concentration of dissolved heavy metals due to co-precipitation, adsorption and precipitation processes. Since the possible acidity of 1g of pyritic sulfur is neutralized by approximately 3g of $CaCO_3$, one of the most widespread remediation methods is the addition of lime (Simon, et al., 2005). During liming, these acidic solutions highly concentrated in Fe and S interact with the carbonate-mineral surface, the carbonate particle is coated with gypsum and amorphous ferric oxy-hydroxides formed from the reaction (Simon, et al., 2005). These (due to a process called liming) minerals neutralize the formed acid and thus try to increase the pH of the acidic soil. This can be represented as follows:

$$Fe_{(aq)}^{3+} + 2SO_4^{2-} + H^+ + 2CaCO_3 + 5H_20 \longrightarrow Fe(OH)_{3(s)} + 2CaSO_4.2H_20(s) + 2CO_2\,(g)$$

Ion exchange through clayey minerals and acid–induced dissolution of other minerals are classified as secondary factors. This reaction affects the quality of seepage, and thus adds

various elements such as Al, Mn, Cu, Pb, Zn and tend to replace Ca and Mg in Carbonates with Fe (Rosner, 2000).

2.4.3.3 Tertiary Factors

These factors depend on the properties of the tailing material and hydraulic condition within the tailing dam. These factors are influenced typically by physical parameters such as the particle size, weathering tendency, water transport and capillary through the tailings. The oxidation rate of pyrite is determined by the surface area of the tailings, the amount of sulfide exposed for the reaction and depth of the oxidized zone. For instance, sand dumps and waste rocks are said to have deeper oxidized zone than the fine- grained tailing because of its coarse–grained material that enables greater influx of oxygen and water. This implies the retention strength of slime tailings is high than that of sand dumps or tailings. Despite this, the slime tailings dam has a large surface area than the rest and therefore constantly undergoes physical weathering which has been the major source of loads of harmful heavy metals and radionuclides. Rosner, (2000) said the surface area and the size of the tailings determine the permeability and this influences the oxygen and pore water movement or capillary. A decrease in permeability will result into a decrease in acid generation, conversely.

In conclusion, minerals that determines the Acidic Potential (AP) of a tailings dam are present in relatively low concentrations (<1%) and usually higher than the Neutralization Potential (NP) (Bezuidenhout & Rousseau, 2006). In the Witwatersrand tailing dams, Acidic Potential is mainly attributed to pyrite, because is the most abundant sulphide mineral (other sulphides occur less frequently). Neutralization Potential is attributed primarily to carbonates of Ca and Mg. Silicates can become important neutralizing minerals in a tailings deposit after all soluble carbonate phases are depleted, because the dissolution of silicate minerals is kinetically limited, the NP of the silicate minerals depends on their respective dissolution rates (Bezuidenhout & Rousseau, 2006).

2.2.4 The Tailings Dam and AMD

The tailings dam remains a major source of AMD in the Witwatersrand, and is commonly the principal cause of pollution for groundwater and soils (Aucamp & van Schalkwyk, 2003). Tailings dams in the Witwatersrand Basin are mostly unlined and many are not vegetated, thus leading to widespread dust pollution, as well as water (surface and groundwater) and soil pollution (AngloGoldAshanti, 2004; Oelofse, et al., 2007) and are situated in urbanized area

or on land used for agricultural purposes in which their role is emphasized (Aucamp & van Schalkwyk, 2003).

Tailings are deposited by sub-aerial slurry, sub-aqueous slurry, paste, and dry deposition method from the mining site depending on the water of the tailings (INAP, 2009). The topography and placement of the dumpsite is well considered before deposition. Available data shows that Witwatersrand tailings materials do not differ in their physico-chemical characteristics, and are typically very large deposits. They are over 1.2km in length and breadth, and up to about 60- 75m high. The actual design and requirement of a tailing dam is to store tailings in such a way the impoundment structure remain stable. This has little or no impact on local residents and the environment. The present changes in the state of the tailing dams in the Witwatersrand now posed a threat to the environment.

In gold mining industry, rocks containing gold ore are rumpled to detach it from the waste rock and then milled (pulverized to a grain size of smaller than 0.5 mm) to extract gold by metallurgical processes. The leftover slurry is then pumped out through pipe into a prepared land dumpsite (which forms the tailings dams) where the fluids and water present are allowed to trench and/or evaporate (Aucamp & van Schalkwyk, 2003). Since the start of tailing disposal in the Witwatersrand, land has been the adopted alternative. This resulted in some environmental implications such as contamination of water-bodies by AMD or due to leaching of tailing dumps, air pollution by wind erosion of dried tailings, denatured environment as well as inhibition of vegetation growth cause by harsh pyritic-tailing soil condition (Oelofse, et al., 2007).

According to reports, there existed only two depositional types or methods as recorded in the literature, which are paddock systems and cyclone tailings deposits (AngloAmerican, 1995; Bezuidenhout & Rousseau, 2006). Cyclone type of deposition occurred in few places in the Witwatersrand (Bezuidenhout & Rousseau, 2006). Despite efforts to minimize the tailing dam contamination effect by creating paddocks, covering of the tailings with stones and bio-vegetative approach (planting of some certain trees), the risk posed can never be underestimated. Many activities, such as illegal mining activities can lead to exposure of underground water to contamination, and dust pollution (another mode of transporting pollutants) by exposing tailing dams' surfaces that contained high or low radioactive substances.

Over a century, most tailing dams in Johannesburg area have remained undisturbed and exposed to oxygen and precipitation (such rainfall). This led to the oxidation of sulphides (prominently pyrite) from the topmost layer of the dumps to several meters thick. Tailings dam can be classified into sand tailings dam and slime tailing dam. Since the sand tailings are more permeable, of large pores and older, they tend to have been seriously affected by the oxidation. Therefore, sand dumps was observed to have been oxidized to a depth of 5m, while the slime (tailing) dam oxidized to the depth 2m. (Marsden, 1986; Oelofse, et al., 2007). The mixture of tailings and used water in mining form slurry, which is pumped to a standing and prepared deposit facility. When dried or drained, the solid fraction of this slurry acts like a soil, but these tailings are unlike the most naturally occurring soils in numerous respects. Since the gold ores, typically containing some base, rare or precious metals and other minerals that are often rich in sulphide, this led to the creation, or making of large amounts of sulphide-rich tailings (Dimitrova & Yanful, 2012).

There has not been much attention to the mineralogical and geochemical interactions occurring inside the tailing dams itself, and this is a major and importance aspect to understand parameters influencing AMD formation and help to develop good and effective prevention methods (Dold, 2005). This study is limited to the state of the slime tailings dams to the depth of about 10m. The tailing dams can be divided into saturated, transition and unsaturated. The oxidized zone (saturated) is between the 0m to 3.5m (Nengovhela, et al., 2006) and the transition zone between the oxidized and un-oxidized zone. The un-oxidized zone is found below to the soil surface underneath. The paste pH of the entire zone is acidic and the presence of trees aided the tailings oxidation, not depending on its age (Nengovhela, et al., 2006). However, the tailing dams that are highly vegetated look more preserved than those poorly vegetated or have no vegetation, preventing dust pollution. The tailing dam accessed is of low and no vegetated surfaces and are closed to a major road R28 linking Randfontein with Krugersdorp and some other communities.

In assessing the extent of pollution in an area, three important stages need to be considered as shown in the figure 2 showing various features of each stage. They are the source of the contamination in which the potential harm posed can be estimated, the pathway of the pollutants showing the route in which the pollutant moved to get to the receptor.

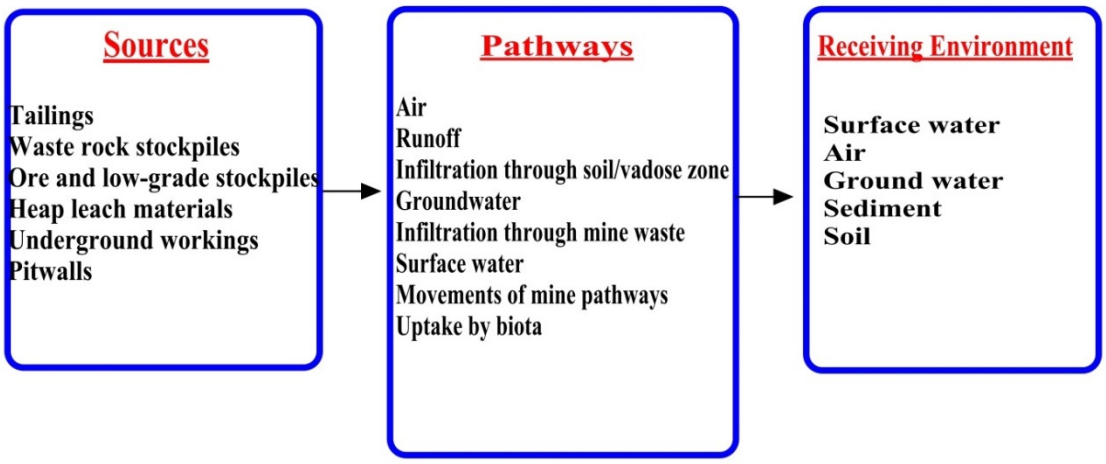

Figure 2: Comprehensive Conceptual Model of Sources, Pathways and Receiving Surroundings at a Mining or Processing Site

The receptor (the receiving environment) is the receiver of the pollutant that houses it and causes several impacts hidden or visible and the overall effect will be detrimental to the ecosystem. Due to the high mobility of most of these AMD heavy metals, the topmost layers of the tailings have been leached of these heavy metals from the overlying materials.

2.2.5 Seepage and AMD

The uncontrollable passage of leached tailings (seepage) has become a major environmental concern in its dissemination and distribution of exchangeable heavy metals in the tailings into the gold mining areas. Only a few paper emphasized on the geochemical characteristics of the seepages of the tailing impoundment. Seepage water is defined as the water derived, collected, or gathered from the outflow point at the toe or feet of the tailings dams (Heikkinen, et al., 2009) while drainage water is equilibrant with surficial conditions and being transported away from the tailing dams. Without seepage, AMD would have been a forgotten because its accumulation leads to drainage water. The quality of this drainage water is determined by precipitation and the sedimentation of secondary mineral, adsorption by suspended–in materials such as clay, organic matter and the mixing and dilution with other surficial material and water bodies along its pathway (Heikkinen, et al., 2009)

The mineralogy of the tailing dams and the chemical reaction occurring in the tailings directly reflect the geochemistry of the tailings' pore and seepage water. In other words, the total geochemistry of the tailing is directly proportional to the mineralogical composition of tailings solids and rate at which the acid buffering minerals dissolve. Therefore, the pH of the

seepage and pore water will determine the balance and correlation between acid producing and neutralizing minerals in the tailing dam. The pH – Eh relationship is a major factor that controls adsorption–co precipitation and dissolution–precipitation components in tailings dams. However, heavy metals and metalloids distribution as well as concentration in seepage and pore waters are majorly dependent on the deposit geology (Heikkinen, et al., 2009). The seepage from these tailings dams is generally characterized by low pH values, high sulphate loads as well as elevated concentrations of toxic substances including radionuclides (Heikkinen, et al., 2009).

2.2.6 Major elements that are responsible for AMD contamination

Mining is one of the most significant sources of heavy metals and responsible for heavy metals impacts on its environment. Heavy metals are the most common pollutants in the ecosystem and are hard to degrade. They can amass throughout the food chain, generating possible human health risks and ecological instabilities (Akpor & Muchie, 2010). Oxides of Fe and Mn are carriers of heavy metal cations in soils and sediments. Normally, heavy metals are not inimical to our environment when present in trivial quantities but are of major environmental pollution concern if found in higher concentration as a result of natural mineralizing procedures and/or human activities (Estifanos, 2013). Heavy metals such as arsenic, mercury, barium, copper, antimony, cadmium, lead, chromium and zinc (Akpor & Muchie, 2010), when found in high quantities, pose great threat to the ecosystem.

The impact of a toxic heavy metal on the ecosystem relies on its solubility in solution under varying pH states, which correlates to the phases of the occurrence of the metal. In other words, a heavy metal is said to be extremely toxic or harmful, if while existing in mineral form, dissolves readily in water. Metal pollution of the environment due to abandoned mining activities is an acute problem nowadays. Mining and smelting of non-ferrous metals has caused soil pollution, metal dusts emanation, water, effluents and seepage (Alloway, 1995). Although mining has been carried out for centuries, until last few decades, relatively little attention has been given to minimize the metal dispersal around these mining areas coming from the indiscriminately dumped wastes. Some heavy metals like lead, arsenic, cadmium and mercury can cause significant adverse effects to human; there are others such as chromium, copper and zinc, taken in lesser amounts that are of important value to healthy life (Akpor & Muchie, 2010). The problems caused by heavy metals differ, for instance, dissolved copper can affect lower trophic levels such as phytoplankton while lead, mercury

and cadmium amassed through the food chain, can pose a lethal risk to organisms higher in the food chain, and finally to humans (Estifanos, 2013). Therefore, the extent of heavy metals toxicity in the ecosystem is influenced by their solubility in solutions of varying pH conditions (Durand, 2012).

Gold tailing dams in the Witwatersrand's basin frequently contain raised levels of radioactive and chemically toxic heavy metals due to transport through seepage, in which dissolved Uranium and other metals migrate from tailing dumps through ground and surface water leach into neighbouring fluvial systems and the biosphere (Winde, et al., 2004). Therefore, elements such as U, Cd, As, Cu, Cr, Pb, Ni and Zn, represent the source of a severe potential hazard when found in elevated concentration that exceeds the required amount safe for the ecosystem (Winde, et al., 2004). Certain elements (heavy metals or trace elements) called chalcophiles (Cd, Cu, Ag, Au, Zn, Hg, Pb, As, Sb, Se, Tl and Mo) are of great affinity towards AMD generation and metal pollution. They are geochemically associated with sulphide minerals such as pyrite (Alloway, 1995).

2.2.6.1 Arsenic

Arsenic is an element of both natural and anthropogenic origin. It is a naturally occurring element found in many environmental compartments and bodies. Arsenic occurs in the pedosphere, the biosphere, the hydrosphere and the atmosphere, contaminates water supplies, and poses a major threat to human health. It is also one of the constituents of a large number of compounds generated by human activities such as, in glass-making industry, precious metals mining, wood processing, pharmaceutical manufacturing, electronics industry, chemical weapons etc. (Smedley & Kinniburgh, 2002; Cheng, et al., 2009).

Arsenic is used for protecting grapevines from excoriosis in fungicide. Acid mine drainage (AMD) is often accompanied with elevated concentrations of arsenic, in the forms of arsenite, As (III), and/or arsenate, As (V). Due to the high affinity of arsenic for sulphide ores, arsenic ordinarily is multivalent and therefore redox sensitive and affects the pH of the solution. Arsenite can be oxidized to the less toxic arsenate form (Cheng, et al., 2009). Some arsenic compounds can be highly soluble, due to the physico-chemical condition of the environment, thus resulting in a high level of bioavailability. The toxicity and bioavailability of arsenic depend on its speciation, which in turn, depends on microbial changes, including reduction, oxidation and methylation. Homogeneous oxidation of arsenite takes place rather slowly while its heterogeneous oxidation on mineral surfaces can greatly improve the

reaction rates (Cheng, et al., 2009). Cheng, et al., (2009) said precipitation reaction reduces the concentrations of arsenic in natural water, while co-precipitation may lead to spontaneous arsenic removal when large quantity of iron hydroxides precipitate out of the aqueous phase on neutralization of the mine drainage.

Both arsenate and arsenite adsorb on clay minerals and common metal oxides through formation of inner-sphere and/or outer-sphere complexes, regulating arsenic concentration in natural water bodies (Cheng, et al., 2009). Arsenite adsorbs less strongly than arsenate in the typical pH range of natural water and is more mobile. Part of the adsorbed arsenic species can be exchanged by common anions (e.g. PO_4^{3-} and SO_4^{2-}), especially phosphate, which leads to their re-mobilization. The knowledge of the geochemistry of arsenic is helpful for predicting its mobility and fate in AMD and natural systems, and for designing of cost-effective remediation/ treatment strategies to reduce the occurrence and risk of arsenic contamination (Cheng, et al., 2009).

It should be noted that the oxidation mechanism converts highly harmful and highly soluble As(III) into less toxic and less soluble As(V). AMD generated by sulfide oxidative dissolution, leads to high concentrations of dissolved metals such as arsenic. This is a major cause of water contamination worldwide (Smedley & Kinniburgh, 2002; Cheng, et al., 2009).

2.2.6.2 Mercury

Mercury (Hg) exists in three chemical states; as an elemental or metallic Hg^0, divalent inorganic Hg^{2+}, or as Methyl mercury. Mercury is noxious to the central and peripheral nervous systems. This is found in trace quantities in gold tailings and tends to pose a threat when released to the environment. Mercury has been attributed to health problems such as changes in vision and personality, deafness, loss of muscle coordination or tremors, numbness, and complications with memory (USEPA, 2010). Mercury can be transferred from pregnant mothers to unborn children and to babies through breast-feeding (foetuses and children are particularly sensitive to the detrimental effects of mercury) (Wright & Welbourn, 2009; USEPA, 2010). Mercury can be related to sulphur forming sulphides, transported along the drainage into the environment. Therefore, inhaling of Hg vapours permits reemission and recycling of Hg into the atmosphere where it is transported to terrestrial and aquatic systems as wet or dry deposition (Wright & Welbourn, 2009)

However, certain bacteria within the environment change inorganic mercury into methyl mercury, which is a more toxic form of mercury well known as being the form that accumulates in fish. Not only does the presence of methyl mercury present a danger to health, it also presents a danger to the livelihood of anyone who relies on healthy stocks of fish (USEPA, 2010).

2.2.6.3 Lead

Lead (Pb), a rare metal in nature released from sulfides and transported at low pH. Lead is neurotoxic, which means it destroys brain and nerve cells. It is found in minerals such as galena, anglesite and comusite. It can cause health problems particularly in children. Lead (Pb) amasses in the body system and can build up to toxic levels under continuous exposure. There is proof that Pb can cause health problems at much lower levels than previously thought, and that no level of exposure to Pb is safe for developing foetuses or children.

Pb exposure has also been associated with attention deficit, hyperactivity disorder and antisocial behaviour. Pb is a probable human carcinogen as defined by the Environmental Protection Agency. Pb accumulates in bones.

Old skeletons have natural deposits of 0.01-0.001ppm as much of Pb as contemporary skeletons that are contaminated by industrial Pb, and these differ isotopically. Lead accumulated not only in bones but also in calcium-based tissues like teeth and eggshells (Wright & Welbourn, 2009).

Lead poisoning termed plumbism from acute Pb exposures affects the central nervous system with stupor, coma and convulsions as well as ‘wrist drop’. This is associated with blood-levels of 70-100 μg dL^{-1}, rare in new aged medicines and environmental exposure. Lead interferes with the haem system, because when Pb concentration increases, the enzymes ferrochelatase and ALAD are inhibited (Wright & Welbourn, 2009).

Haemoglobin synthesis in haemopoteric system decreased with increasing Pb concentrations; in which starting at low concentrations anaemia with pallor also been recorded.

2.2.6.4 Nickel

Nickel is one of the most frequently occurring chemicals in waste sites in the United States (Haber, et al., 1998). Nickel sulphate generated from the oxidation of its sulfide, leads to skin irritation and is cancer-causing (USEPA, 2010). The presence of Ni in Witwatersrand tailings

dam is significant and usually found in its sulphide state. The primary uptake of Ni is inhalation and minor amounts via ingestion, which is excreted through faeces. Some urea contains Ni as an essential element in vertebrates, invertebrates and cyanobacteria. Aquatic organisms' uptake of Ni is influenced by water hardness, therefore Ni toxicity decreases with increasing hardness (Wright & Welbourn, 2009). Water diffused Ni enters organisms by diffusion or through Ca^{2+} channels, accumulating in cell cytosol until equilibrium is reached or until the membrane, binding sites become saturated (Wright & Welbourn, 2009). Nickel ions in the cytosol become bound to proteins and low-molecular weight ligands including amino acids like cysteine and histidine, they bind to albumin in blood, before elimination in the urine. Chronic Ni exposure inhibits reproduction and growth in invertebrates at concentrations that are two orders of magnitude lower than the reported acute levels (Wright & Welbourn, 2009)

2.2.6.5 Uranium

Uranium is a radioactive heavy metal, with an average natural background concentration ranging from <2 to 4 mg/kg (ppm) (Rosner, 2000). Uranium occurs in natural waters in three oxidation states, uranium (IV) (e.g. U^{4+}), uranium (V) (e.g.UO_2^{+}) and uranium (VI) (e.g. uranyl ion UO_2^{2+}) (Wade, et al., 2004; Wade & Coetzee, 2008). In auriferous ores of the Witwatersrand, U is accumulated up to 1000mg/kg (0.1%) compared to 0.3 -6% grades in mines from Canada and Australian. Therefore, the auriferous ores of the Witwatersrand is known as a low grade Uranium ore. Uranium is produce as a by-product of gold to subsidize the mining cost in South Africa. About 6000 tons of U was reported to be annually disposed into slime dams by gold mining activities in South Africa (Winde, et al., 2004). Few old slime dams however were later refined to recover U because they contain U in elevated concentration as found in mineral ore. Winde, et al., (2004) said that transport of dissolved U from slimes dams is a major pathway for environmental contamination of stream water, groundwater and sediments. In contrast to erosion of U-bearing particles, where U is 'diluted' by uncontaminated material along the pathway; solute transport is associated with chemical re-concentration of U in the environment. Co-precipitation of U along with calcium carbonate and iron/manganese compounds is the main reason for higher immobilization rate in the flowing water system (Wade, et al., 2004).

Oxidation-reduction conditions are important in the geologic transport and deposition of uranium. Oxidised forms of uranium (U (VI)) are quite soluble and leached from the rocks

and transported into the environment. When strong reducing conditions are faced (e.g. presence of carbonaceous materials or H_2S), precipitation of the soluble uranium will take place (Wade, et al., 2004; Wade & Coetzee, 2008). Besides the migration of dissolved or suspended uranium due to the movement of water in the environment, the transport and dispersion of uranium in surface water and groundwater are affected by adsorption and desorption of the uranium on surface-water sediments (Wade, et al., 2004). In addition, uranium removal from solution by physical adsorption processes, such as adsorption onto oxides of Fe or Mn occur as coatings on the particles of soil and sediment. Uranium mobility tends to rise due to the formation of soluble complexes with chelating agents generated by microorganisms in the soil (Wade, et al., 2004; Winde, et al., 2004). Transportation of uranium to vegetation could be by direct deposition or re-suspension (by air or by water) in which it is deposited on the plants themselves, or adhere to the outer membrane of the plant's root system with potential limited absorption. Similarly, uranium is deposited on aquatic plants or in water bodies, by adsorption (Wade, et al., 2004; Winde, et al., 2004; Wade & Coetzee, 2008).

2.2.6.6 Cobalt (Co)

Co is found naturally in water, air, rocks, soil, animals and plants but relatively low abundance. Cobalt chloride and cobalt sulphate are very soluble and are often found in solution. In solution, Co ions occur in a valence of II or III, in which Co^{2+} is more stable. This forms divalent complexes of cobalt in aqueous solutions. In aqueous solution, cobalt is mostly precipitated as highly insoluble cobalt sulphide (CoS).

In acidic soil condition, Co is highly mobile because of its increase sorption on silicate clays, oxides and organic matters as compared to its low mobility in neutral soil condition (Rosner, 2000). Therefore, in highly reducing conditions, the precipitation of Co-sulphides may hinder its mobility.

Extremely high concentration of cobalt can damage human health causing lung effects such as pneumonia and asthma, heart problems, impaired vision and thyroid damage. In addition, cobalt could form radioactive isotope and cause radiation into the environment.

2.2.6.7 Zinc

Zinc is an important element for the human body. It is found in enzymes and zymo-excitators, which improves growth, tissue regeneration and the immune system. Excessive

zinc consumption and its long-term accumulation led to nausea and vomiting, stomach cramps, cholesterol imbalance, immune system malfunction and infertility (Zhang, et al., 2012).

Zinc has an oxidation state of +2 and is normally found in form of sulphide as sphalerite (ZnS or zinc blende) in soils and ores. Zinc ion is the most mobile and soluble trace metallic ions in acidic soil conditions causing AMD. Its high mobility exposed it to leaching during oxidation process that starts AMD generation and ZnS is oxidized. The oxidation of zinc sulphide and presence of zinc can increase the acidity of waters. During AMD neutralization, Zn is removed through co-precipitation and sorption into Fe and Al hydroxides precipitates.

2.2.6.8 Copper

Copper is a transition element, which normally occurs in valence of II or I (Cu^{+}, Cu^{2+}). Copper ions are released into the environment by human activities and natural sources, through a transport medium. Naturally, Cu is found in natural deposits such as various ores containing other elements. Cu is usually found in gold ore as chalcopyrite ($CuFeS_2$), showing great affinity for iron sulphide.

According to USEPA (2009), the maximum contaminant level goal for Cu is 1.3ppm in drinking water. Soluble compounds of Cu generate the highest risk to human's health. In a reduced environment, the mobility of Cu is low since it is a chalcophile. Absorption into Mn/Fe and Al oxides increases as the soil pH increases. Cu^{2+} also form complex compounds, a property peculiar to transition elements.

Excessive concentration and accumulation of Cu could lead to irritations, headaches, diarrhea, liver and kidney damage. Considerable amount of Cu is found in the gold tailings and are mostly associated to iron sulphides present. When sulphides of Cu are exposed to oxidation, they generated acidic leachates.

2.3 Mineralogical composition of the Witwatersrand gold tailing dams

Available data indicate that Witwatersrand fine residue materials do not vary greatly in terms of their physico-chemical characteristics. Witwatersrand gold tailings are constrained within a relatively slender compositional range. They are described as consisting of between 70% and 90% quartz, 10% to 30% phylosilicates (mainly sericite) and 1% to 2% consisting of minerals such as uraninite, monazite, chromite and rutile; besides quartz, the minerals found

in tailings included muscovite, chlorite and pyrophyllite (Table 1) (Rosner, 2000; Rösner, 2001; Nengovhela, et al., 2006; Oelofse, et al., 2007).

Nengovhela, et al., (2006) investigated the climatic, mineralogical, hydrological and oxygen diffusion properties of the some selected tailings. The study inferred that that the flow of oxygen in the Witwatersrand tailings dams is controlled by secondary porosity (i.e. cracks caused by roots of plants on the dam surface. AMD processes take place within the first 3m of the dams, that is, the oxidation zone. However, the amount of rainfall plays a crucial role in determining the extent to which an oxidized zone is oxidised down depth. The average oxidized zone in the five sites is 2.4 m ranging from 0 to 3.5 m.

From previous researches, the mineralogy of the gold tailings contained mostly quartz of about an average of 78%, pyrite, gypsum, jarosite, clinochlor, muscovite, and pyrophyllite. Due to the high weathering resistance of quartz, this contributed to its abundance in the tailings composition. Pyrite remains a major sulphide that generate AMD in Witwatersrand's tailings(Table 1), and it is hardly found on the topmost part or even few centimetres down the tailing, because it would have been oxidized and have yielded some secondary oxidation products such as gypsum and jarosite predominately.

These secondary products are present mainly at the foot of the tailing in areas where the discharge of seepage occurs. Muscovite, pyropyllite and clinochor are other primary minerals phase found. The primary minerals are similar in concentration as compared to the general Witwatersrand basin mineralogical composition as shown in table 1.

2.4 Geochemical composition of the Witwatersrand gold tailing dams

The general chemical properties of the Witwatersrand basin and its gold tailings dams have been well-documented.

The constituent of gold tailings varied from one site to another depending on the method of extraction, the efficiency of the extraction method, changing ore body geochemistry and weathering process within the gold tailings dam.

In addition, the mineralogy, permeability, oxygen concentration and other factors affect the AMD formation variation from one site to another.

Table 1: General Mineralogy of Witwatersrand basin (Rosner, 2000)

Minerals	Abundance
Quartz(SiO_2), primary and secondary	70 - 90%
Muscovite and other phyllosilicates	10 - 30%
Pyrite	3 - 4%
Other sulphides	1 - 2%
Grains of primary minerals	1 - 2%
Uraniferous Kerogen	1%
Gold	approx. 45 ppm in the Vaal Reef

Table 2: The average major elements concentration of 5 different gold tailings dams in the East Rand area (Rosner, 2000)

Major element (%)	Site 1	Site 2	Site 3	Site 4	Site 5
SiO_2	80.44	84.14	82.33	83.44	77.63
Al_2O_3	8.24	6.33	8.05	5.68	9.77
Fe_2O_3	3.66	3.23	3.65	3.66	3.6
TiO_2	0.49	0.48	0.47	0.27	0.6
MnO	0.02	0.02	0.01	0.01	0.01
CaO	0.28	0.55	0.12	0.43	0.2
MgO	0.94	0.77	0.6	0.29	0.6
K_2O	1.91	1.34	1.95	1.1	2.7
Na_2O	0.15	0.21	0.19	0.17	0.22
P_2O_5	0.03	0.04	0.04	0.03	0.03
$(Cl)^-$	0.02	0.04	0.03	0.03	0.03
$(F)^-$	0.02	0.01	0.01	0.01	0.01
$(SO_3)^-$	0.1	0.12	0.02	0.08	0.06
LOI	3.46	2.36	2.32	4.31	4.24
Total	99.76	99.64	99.79	99.51	99.7

Rosner, (2000) presented the average major elements in tailings dams from five different sites in the East rand area as shown in Table 2. High SiO_2 values are recorded in all the sites. This

conforms to the high quartz content in the gold ore (Table 2). Al_2O_3, Fe_2O_3, LOI and K_2O show percentage weight concentration greater than 1.

Other major elements concentration is less than 1. The presence of carbonates is not prominent in the gold tailings and is too low to provide sufficient neutralisation potential or capacity to prevent AMD generation (Rosner, 2000). LOI reflects the presence of organic materials and volatile elements.

High Al_2O_3 and K_2O suggests the presence of clayey related materials such as the phyllosilicates. With the oxidized zone (2-3m), the sulphide is said to be depleted because of its reaction with oxygen and moisture. This results in high sulphate loads in tailings.

2.5 Relationship between the gold tailings dam and its age of formation

Different views exist in the effect of age of dam on AMD generated. The age of formation of the gold tailings dams affects its mine waste leachates (Saria, et al., 2006). Samples collected from the fresh tailings dams, less than one year and over a year indicate a variation in pyrite oxidation.

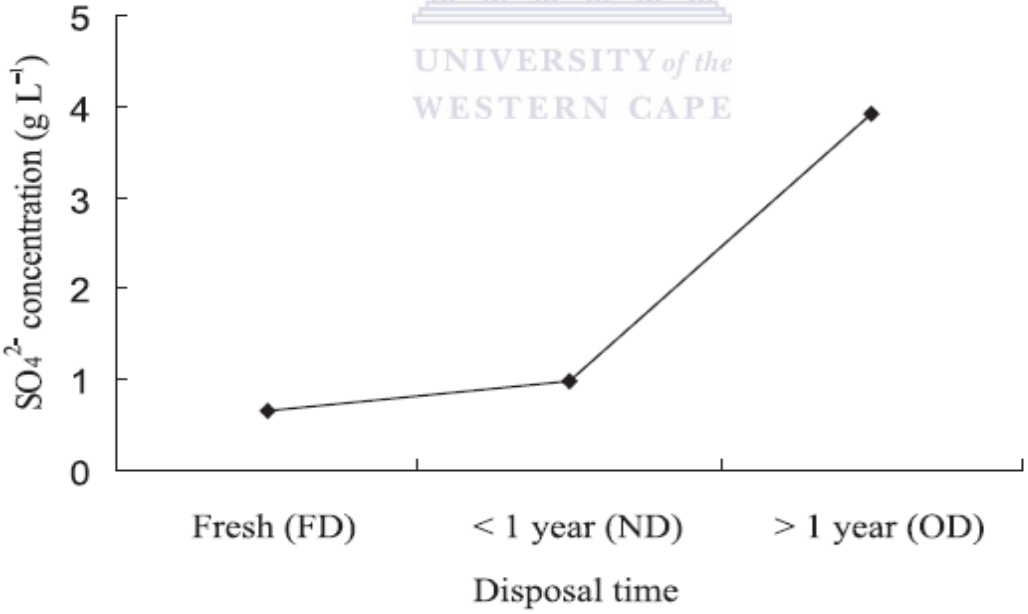

Figure 3: SO_4^{2-} concentration in leachates from different waste rocks (fresh dump-FD, tailings dam less than a year –ND-new dump, tailings dam over a year – OD-old dump) (Saria, et al., 2006)

The result from Figure 3 shows the tailings dams that have been formed or dumped for a longer period are more pyrite-oxidized based on the sulfate concentration present (Saria, et

al., 2006). Therefore, the rate of pyrite oxidation was in the following sequence: tailings dam over a year> tailings dam less than a year> fresh tailings (Saria, et al., 2006).

2.6 Mineralogical Characterization with XRD

X-Ray Diffraction (XRD) method and petrographical studies are helpful in the determination of changes in the initial mineralogical assembly of minerals brought about by reaction with water. However, XRD is often not sensitive to the development of small, but potentially important, quantities of secondary mineral phases (Doye, 2003).

The mineralogy of the Witwatersrand is well known and has been a basis for other researches that have come up. The knowledge of the minerals present in the tailing dam can help determine the extent, effect and state of AMD present at any given time of research.

Due to the leaching of the surface tailings of the Witwatersrand that is visible, constant check and monitoring, remain inevitable because it will help to determine the extent of the threat posed since the depth of oxidation of the tailing indicates the damage it has caused.

2.7 Geochemical Characterization with XRF

X-ray fluorescence (XRF) is a well-established analytical and geochemical method capable of determining the concentrations and composition of a wide variety of economically and petro-genetically useful elements in geological materials (such as rocks, overburdens, and sediments) (Norrish & Thompson, 1990; Weltje & Rik, 2008). XRF analysis is built on the principle of exciting electrons by incident X-ray radiation. Discharge of electrons from inner atomic shells produces vacant spaces filled by electrons subsiding back from the outer shells, whereby excess energy is released as a pulse of secondary X-ray radiation. Fluorescence energy released or emitted and wavelength spectra are typical for atoms of specific elements, which allow the estimation of their relative abundances.

In XRF analysis, procedures for sample preparation are quite simple, but sulphide ores involve specialized handling compared to silicate rocks. Some elements like sulphur, iron, copper and tin may be lost to the platinum crucibles normally used for preparation of fused glasses or volatilized (Norrish & Thompson, 1990; Norman, et al., 2003). For instance, high Lead contents in particular pose problems for many elements in the accurate analysis of sulphide samples by XRF because of significant spectral interferences and matrix effects.

2.8 Geochemical Characterization with ICP-MS

Inductively coupled plasma – mass spectrometry (ICP-MS) is a well-established analytical and geochemical method capable of determining the concentrations and composition of a wide variety of economically and petro-genetically useful elements in geological materials (such as rocks, overburdens, and sediments) (Norrish & Thompson, 1990; Weltje & Rik, 2008). ICP-MS uses a plasma torch generated by the interaction of an intense magnetic field on a tangential flow of gas in which the ionized the gas coupled with a source of electrons from a high-voltage spark, forms a very high temperature plasma discharge (~10,000 K) at the open end of the tube.

Unlike ICP OES, the plasma is positioned horizontally; generating positively charged ions rather than photons and giving it distinctive ultra-trace detection capability, due to the production and detection of large amounts of these ions (with the use of the mass spectrometer compartment).

Compared to XRF, ICP-MS analysis can offer improved detection limits and a much more list of elements, with the shortcoming of using the conventional approach in which solution nebulization needs the sample to be completely digested, but experience difficulties if some minerals present are resistant to acid attack. This implies that, the sample digestion procedures for solution nebulization ICP-MS of geological materials, such as rocks, minerals and soils are particularly problematic, time consuming and expensive and can be subject to a variety of sources of error.

This led to the invention of another method that will not involve digestion in determining major- and trace element concentrations using a laser-ablation coupled with ICP–MS (LA–ICP–MS) for the analysis of samples (GuÈnther, et al., 2001). Therefore, alternative and precise instrumental procedures for routine trace element (e.g. rare earth elements and Zr, Nb) analysis are of paramount interest. Laser ablation-inductively coupled plasma mass spectrometry (LA-ICP-MS) has been reported as a technique for the accurate determination of elements using Ba as the internal standard and matrix matched calibration.

2.9 Statistical Evaluation in the study of AMD

Statistics is receiving more and more attention in environmental geochemistry. However, it is important to know the functions and limitations, the advantages and disadvantages of these techniques for better understanding of their applications. The use of statistical analysis can be

a useful tool in finding groupings and correlations among many parameters in a large data set. For instance, water quality results may be grouped into set or values that may relate to various hydro-geochemical processes. Univariate statistics is useful for calculating averages, identification of probability distribution and outlier detection. Multivariate analysis plays an important role in the study of relationships among variables (Zhang & Selinus, 1998).

Spatial analysis makes use of the spatial coordinate information of the variables, and considers the spatial correlation. However, these pure mathematical methods are still unsatisfactory as the nature of environmental geochemistry is far from being so simple. Multivariate method of analysis such as the principal component analysis (PCA) and cluster analysis (CA) will be used in this study. This is as to discover the prominent and emerging sources of heavy metals. The value of the statistical analysis for evaluation and interpretation of the data is used to determine the major pollutant sources. Thus recommending ways the pollution and damage caused by the AMD heavy metals (directly or indirectly) can be alleviated and shows why there should be urgent attention to the abandoned mining sites and management of the active mines in the West Rand. An environmental information system, with the integration of statistics, GIS, expert systems and environmental models should be established to further the study in environmental geochemistry, as well as to provide decision support (Zhang & Selinus, 1998).

2.10 Geographical Information System (GIS)

GIS is computer-based software that combines mapping, database management and analytical functions. All spatial data are recorded as points, lines or polygons in space. GIS enables the user to overlay different layers/themes of spatial data and interpolation (such as kriging and IDW) to analyse the relationship between the various themes. It can also display new themes based on the pre-selection of tabular data such as displaying a map of all the gold deposits in the Gauteng Province. GIS can be used to monitor the environmental impact of mining, and to identify natural hazards and environmentally sensitive areas, be a connection to an external access database to facilitate the integration of mining applications and finally used for the production of small map products (Zhang & Selinus, 1998).

Adopting GIS software (such as Arc GIS 10.2 used), various thematic layers can be overlaid to assist the user with environmental impact assessments. Integrating thematic layers such as topography, land ownership, land use and geology can facilitate the objective selection of economically and environmentally preferable alternatives. Buffers created around selected

features to identify zones of no interference or development (Kumar, 2010). Other factors that play a role in the process of a mining application such as property ownership, lease holdings and mineral rights can also be successfully managed within GIS (Zhang & Selinus, 1998). The most progressive means of mapping is with Geographic Information Systems (GIS) as it enables sound cartography as well as a holistic analysis of an area.

GIS is a digital cartographic tool used for generating, integrating, storing, editing, analysing, sharing, and displaying geographically referenced data. It allows users to make queries, analyse spatial information as well as editing and managing data with a final output being the formation of maps to aid visual data interpretation. Data used in GIS are available in many different forms, ranging from simple point co-ordinates to advanced remote sensing performed on satellite imagery.

However, pure mathematical methods are still unsatisfactory as the nature of environmental geochemistry is far from being so simple. GIS provides visualization and some spatial analysis functions with spatial information involved. An environmental information system, with the integration of statistics, GIS, expert systems and environmental models should be established to further the study in environmental geochemistry, as well as to provide decision support (Zhang & Selinus, 1998).

2.11 Geochemical Mass balance (GMB) and AMD

Presently, there are no studies on Acid Mine Drainage prediction in the Witwatersrand, which have utilised the geochemical mass balance approach, but it has been used in alteration process determination. If AMD is generation from mine wastes, this indicates that an alteration process has occurred within the mine wastes system. The knowledge of the level of weathering can ascertain the degree of oxidation of mine waste and highlight the mobile elements that are of great threat to the surroundings.

The origin of the study and application of geochemical mass balance was set by (Gresens, 1967), who proposed the affiliation of change in volume, composition and density of an altered rock to its original composite (protolith) in a metasomatic systems.

GMB is generally applied to all kind of alteration processes, if its original composition is known (Mukherjee & Gupta, 2008; Lo´pez-Moro, 2012). Nonetheless, Grant (1986, 2005) offered a modification of Gresens' mass balance equation in which he replaced volume and density by mass, allowing a direct evaluation of mass transfer to composition of the original

composite and to the altered rock through the ISOCON diagram (Mukherjee & Gupta, 2008; Lo´pez-Moro, 2012).

Based on this mass balance alteration, the estimation of geochemical Mass Balance in determining the alteration processes in rock materials is done in numerous ways, in which ISOCON method of mass balance is widely used. This is because of its simplicity, in terms of its flexibility and its graphical approach. Despite that, the reference frame for Mass Balance got by best-fit regression is partial to the element scaled upward; data points with higher numerical value control the scaling factor of the ISOCON analysis slope in the plot (Mukherjee & Gupta, 2008).

This slope of the best-fit ISOCON line may differ within the scope of slopes well-defined by specific conserved elements plots far from the origin. If identical weight is given to all elements, irrespective of their concentration level, the mean of slopes of the immobile elements (which implies the ratio of the concentration in altered to unaltered elements) may offer a better estimation for reference frame without option to graphical plot and ISOCON solution. Therefore, an appropriate identification of the conserved species is a vital requirement to fruitful application of mass balance computation reducing the characteristic errors of the ISOCON technique (Mukherjee & Gupta, 2008). Therefore, the method of Isocon analysis was applied to the altered and the unaltered (or least altered) tailings (from samples in each altered layer) so as to estimate the geochemical variations during alteration. A Microsoft Excel spreadsheet known as EASYGRESGRANT was used in this study. It allows accurate selection of immobile elements from clusters of slopes, volume factors, and an enhanced isocon diagram, thus giving an error-free modelling of mass-balance for application in metasomatic systems (Lo´pez-Moro, 2012).

This was applied to the altered and the unaltered (or least altered) tailings (from samples in each borehole) so as to help in estimating the geochemical variations during alteration based on the gain or loss of constituents present. Samples taken from the bottom depth of all boreholes was used as the unaltered sample based on the petrography (that is, in this study, the bottom samples of the each borehole were selected as the “least altered equivalent” because the far end of the borehole have undergone the shortest period of weathering or non-weathered). If leaching, mobilisation and transportation or precipitation and accumulation of element(s) have occurred, a total mass change between the unaltered sample and the altered sample can help in identifying the elements involved based on a regression value of approx.

1. Because of this, the enrichment or loss in elements can be identified from each layer and within each borehole sampled. The elements of similar trend in mass balance results in each borehole or to a layer might link to peculiar geochemical process.

CHAPTER 3 Geology of the study area and its Climate

3.1 Climate of the Study Area

The study area is situated along Krugersdorp R28 road, which is adjacent to a residential area known as west village in Randfontein. Along this R28, other tailing dams are under intense watering to prevent dust pollution. The tailing dam was constructed around 1952 and it is about 70m deep from the top to the ground surface.

The climatic condition of this area is well known. It has a similar condition with Johannesburg since it is situated in its north west. The annual rainfall in Johannesburg and its environment is about 750 mm, and is intensely seasonal, while potential evaporation is about 1600 mm/annum (Dyson, 2009). Most rain falls during the summer, between October and February. Thunderstorms of short duration accompanied most of the rainfall. Temperature averages showed about 20 C during the summer months and about 15 C in winter (Naicker, et al., 2003).

Due the fact that the Johannesburg weather station (JHB BOT TUINE STATION) information covers through areas with coordinates of -26.1500, 28.0000 in which the study area falls, temperature, rainfall, wind speed and direction, and pressure data were collect for years between 2003 to 2012 (Table 3). These data collected were processed to get the average values for each criterion over the period of 2003 to 2012.

Table 3: Summary of the weather data collected from the South Africa weather bureau, for Johannesburg weather station (JHB BOT TUINE STATION) “-26.1500, 28.0000” from 2003 to 2012

MONTH	JAN	FEB	MAR	APR	MAY	JUN	JUL	AUG	SEP	OCT	NOV	DEC
Av. Rainfall(mm)	143.8	72.74	67.14	32.58	12.61	11.14	1.34	4.54	6.96	48.26	43.32	107.56
Av. Max Temp oC	26.78	27.06	25.32	22.81	20.92	18.19	18.35	21.09	25.01	26.36	26.67	27.32
Av. Min Temp oC	15.88	15.48	13.3	10.39	6.44	3.48	2.77	5.16	8.69	11.97	13.53	14.81
Av. Speed(m/s)	1.14	0.98	0.7	0.49	0.43	0.46	0.39	0.61	0.84	1.31	1.31	1.35
Av.Pressure(hPa)	840.3	841.38	841.7	843.16	843.56	844.85	845.72	843.96	843.36	842.04	840.68	839.97

The amount of rainfall was observed to be high between October and March (during summer). Low amount of rainfall is observed during the wintertime according to the data obtain (Figure 5).

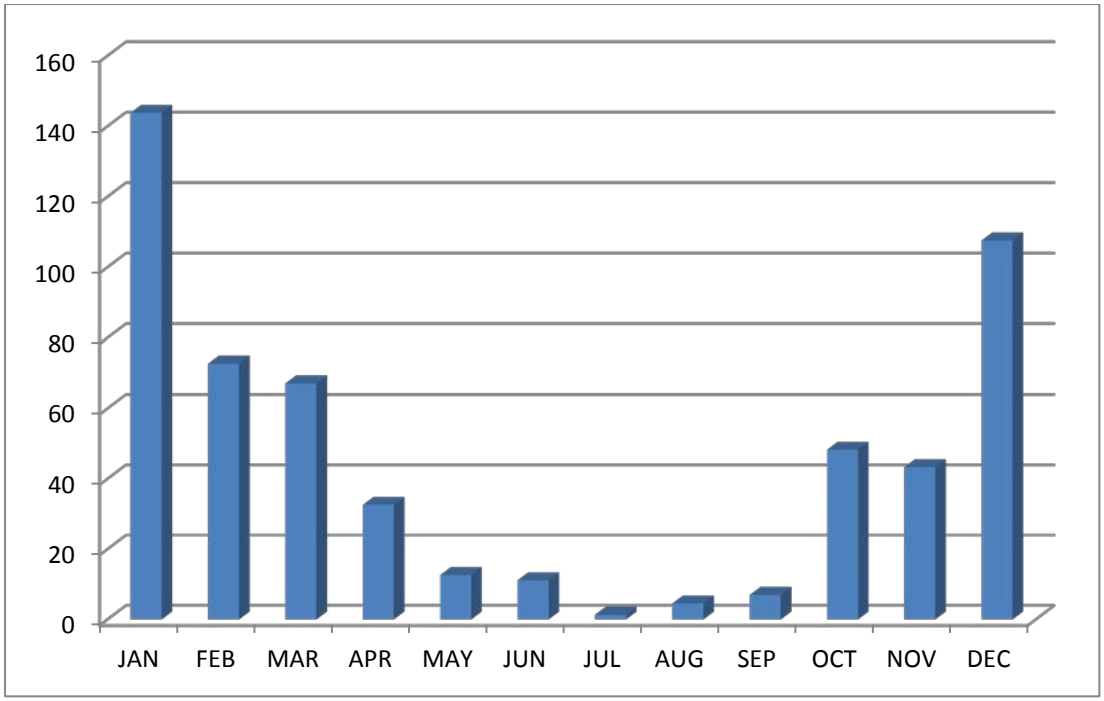

Figure 4: Graphical representation of the Average daily rainfall in (mm) from 2003-2012

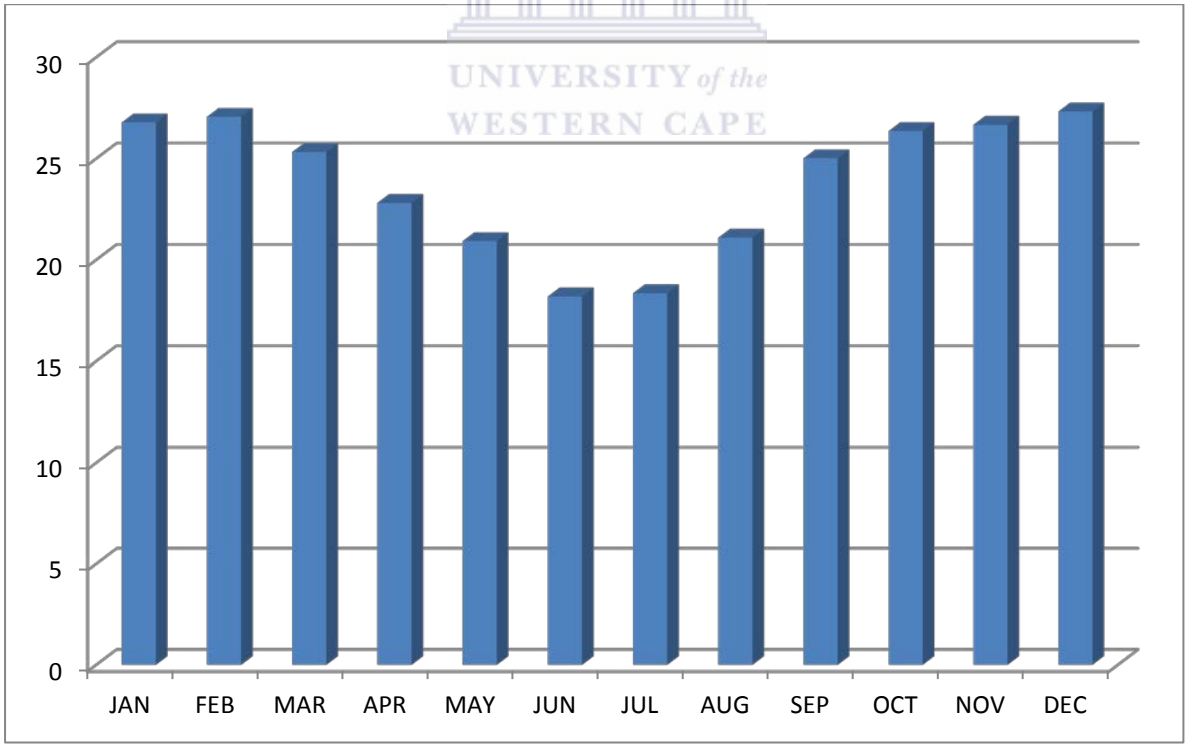

Figure 5: Graphical representation of the Average maximum temperature between 2003 - 2012

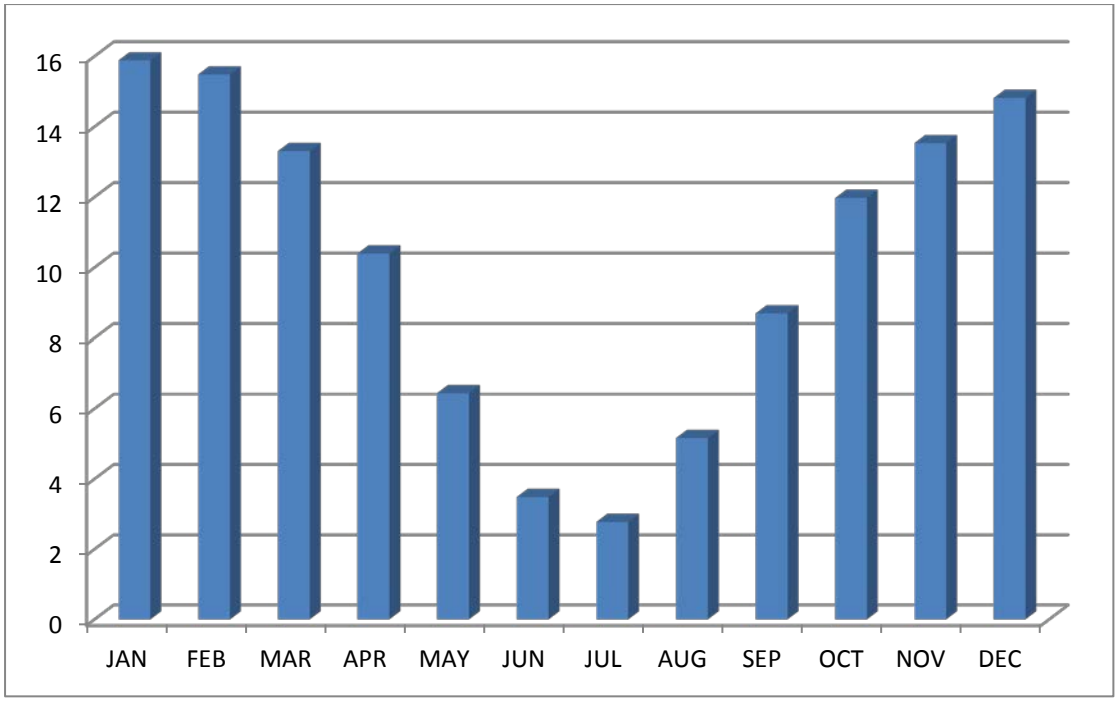

Figure 6: Graphical representation of the Average minimum temperature from 2003-2012

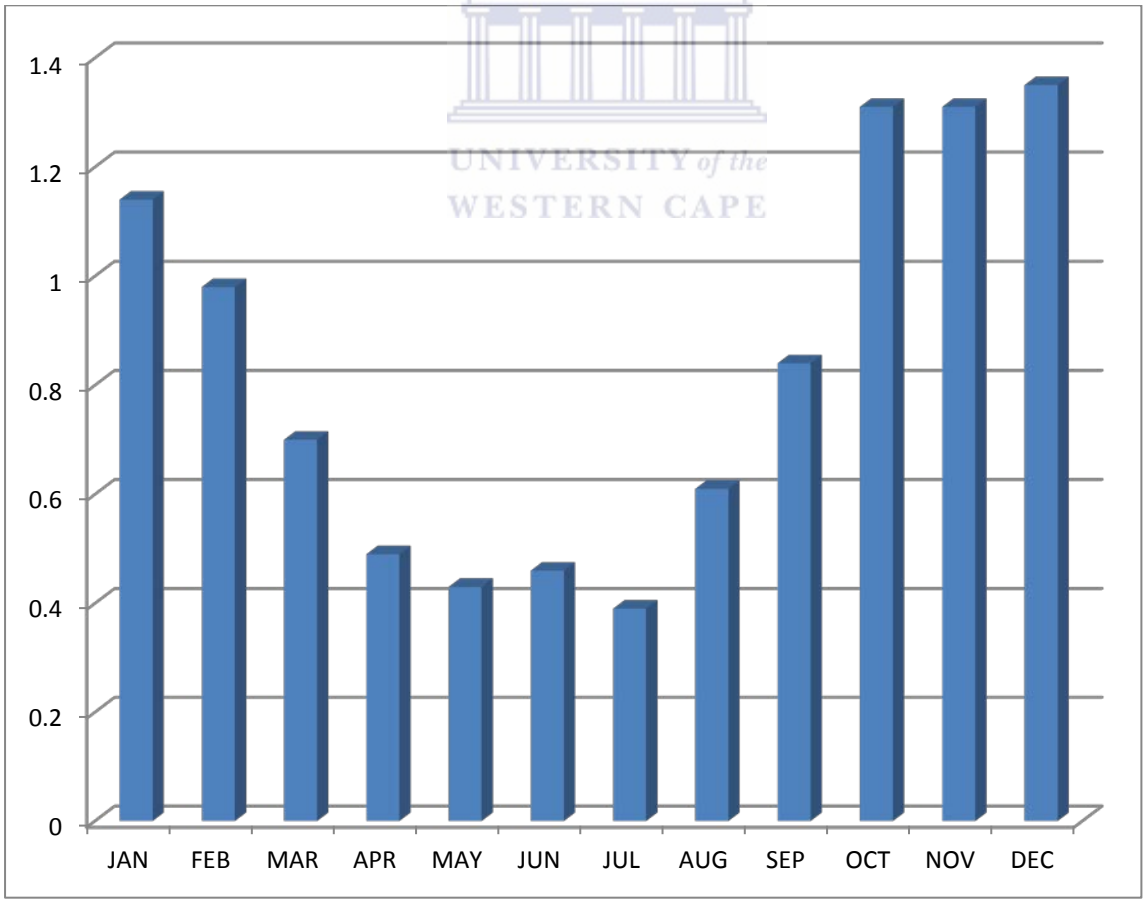

Figure 7: Graphical representation of the Average wind speed from 2003-2012

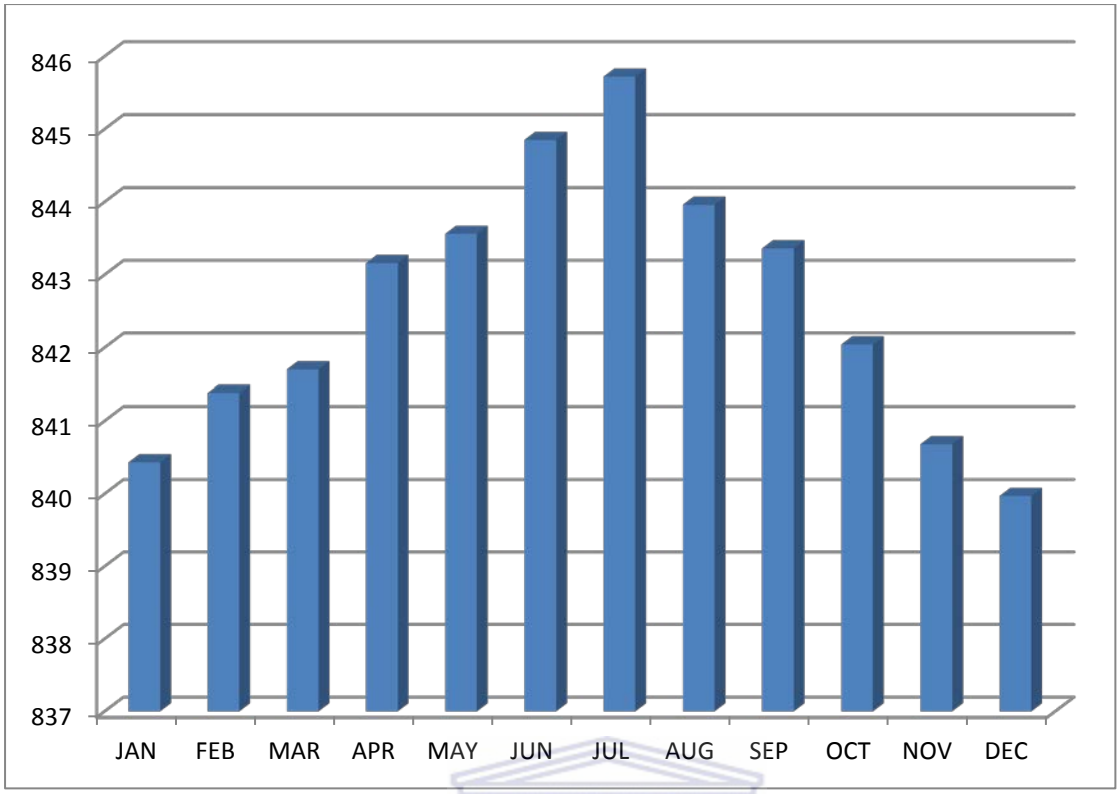

Figure 8: Graphical representation of the average pressure for 2003-2012

From graphical representation of data (Figure 4-8), the average daily rainfall was relatively low and falls between May to September and high between October to April which corresponds to the winter and summer period respectively. Compared to previous rainfall data from (Rosner, 2000) (though numerically there have been difference), the average rainfall over 2003 – 2012 is 551.99mm. Though smaller, it indicated change in weather, which could be linked to increase in man's activities overtime. This could be because of climate change overtime.

The average maximum temperature recorded was 27.32^{o}C in December, which falls in the summer time, while the average minimum temperature was 2.77^{o}C in July that falls in the wintertime.

The wind speed is more prominent during summer period than winter. The average wind speed ranges from 0.39-1.35m/s. According to the data, the most prominent wind direction is from the north through north eastern direction, which is followed by the south western direction with an average of 0.834m/s (movement to the north is scanty).

Finally, the average pressure is almost of the same values throughout the months.

3.2 Regional Geology and Structural Setting of the Witwatersrand Basin

Major mineral deposits of the world formed because of some irreversible series of geological events that cannot be recurrent overtime (Robb & Meyer, 1995). This kind of events led to the formation of the Witwatersrand basin.

Globally, the Witwatersrand basin is the largest gold region. The metamorphic hydrothermal model and the modified placer model are the two main models that have been recommended as the source of its mineralisation (Frimmel, et al., 2005; Law & Phillips, 2005; Rasmussen, et al., 2007).

The formation of the Witwatersrand basin occurred over a period of 360 Ma, between 3074 and 2714Ma. Before the formation Witwatersrand, the Kaapvaal Craton, which is the term given to the ancient section of continental crust was formed between about 3.7 to 2.7 Ga in southern Africa (Rasmussen & Muhling, 2009).

It contains 4 major volcano-sedimentary successions and 3.7–3.1 Ga granite-greenstone terranes within the overlying Witwatersrand basin (Rasmussen, et al., 2007). A series of events (episodic) led to the pulses of sedimentation within the sequence and its precursor. These events occurred between 3086-3074Ma (Dominion Group), 2970-2914Ma (West Rand Group) and 2894-2714Ma (Central Rand Group) (Robb & Meyer, 1995) which are the four major volcano sedimentary successions.

In 2500, 2300, and 2000Ma, the metamorphism of the Witwatersrand basin occurred. The earlier two events occurred concurrently with the increasing intrusion by Venterdorp and Transvaal Formation sequences. The last event shows the intrusion of the Bushveld complex and/or the Vredefort syndrone (Robb & Meyer, 1995).

Various structural models published such as regional strato-tectonic models, which are based on relatively local tectonic or goldfields datasets, and hydrothermal models, are strengthened by the hypothesis that structural architectures have acted as channels, controlling the deposition and remobilization of economic gold throughout the goldfields in the Witwatersrand basin.

Despite this, few studies have recognized the basin-wide structural character or looked for structural correlations, after years of published researches.

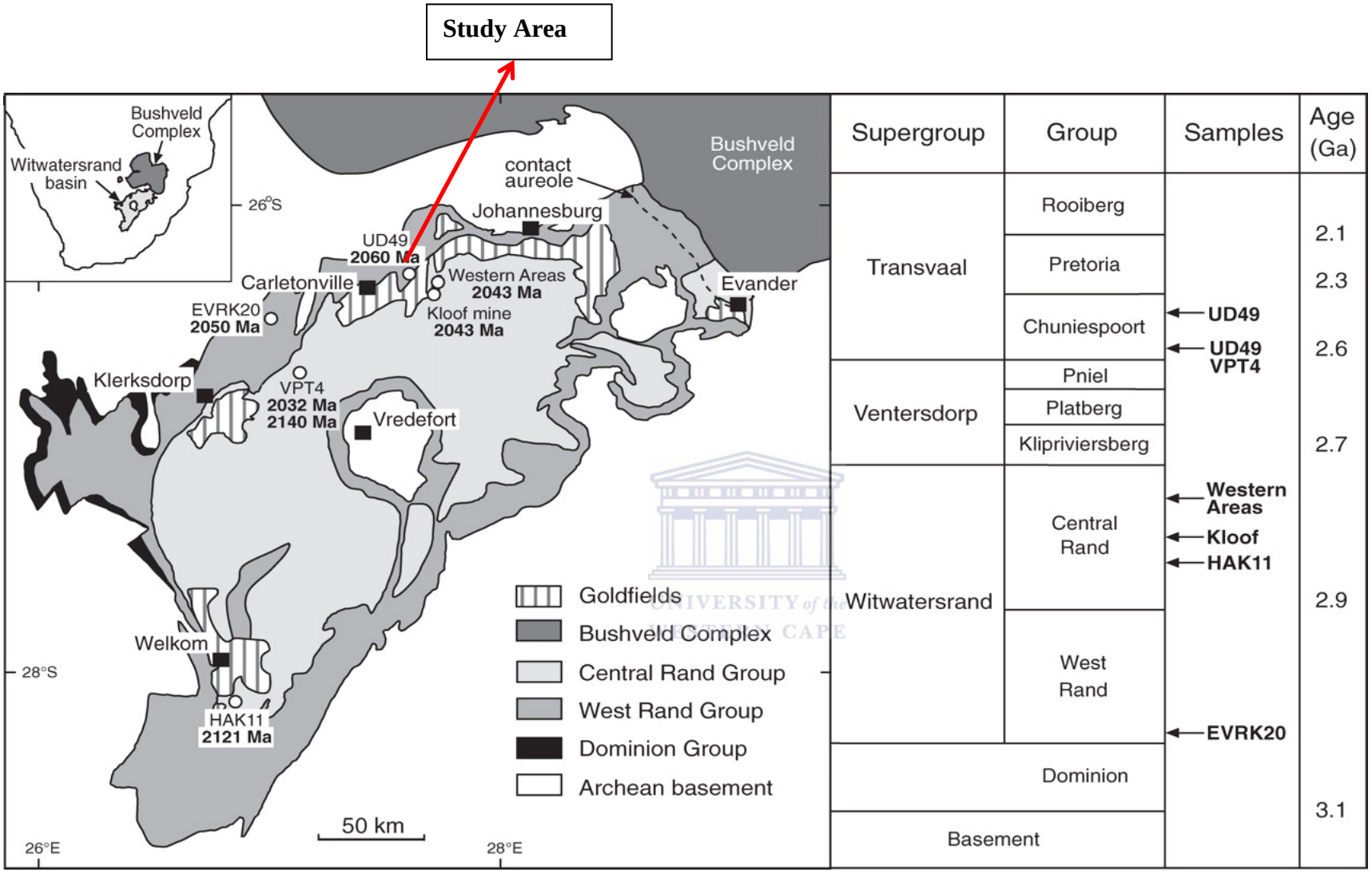

Figure 9: Map of Witwatersrand basin and adjacent Bushveld Complex, South Africa, and generalized stratigraphic column for Witwatersrand, Ventersdorp, and Transvaal Supergroups (Frimmel, et al., 2005; Rasmussen, et al., 2007)

An enhanced and model understanding of processes of formation of basin (Archean-Proterozoic tectonics) and the application of modern structural geology needs to be implemented by evaluating the existing and previous structural dataset to test and confirm strato-tectonic models of the ore formation (Jolley, et al., 2004; Dankert & Hein, 2009).

The Figure 9 above shows the geological map and the various Formations that underlies the Witwatersrand basin. This shows the three major Super Groups: the Ventersdorp, the Transvaal and the Witwatersrand Super Group that overlies the Archean Basement.

The Dominion Group (3074±6Ma, single zircon U-Pb SHRIMP) (Dankert & Hein, 2009) overlies the Archean Basement (ca. 3.6–3.2 Ga) and comprises volcanic rocks and rift-related sedimentary rocks of about 2.5 km thick, which were deposited showing deformed enlargement, moderate- to the finest granite–greenstone basement (Rasmussen & Muhling, 2009).

The overlying Witwatersrand Super Group is about 7.5 km thick. This is subdivided into the upper unit called the Central Rand Group and the lower unit called the West Rand Group (shallow-marine and subtidal sandstone and shale) (Rasmussen & Muhling, 2009).

The West Rand Group is divided into hospitals hills series, the government reef series, the Jeppesstown series, and all in ascending order and each division corresponding to shales and quartizite groups (Viljoen, 1999; Mccarthy & Rubisge, 2005). Its main reef Groupings are the Ventersdorp Contact Reef (VCR), the Carbon Leader Reef (CLR) and the MondeorReef. It comprises of a lower division of about 15,000 feet thick, containing inter-bedded shale and quartzite predominated by the shales and an upper part of about 9000 feet thick that are actually predominated by the quartzite (Durand, 2012).

The Central Rand Group can be subdivided into the Johannesburg sub group and the Turffontein named from the area it was first described but not limited to it (Durand, 2012). In addition, it is classified into the main Bird series, which includes the strata from the basal contact to the Kimberly shales and the Kimberley – Elsburg series which also comprises strata from the Kimberley shales to the top of the system (Durand, 2012). The Johannesburg Sub Group of the Central Rand Group contained the richest deposit of gold and was mined extensively throughout the Witwatersrand basin.

According to (Schneiderhan, 2008), 1600m thick lavas of the Venterdorp Super Group which are deposited between 2.714 and 2.665Ga overlie the Witwatersrand Super Group (Figure 9).

Below the Ventersdorp super group (which consist mostly a sequence of igneous rock) lie a layer of sedimentary rock known as the Ventersdorp contact reef. This gold-bearing layer consists of the sediments deposited as a result of partial erosion of the Witwatersrand super group discordantly (Durand, 2012).

The Ventersdorp Super Group is overlaid discordantly by the Transvaal Super Group that is embedded with a basal layer sequence called the siliciclastic Black Reef Formation, (which consists of sedimentary rock of limited gold deposits) ,up to 2 km of dolomite (Durand, 2012). It is overlaid by banded iron formation (a part of Chuniespoort Group), and about 2–3 km of sandstone and shale, with minor volcanic rocks (Pretoria Group) (Rasmussen & Muhling, 2009; Dankert & Hein, 2009).

Viljoen & Reimold, (2002) said the area occupied by the Witwatersrand basin sediment experienced heavy erosion by an extension northwards–flowing river system more than 2.2Ga. The part (channels) formed by the river system were filled in by the sediments that formed by the river system and formed the black reef with an average thickness of 1 to 10m. This is found in the tens of meters thick in Randfontein but has been extensively mined (Mccarthy & Rubisge, 2005; Durand, 2012).

The black reef formation underlies the Chuniespoort group of the Transvaal super group, which consist of chemical, and biochemical sediments including stromatolitic carbonates and banded ironstone. This stratum is between 1200 and 2000m thick in Gauteng and the North West province, and set down during the transgression of the Transvaal super group epeiric sea approximately 2.67 – 2.46Ga (Eriksson, et al., 1995; Durand, 2012)

The carbonates which were set down 2.643 -2.520Ga, are distributed into several formations of abundantly dolomitic and partially silicic (Eriksson, et al., 1995; Durand, 2012). Below the Chuniespoort group is the Malmani subgroup, which is peculiar in the Southern Gauteng and the gold mining area of the North West Province. The geological sequence consists of sediments that have been deposited against basement granites and greenstones.

Therefore, the Witwatersrand sediments containing the gold bearing conglomerate layers (Reefs) consist of interbedded shale and quartzite with numerous conglomerate bands. Andesitic lavas of the Ventersdorp Supergroup, which, in turn, are unconformably covered by approximately 1,200m of Transvaal Super group dolomite, un-conformably overlie these

sediments; the dolomite thickens toward the south. Shale and quartzite of the Pretoria Series finally cover the dolomite conformably.

Karst topography and cave systems have developed within the dolomite. This has caused substantial subsurface secondary porosity, which has been an outlined and drawn using geophysical technique. It showed its relation to water-table levels, both historic and present, the nature of the sediments and relationships to intrusions. Since water levels are related to the topography studies of the paleo-topography have been used to understand the karst distribution.

Tectonic activity gave rise to block faults and open folds. The pre-dolomite Formations have been widely faulted; these faults and erosion are responsible for the main spreading of these Formations and hence the position of the mines. In the northeastern part of the area, Witwatersrand sediments outcrop due to a combination of faulting and folding. There are three major faults: The Witpoortjie, Panvlakte and Bank faults (Dankert & Hein, 2009).

Although much of the faulting was pre-dolomite, there are faults that either continue into the dolomite due to rejuvenation of the pre-existing faults or continued activity. It is these faults and, sometimes, opens joints that connect the water bearing features in the dolomites within the mine openings, which have been developed at depth. Mostly, there is a considerable thickness of impervious strata between the mines and the water-bearing features in the dolomites.

Dykes of younger age than the previously described features have intruded the area; many are roughly parallel with north-south orientation. These dykes have divided the dolomites into compartments and controlled groundwater movement in pre-mining times.

Since mine development and dewatering, the dykes still affect the movement of groundwater, but have been mined through in many places. Thus, it is suspected that the pre-mining groundwater conditions will never be repeated, even when the mines have stopped operation and are flooded.

From the study of Jolley et al, (2004), thrust-fracture networks can be channels for hydrothermal reworking of gold at range of microscopic to macroscopic measurement. The tectonic and metallogenic models have been the basis of the structural geology of the Witwatersrand basin (Dankert & Hein, 2009).

3.3 Local Geology and Structural Trend

The project area lies in the Randfontein in the West Rand region. The West Rand region of Gauteng encompasses the towns Carletonville, Krugersdorp, Westonaria, Randfontein, Soweto, Western Gauteng, the Magaliesburg and all their surrounding areas, all of which have been incorporated into the new West Rand District Municipality. The West Rand gold field lies 25 km west of Johannesburg and extends from Roodepoort, in the east, to Krugersdorp in the north and south towards Westonaria. The geology of the West Rand has been discussed by (Hobbs & Cobbing, 2007), shedding more lights on its geological formation, hydrology, litho-stratigraphy, and structural geology.

The West Rand Basin is underlain primarily by sedimentary strata (quartzite and shale) related to the Witwatersrand Super Group, and younger sediments (dolomite, quartzite and shale) related to the older strata of the Transvaal Super Group (The West Rand area of Gauteng is underlain by dolomite of the Transvaal Super Group).

Systems	Sub-group	Formation	Rock
Transvaal Supergroup (West Rand Basin)	Chuniespoort Subgroup	Black Reef Witpoortjie and Panvlakte Horst blocks	Dolomite, chert, dolomitic limestone
		Kimberly Reef	Feldspathic quartzite, shale and conglomerate
Ventersdorp Supergroup (Far West Rand Basin)	Malmanini Group	Ventersdorp Contact Reef	Conglomerate, lava (amygdaloidal andesite and dacite, and quartz porphyry), sediments(quartzite, grit and conglomerate)
		Middelvlei Reef	Agglomerate, tuff, chert and dolomitic limestone
		Mondeor Reef	Conglomerate

Figure 10: A summary of the formation and rocks peculiar to West Rand Area or District (the West Rand and the Far West Rand)

The dolomitic strata underneath the West Rand (gold-mining) Basin are related to the Vaalian (2.65 to 2.43 Ga) Chuniespoort Group, and in particular the Malmani Subgroup within the lithostratigraphic unit and are responsible for recharging aquifers. These strata are

compressed within Black Reef Formation quartzite, which, in turn, is enclosed and underlain by older Randian (3 to 2.75 Ga) basement rocks related to the Witwatersrand Super Group (Figure 10).

Faults and dykes are found in which faults cut through strata along the litho-stratigraphy. (Hobbs & Cobbing, 2007) negated the notion of (Coetzee, 1995; Van Biljon, 2007) referring to the dolomitic strata as an inlier but an outlier. The Sterkfontein Caves that formed within this dolomitic rock was declared a UNESCO World Heritage Site in 1999 and have delivered many anthropological finds. The most important and of these finds are "Mrs Ples", a 2.1-million-year-old Australopithecus skull, and "Little Foot", an almost complete Australopithecus skeleton dating back more 3 million years (Durand, 2012).

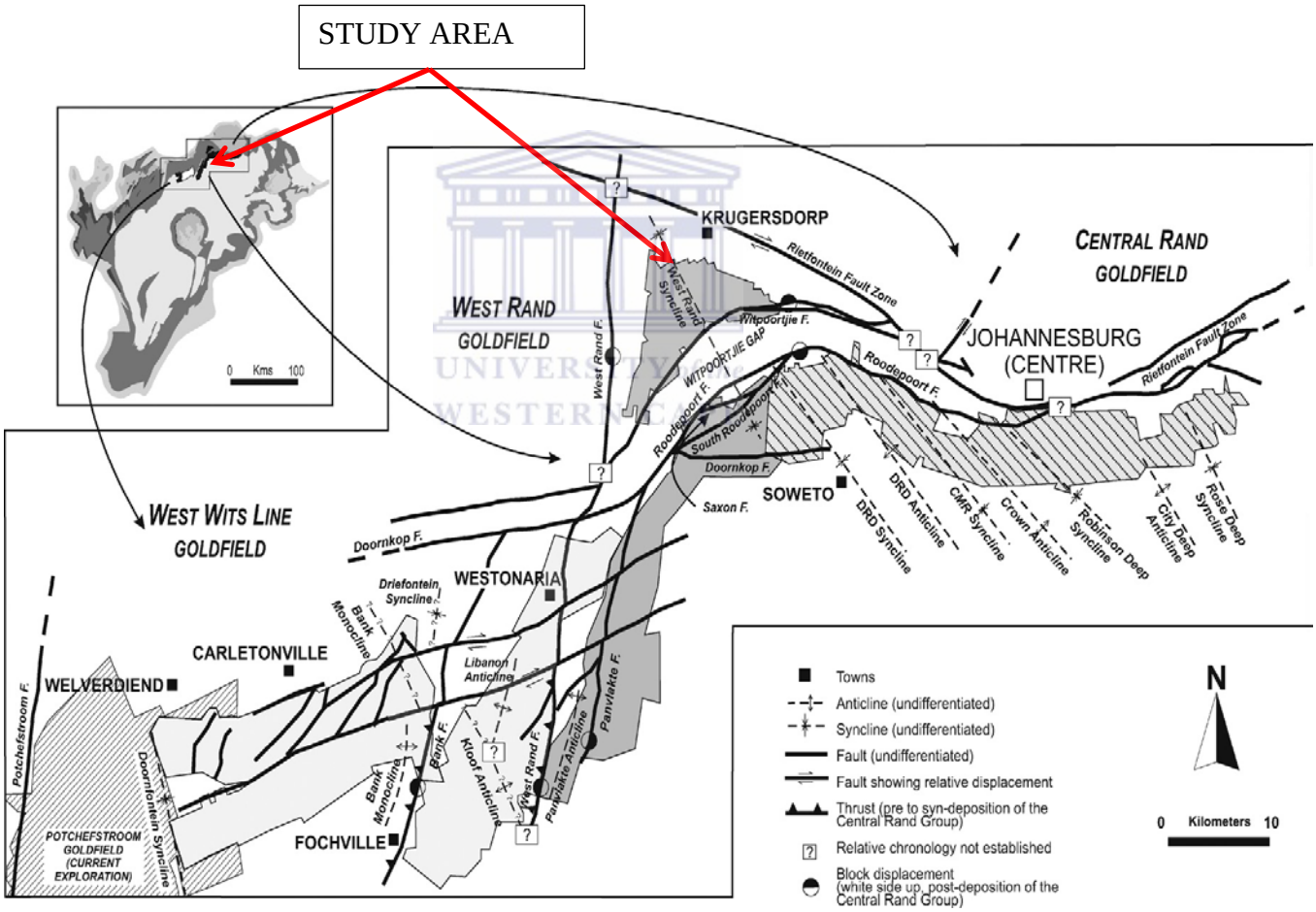

Figure 11: Geological map of first-order structures in the Witwatersrand Super Group in the West Wits Line, West Rand and Central Rand goldfields with the younger cover removed. Extracted from (Dankert & Hein, 2009)

Most of the original mines of the West Rand gold field have been exhausted. Cooke Section currently derives its ore from the Composite Reef, which represents at least two conglomeratic horizons (E9 and UE1). The Western Areas Gold Mine exploits ore from three conglomerate reef horizons – the Composite Reef, the 'Massives' and the Ventersdorp Contact Reef.

On Randfontein Estates Gold Mine, the Kimberley and South Reefs are mined in the Doornkop Section while the White Reef was exploited in the past, mainly for uranium. It comprises of quartzite, shale, dolomite limestone and the conglomerates (a peculiar feature of the Witwatersrand) (Norman & whitfield, 2006).

The quartzite (metamorphic, which is a rock composed of sand particles, bonded together by heat, pressure and rock cement that makes it a hard resistant rock) and shale formed from mud and silt and bonded by rock cement(despite forming a softer rock) are the 2 major rock types of the Witwatersrand super group.

Others less prominent are the conglomerate formed from rounded pebbles in a sandy matrix, ironstones rich in iron oxides and silica. It should be noted that the knowledge of the rock types would aid the study by providing basic information of minerals of great abundance, which are peculiar to the pollution source (Mendelsohn & Potgieter, 2001). Most rocks layers particularly the softer varieties are not exposed at surface but are covered by soil.

The general direction of meta-sedimentary sequences of the Witwatersrand Super-group in the southwest of the goldfield is SW trending and SE-dipping, and in the northeast of the goldfield, west trending, south dipping as shown in Figure 11 (Dankert & Hein, 2009).

Some researches provided a comprehensive overview of major faults and folds in the West Rand region. These regional faults include the WNW-trending extension of the Rietfontein Fault Zone, the arcuate Witpoortjie and Roodepoort–Saxon–Panvlakte faults, the north-trending West Rand fault, and the WSW-trending Doornkop fault and WSW-trending faults south of Westonaria. The latter dextrally displaces (apparent) the West Rand and Saxon–Roodepoort–Panvlakte faults (Figure 11) (Dankert & Hein, 2009).

CHAPTER FOUR: Research Methodology

4.0 Introduction

This chapter entails the general overview the method of sampling and instrumental technique used for the investigations. Before embarking on this research, literature study was done to get ample information about and know the gold tailing dam environments in Witwatersrand. Contacts were made to various gold mining companies in-charge of the tailing dams. Site investigation was done for a week to help in choosing the tailing dam of interest. The criteria used was based on its location, accessibility, proximity to residential area, the physical state of the dam (some dams are being or totally reclaimed), and how long it has been constructed. The site chosen was also within one kilometre away from the residential area.

4.1 Field Work

After a week of site investigation, Mogale Tailing dam MT became a site of interest because of its nearness to residential areas, farms and major road and the present state of the dam. Samples were taken from the tailing dams at an interval of 1m each down hole using a hand auger. All drill holes location coordinates were recorded using a GPS (Global Positioning System). Five holes were drilled with the use of a hand auger to a depth of 10.2 meters measured constantly (as auger moved down) with a strong metallic meter rule. The drill holes were marked as T004, T008, T009, T010, and T011 respectively. Each hole drilled was carefully examined, logged to show the variation in color, grain size and mineralogy. Since there is much similarity in the texture and size of gold tailing dams, only the colour difference and moisture were prominent. Samples collected were place in an airtight and properly sealed polythene bag and kept in dark container to minimize further oxidation. Afterwards, the samples were transported to the Earth Science Department laboratory of University of the Western Cape for sample preparation and analyses.

4.2 Sample Preparation

Before every analysis, it is important that the samples are well prepared because it determines the outcome of the analyses because of the possible influence of external bodies (such as impurities) and mixing. Prior to geochemical analysis, all tailing samples were dried at 40^{o}C for 16 hours and afterwards pulverised by Dickie and Stockler milling machine (TS-250mill) into powdery form without sieving. This is because a complete elemental analysis was needed to be done. The milling machine was properly cleaned with soapy water and acetone

before and after milling each sample. Samples were sent to Itemba Labs for XRD analyses and Acme Analytical Laboratories (Vancouver) Ltd for geochemical analyses in which the XRF and LA-ICP-MS were used.

4.3 Mineralogical analyses procedure of XRD

The mineralogical composition of the 37 tailing samples was done using the BRUKER AXS D8 Advance X-ray diffraction spectrometry (XRD) machine of ϑ-ϑ scan in locked coupled mode at the Itemba labs. These thirty-seven samples were selected based on the colour, texture and mineralogical variations down hole. Samples from layers that are distinct are considered.

The X-ray tube Cu-Kα radiation ($\lambda K\alpha_1$=1.5406Å) and the Detectors are Position Sensitive Detector Vantec-1 appropriate for mineralogical studies.

For each sample, 1.2 g of powder specimen was deposited in the centre of the sample holder, which consists of a 20mm, by 20mm corning glass (Tube voltage: 40kV, Tube current: 40mA, Slit system: V20 variable slit). The heap of powder was smoothly flattened into a disc shape of 15mm diameter and 1mm thickness by means of circular motion of a microscope glass slide until the zero level for a correct sample height was achieved.

4.4 Geochemical Analyses

The geochemical analyses were done in the Acme Analytical Laboratories (Vancouver) Ltd (Table4). Fifty-one (51) tailing samples were analysed, spanning over the five boreholes drilled.

Five grams of each sample was analysed by $Li_2B_4O_7$/ $LiBO_2$ fusion analysis by X- ray Fluorescence (XRF). The $Li_2B_4O_7$/ $LiBO_2$ fusion analysis by X- ray Fluorescence (XRF) was used to analyse the percentage concentration of the 12 major elements and the loss of ignition (LOI, SiO_2, Al_2O_3, Fe_2O_3, CaO, MgO, Na_2O, K_2O, MnO, TiO_2, P_2O_5, Cr_2O_3).

A measure of 0.1g of each sample was analysed for the total percentage of carbon and sulfur present using analysis by Leco.

Using Aqua-regia / ICP-MS method, ultra- trace element determination was performed for Mo, Cu, Pb, Zn, Ag, Ni, As, Au, Cd, Sb, Bi, Hg, Ti, and Se.

Laser Ablation Inductively Coupled Plasma Mass Spectroscopy (LA ICP –MS) coupled with $LiBO_2/Li_2B_4O_7$ fusion analysis was used to analysed the rare earth elements and Ba, Be, Co, Cs, Ga, Hf, Nb, Rb, Sn, Sr, Ta, Th, U, W, Zr, and Y.

Standard quality control was used during geochemical analysis (such as standards, blank samples and pulp duplicates) and reference materials.

Table 4: Sample preparation and analytical procedures in Acmelabs

Method Code	Code Description	Test Wgt (g)	Standard used
4X	**Li2B4O7/LiBO2 fusion, analysis by XRF**	**5g**	**STD OREAS72A/ STD SY-4(D)**
2A Leco	**Analysis by Leco**	**0.1**	**STD GS311-1/ STD GS910-4**
4B02	**LiBO2/Li2B4O7 fusion ICP-MS analysis**	**0.2**	**STD SO-18**
1DX	**Aqua regia /ICP-MS analysis**	**2g**	**STD OREAS45EA/ STD DS9**

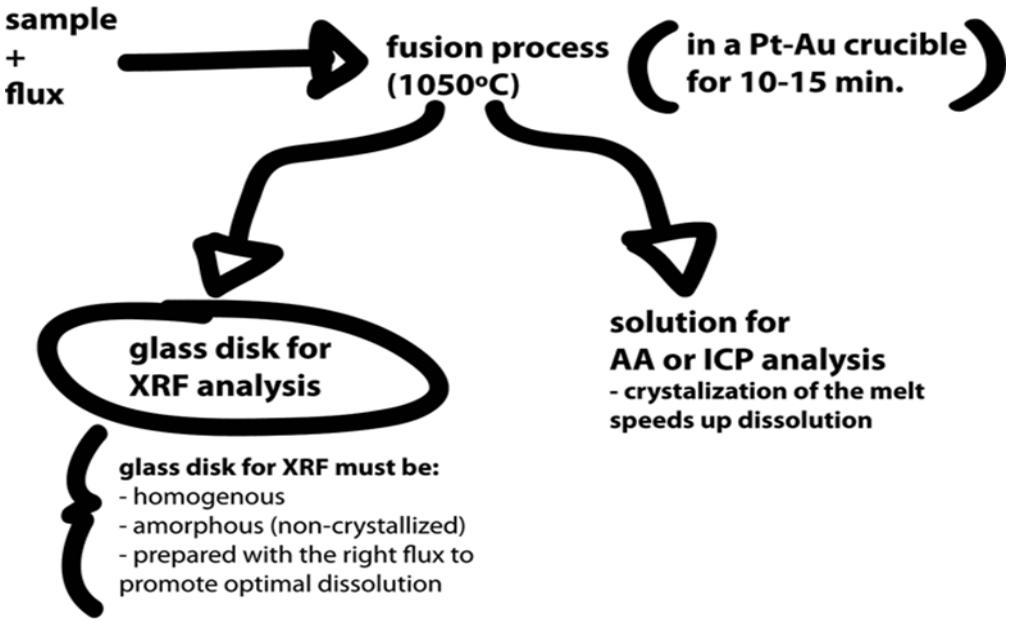

Figure 12: Graphical representation of the generalised lithium borate fusion procedure as used by ACME lab.

4.4.1 Lithuim borate fusion method/ XRF

Fifty-one tailing samples from the investigated site were analysed by lithium -borate fusion (sample digestion method) with X- ray Fluorescence (XRF) spectrometry at the acmelabs, Vancouver, Canada. A predetermined amount of sample was roasted at 950^{o}C to determine the loss on ignition (LOI) which is calculated as a function of weight loss after roasting(Loss on ignition (LOI) is determined by igniting a sample split then measuring the weight loss).

Five grams of sample pulp was roasted to 1050^{o}C and the roasted sample was then fused in a platinum-gold crucible with a commercial lithium tetraborate flux (Figure 12). The molten material was cast in a platinum mold. Fused discs are analysed by XRF spectrometer, which was calibrated with calibrated by certified reference materials. For XRF analysis, the creation of an homogenous glass disk decreases effects linked with particle size, mineralogy and matrix to attain better accuracy than pressed powders. However, for the preparation of a glass disk, 35% Lithium tetraborate /65% Lithium metaborate instead of 100% Lithium metaborate was used to avoid crystallization.

The samples were analysed for LOI, SiO_2, Al_2O_3, Fe_2O_3, CaO, MgO, Na_2O, K_2O, MnO, TiO_2, P_2O_5 and Cr_2O_3 using XRF.

4.4.2 Method of Lithium metaborate/tetraborate fusion/ LA-ICP MS

The technique of using inductively coupled plasma-mass spectrometry (ICP-MS) is well known as a quick and accurate process for the determination of the trace elements in geologic samples and rare earth elements (REEs) (Longerich, et al., 1990). Nonetheless, absolute sample digestion is vital for precise results. For instance, mixed acid open-vial digestions on a hotplate work is good for basaltic and almost all ultramafic samples, on the other hand may well fail to totally breakdown many trace mineral phases found in more silica containing samples. These resistant phases, such as zircon, tourmaline and garnet, may have a significant percentage of the total trace elements in a specified sample. Therefore, high-pressure bombs are employed and thus effective at achieving complete digestion, but are complicated, sluggish, and labour intensive.

Since the method of using fusion with a flux may require large dilutions to avoid unacceptably high levels of total dissolved solids, a combination fusion-dissolution method that effectively decomposes refractory mineral phases and removes the bulk of unwanted

matrix elements is applied. The method consists of a low-dilution fusion with lithium metaborate/tetraborate fusion is used for digestion.

In this study, this method helps to analyse for 14 REEs and 16 additional trace elements in the tailing samples without having to bother any form of element loss from or to resistant mineral phases. The dissolution with HF afterwards accurately removes silica and more than 90% of the flux as gasiform fluorides, leaving clear and steady solutions for analysis on the ICP-MS. The Flux used for the fusion is lithium metaborate/tetraborate fusion 0.2g of the prepared and powdered samples are mixed with an equal amount $LiBO_2/Li_2B_4O_7$ flux placed in a carbon(graphite) crucible and fused at 1050° C in a muffle furnace for 30 minutes (crucibles are fused in a furnace).

The bead is allowed to cool and after cooling, the resultant fusion bead is dissolved in ACS grade nitric acid (the fused crucible was dropped into a mixture of 5% nitric acid). This fusion process uses lithium metaborate and lithium tetraborate mixed with the sample in graphite crucibles and fused in induction furnaces at 1150^{o}C. The resultant molten mixture is dissolved and will result in total metals extraction and is ideal for litho-geochemistry including major oxides and trace elements including REE and other high field strength elements. All water used is >18 M deionized water from a Nanopure analytical grade water system

Samples are prepared and analysed in a batch system. Each batch contains a method reagent blank, certified reference material and pulp duplicates (samples are mixed with a flux of lithium metaborate and lithium tetraborate and fused in an induction furnace). The molten melt is immediately poured into a solution of 5% nitric acid containing an internal standard, and mixed continuously until completely dissolved (~30 minutes). The samples are analysed for elements (Code group 4X) with STD OREAS72A/ STD SY-4(D) standards used.

The samples were analysed for the rare earth elements and Ba, Be, Co, Cs, Ga, Hf, Nb, Rb, Sn, Sr, Ta, Th, U, W, Zr, and Y using LA ICP-MS.

4.4.3 Aqua-regia digestion

Aqua regia digestion is a popular digestion method for multi-element analysis and requires two acids (hydrochloric acid and nitric acid) in a 3:1 ratio, forming nitrosol chloride for ultra-trace element analysis (1DX). This digests the mineral matrix and helps release the metals present in solution and assisted by gentle heating. According to the method discussed by

(Chen & Ma, 2001; Kisser, 2005), the nitric acid reacts with concentrated hydrochloric acid to form aqua regia:

$$3HCl + HNO_3 \longrightarrow 2H_2O + NOCl + Cl_2.$$

The aqua regia digestion was performed in 250-mL glass beakers covered with watch glasses. A thoroughly mixed sample of 0.5000 g was digested in 12 mL of aqua regia on a hotplate for 3 hours at 110^{o}C to evaporate. After evaporation to near dryness, the sample was diluted with 20 mL of 2% (v/v with H_2O) nitric acid. Afterwards, it was taken into a 100-mL volumetric flask by filtering through Whatman no. 42 paper. Then, it was diluted to 100 mL with deionised distilled water (DDW) which is then analysed in ICP-MS. The standards STD OREAS45EA and STD DS9 were used in the analysis. The samples were analysed for Mo, Cu, Pb, Zn, Ag, Ni, As, Au, Cd, Sb, Bi, Hg, Ti, and Se using this method (1DX).

4.4.4 Leco Analysis

Leco analysis was done to determine the total sulphur and total carbon present in the sample. The Total Carbon and Sulphur are determined by the Leco method (Group 2A)

Total sulphur was determined using a Leco sulphur analyzer. For all samples, 0.1g was ignited in an induction furnace to about 1350 °C while a stream of oxygen was passed through the sample. The amount of sulphur dioxide released from the sample is defined by an IR detection system (that is, infrared spectroscopic analysis), which is used to generate the Total Sulphur result.

Total carbon was determined using a Leco carbon analyser. For all samples, 0.1g was combusted in high temperature of 1350 °C in an induction furnace while a stream of oxygen was passed through the sample. The total carbon was calculated from the infrared spectroscopic analysis of the carbon dioxide generated.

4.5 Paste pH and EC

Paste pH and EC test was done by dissolving a 1-part portion of the tailing sample to 2.5 part of water, after shaken properly, and then the values are measured using a multi-meter pH- EC Electrode (TMH1, 1986; Price, 2009; INAP, 2009).

Paste pH remains a modest and economical method that assist to indicate the presence of reactive carbonates or relative extent of acidity. In this study, milled tailings samples and water were mixed to form a paste in a specific proportion.

The pH was first calibrated using buffer solution of pH 4 and pH 7 and the EC. 5g of tailing samples was measured into the test tube and 15ml of distilled water was added and mixed thoroughly. The sticky solution was then measured for paste pH and EC.

4.6 Quality Assurance and Quality Control (QA/QC)

QA/QC is a major and important aspect of modern analytical geochemistry. A well-monitored QA/QC method gives a way of establishing confidence level in and evaluating the limitation of the analytical data, thus, detecting the origin of analytical error. The method includes the determination of the precision, accuracy and potential contamination load from sampling to analysis. The advancement of instrumentation technology over the years has resulted in high demand for high precision and accuracy of litho-geochemical data in research, and mineralisation studies and development (Abzalov, 2008; Piercey, 2014).

Due to the tendency of uncertainty that can seldom surrounds the quality of litho-geochemical data, proper record of QA/QC is required before the data can be publicly reported and accepted. This has led to the requirement from research community suggesting the availability of standardised information about all analytical data, including a well-known QA/QC procedure.

4.6.1 Definition of terms

Lower limit of detection(LOD)

This is the lowest concentration for every instrument used to analyse a particular element that it can identify above the background signal. This can be determined by the signal in the blank samples.

Upper limit Detection(ULD)

This is the highest concentration that a specific instrument can reliably quantify without any major error expectancy.

Reference or Standard materials

These standard materials possess certified or approved values for a given element of interest.

Duplicates

These are the replicates of samples, its pulps, coarse reject, or analysis performed at random to determine the error created during sampling and preparation

Blank Sample

This is a sample or sample solution that does not contain identifiable concentration of the elements of interest using designated analytical methods. This represents a method for monitoring contamination during the sample preparation and analysis.

4.6.2 Precision

Precision is the measure of the reproducibility of a specific measurement performed. Precision is determined using systematic introduction of sample, pulp duplicates, and sometimes reference materials. Evaluation of data is done using scatter plots, statistical test, Thompson-Howarth plots and average coefficient of variation.

In this study, pulp duplicates of some selected samples will be used to calculate precision with the use of scatter plot. It should be noted that reference or standard materials have recognised values but limited ranges of values for a given element; and at such, do not give the true measure of precision. That is why duplicates samples are used.

Scatter plots provide a means of visualizing the pulp duplicate result from data collected by plotting the duplicate sample results on the y-axis and the initial results plots on the X-axis with control lines that depicts a specified level of precision (i.e. 5%, 10%, 20%, etc.).

If all data falls within the control line then the data is said to be precise based on the set precision, if outside, it indicates that the data is not precise at the set precision.

4.6.2.1 Precision results for major elements

From the scatter plot for LOI, SiO_2, Al_2O_3, Fe_2O_3, and CaO, the data fall within the control line of 5%, indicating that it is <or =5% precise, and MgO, K_2O, and TiO_2 data fall within the control line of 10% (Figure 13). Other scatter plot chart are displayed in appendix E.

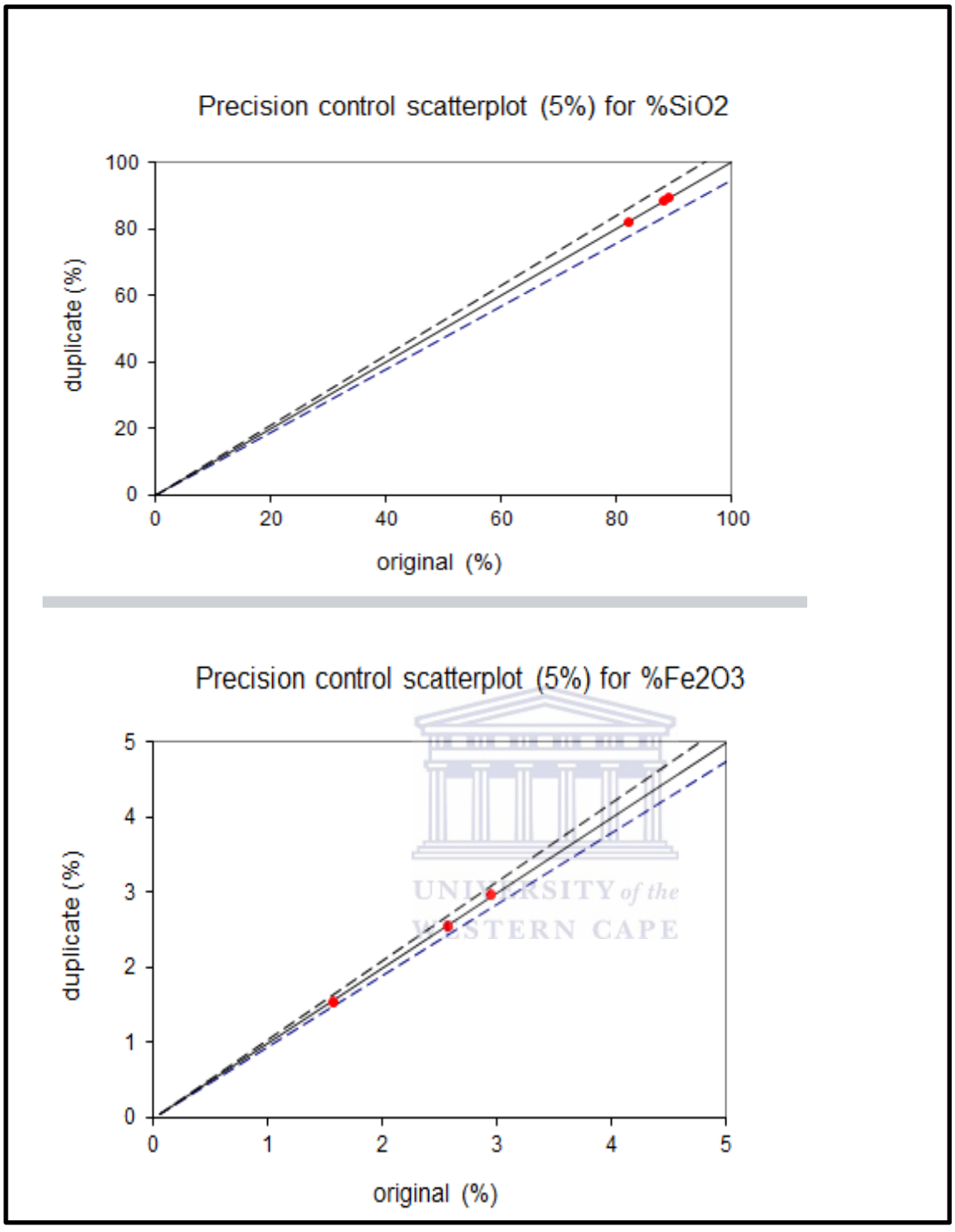

Figure 13: Precision results with precision control scatterplot of 5% for SiO_2 and Fe_2O_3

4.6.2.2 Precision results for trace elements

Mostly, trace elements data in this study fall within the control line of 10%, indicating a less or equal 10% precision (Figure 14). The scatter plot chart for precision is shown in appendix E.

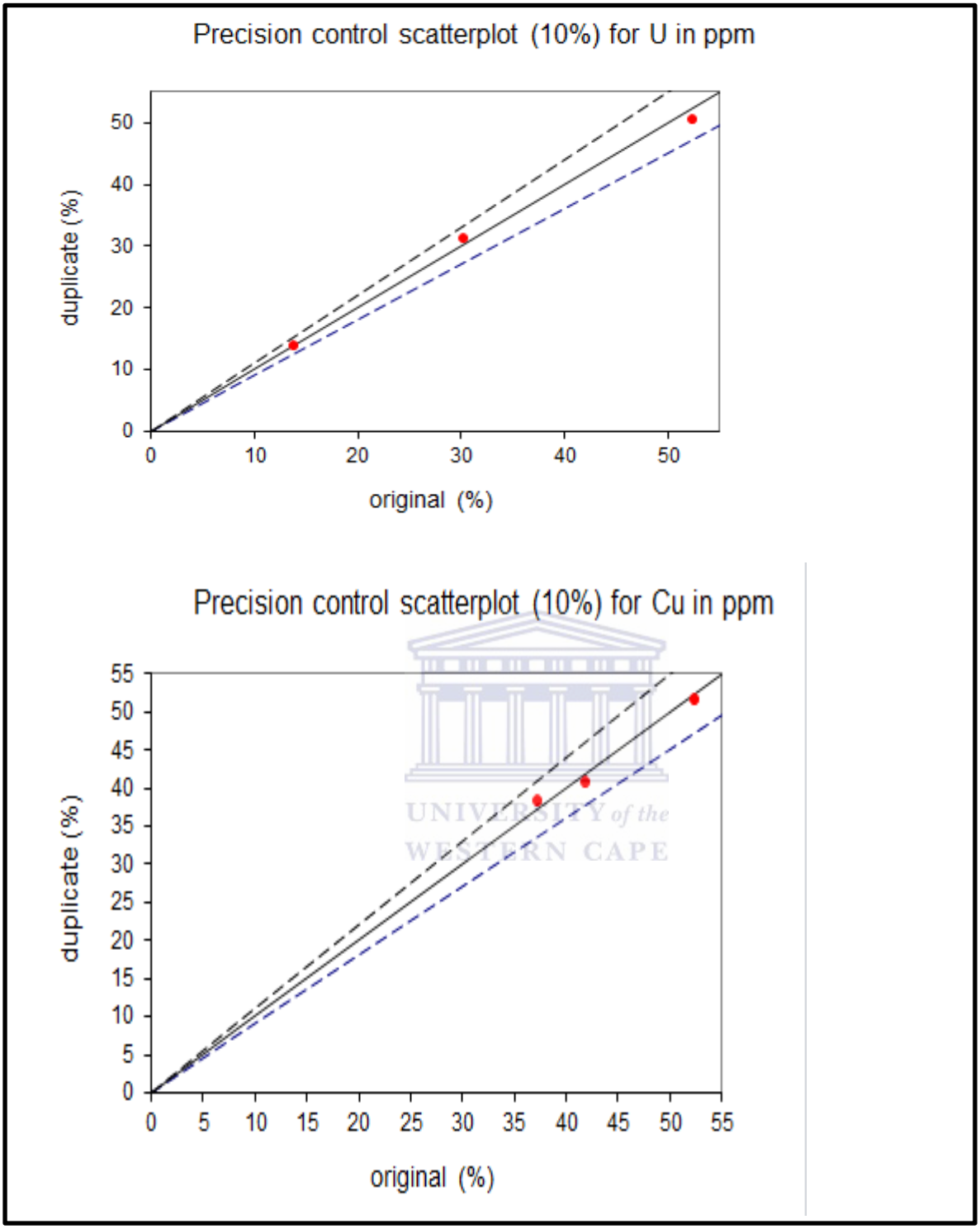

Figure 14: Precision results with precision control scatterplot of 10% for U and Cu

4.6.3 Accuracy

Accuracy is defined as the determination of the degree of closeness of a calculated or measured value to its known and accepted value. This is determined using the analysis of reference or standard materials using some formulae, statistical test and shewart control

charts. In this study, the percentage relative difference is used, which is a result of the percentage difference of the expected or known reference material and the measured or analysed reference material. This is calculated from the replicates analyses of reference materials as follows.

Percentage relative difference **(%RD) = 100* (M*e* –STD*e*)/STD*e***

Where M*e* = mean value of element *e* in the standard over a number of replicates analyses results of the reference or standard material.

STD*e* = the certified or known value of element *e* for the standard or reference materials used

% RD can be negative or positive, that is <0 or >0. Generally, when %RD values are +3% or -3%, the data accuracy is considered excellent, if between 3-7%, it is termed very good, 7-10%, it is termed good, if above 10%, it is not accurate.

Some elements such Au could have an accuracy over 10% because of its nugget nature; therefore a standard accuracy is given for this elements. The results for % accuracy for major and trace elements is shown in appendix E

4.7 Data evaluation

Statistical analysis and geochemical mass balance techniques were used to evaluate the data from the mineralogical and geochemical analyses. The descriptive statistics of the tailing dam's major oxides and selected trace elements was done.

4.7.1 Statistical Analysis

Bivariate and multivariate analysis was performed using SPSS 21® software. Correlation coefficient, Hierarchal-clustering and factor analysis was performed based on the method described by (Zhang & Selinus, 1998; Alkarkhi, et al., 2009).

4.7.1.1 Correlation coefficient analysis

Correlation coefficient analysis was performed for elements occurring in the samples from all the five boreholes to identify bivariate trends between two variables using Pearson's correlation method. The correlation coefficient r ranges from -1 to +1 (that is r = -1 or r = +1) representing a perfect linear relationship between two variables, showing a direct or indirect relationship with each other. When r is negative, it shows there is a negative trend (correlation), if r is positive, there is positive correlation and if r is 0, it shows no trend at all.

Correlation coefficient r can be defined as:

$$r = \frac{n(\Sigma xy) - (\Sigma x)(\Sigma y)}{\sqrt{\left[n\Sigma x^2 - (\Sigma x)^2\right]\left[n\Sigma y^2 - (\Sigma y^2)\right]}}$$

Where x and y are the two selected variables correlated.

4.7.1.2 Cluster analysis

In cluster analysis, geochemical data for the major oxide was analysed using hierarchical cluster analysis with a statistical agglomeration schedule under an initial none cluster membership. Cluster analysis was used to generated the prominent clusters present at r= 0.05(dendrogram) in which hierarchical cluster analysis was done using nearest neighbour linkage and Euclidean distance as a measure of proximity between samples.

The ward method under the Euclidean distance interval was used and a dendrogram was plotted. Cases were labelled based on the sample no and sample ID. Box plots was used see the variation of a specific element in each group (cluster).

4.7.1.3 Factor analysis

Factor analysis on the other hand, narrows down to the elements the are playing major role in the composition of the samples and helps in group based on elemental relationship. Factor analysis was done using principal component analysis extraction method to find and estimate the relationships among variables. This will make the interpretation of the analytical results by reducing the no of variable that are the determinant factor, thus, narrowing the interpretation of variables distribution as a function of its geochemical and sedimentological activities and common origin.

Therefore, Principal component analysis (PCA) was done to create possible factors that responsible and determinant of the metal concentrations and source allotment. All dataset was subjected to factor analysis (FA).

The number of significant principal components (PC) was selected based on Varimax orthogonal rotation with Kaiser normalisation with eigenvalue greater than 1. This implies that factors with eigenvalues greater than 1 was considered and varimax orthogonal rotation was used to transform the matrix and reduce the no of variables loaded in each factor.

4.8 Geochemical Mass Balance

The geochemical mass balance calculations were done using EASYGRESGRANT software by Lopez-Moro, (2012). The mass balance results were expressed in gain/loss percentage weight and ppm of oxides and trace elements respectively (Mukherjee & Gupta, 2008).

In this study, the bottom samples of the each borehole were selected as the "least altered equivalent" because the far end of the borehole have undergone the shortest period of weathering or are non-weathered. The degree of mobility of a material in a natural system was computed by (Gresens, 1967) according to the formula $\Delta m_i = fv(\rho_a/\rho_0)C_a^i - C_0^i$. In addition, the gain and loss of materials is calculated by the equation $(\Delta C_a^i/C_0^i) = (m_a/m_0)(C_a^i/C_0^i) - 1$ and based on ΔC_a. Where *0* and *a* represent the original and the altered tailing materials respectively, and ρ0 and ρa signify densities; m_i is the mass change in material *i*, C^i_a and C^i_0 are the initial and final concentrations in material *i* respectively, and *fv* is the volume factor or ratio of the final volume to the initial volume. $\Delta C^i_a / C^i_0$ is the change in the ratio C^i_a and $C^i_{0,}$ m_a and m_0 are the masses of the altered and original material.

The mass balance calculation was based on the Gain/Loss relative to C_i^0, represented as ΔC_i and $\Delta C_i/C_i^0$. Where (i) stands for the element analysed for, (0) represents original value, C_i represents the average value of element (i) in the specific layer, C_i^0 is the average value of element (i) in the bottom samples, ΔC_i represents (C_i - C_i^0), and when ΔC_i is +ve, there is gain /enrichment, when –ve, there is loss/depletion (Mukherjee & Gupta, 2008). The average values of all major oxides and elements found in the each layer as described by the petrography was used to calculate the mass balance.

4.9 Inverse Distance Weighted (IDW) Analysis (interpolation) using Arc GIS

The spatial analysis of the data in which was done using Arc Map 10 software. The data was subjected to the Inverse Distance Weighted Analysis for the distribution of individual elements in layers of 1m down depth. An excel sheet containing the coordinates of each drill hole was converted into a shapefile (saved as drillhole) and geo-referenced into the coordinate system of the base map (map of the study area) used.

Using the data management tool in the arc tool box, IDW interpolation method (Setianto & Triandini, 2013) was used. The input point feature was the drillhole, the Z-value field is the element analysed for. This was done for each meter (1-9).

The layer properties of the IDW interpolation is displayed with classified symbology with polychromatic colour. The distribution of value of element was based on quantile range and four classes with none normalisation. The layer display is exported as a jpeg and all display for each element is displayed from 1-9m.

CHAPTER 5: Petrography

5.1 Introduction

The physical characteristics and knowledge of the tailing dam constituent can help determine AMD potential of the tailing dam. Petrographic and mineralogical studies of the tailings will provide ample information on the state of oxidation of the tailing dam constituent and the relationship between the oxidised and unaltered tailings. The petrographic work will serve as the foundation of study on which the element variation pattern can be used as an effective explanation.

This chapter gives the detailed description of the borehole drilled and its mineralogical composition. Therefore, it is pertinent to know that the mineralogy of the tailings controls the pore water chemistry and affects the chemical composition of AMD.

5.2 Site Description and location of drilled holes

The study area is situated along R28 main road in Randfontein, which is adjacent to a residential area known as west village in the West Rand area as shown in Figure 15. This tailing dam is owned by Mogale Gold Company and partially vegetated (some parts are vegetated and others non-vegetated). The tailing dam was constructed around 1952 and it is about 70m deep from the top to the ground surface).

From the Figure 15 below, the tailing dam is about 2.1km long and 1.4km wide. The eastern parts of the tailings dam have been exposed to reclamation processes to extract gold. This made some parts of the tailing dam unreachable. Therefore, the sampled boreholes fall within the vegetated and non-vegetated surface that is accessible. In addition, at the opposite side of the tailing dam that is across the road two other dumps that are exposed are found. A wet land was found on the side of the road closed to the tailing dam, and from the information gathered; it is very active during the wet season and is an extension of the Wonderspruit. Along the road, it is observed during that sampling period that a water system is used to spray water on the mine dumps to minimise wind pollution. Closed to the tailing dam, excavation is still in process to mine for gold and waste rock deposit from the excavation. At the western part of the tailing dam is the manganese mill and processing plant and excavation is done for manganese mining. At the back of the tailing dam is the presence of a non – perennial river body, which will surely be affected, if the tailings are leached towards the direction of the river. Also, the tailing dam is closer to Krugersdorp. In Mogale Tailing Dam 1L23, five

boreholes drilled and named T004, T008, T009, T010, and T011. For this study, 41 samples are analysed.

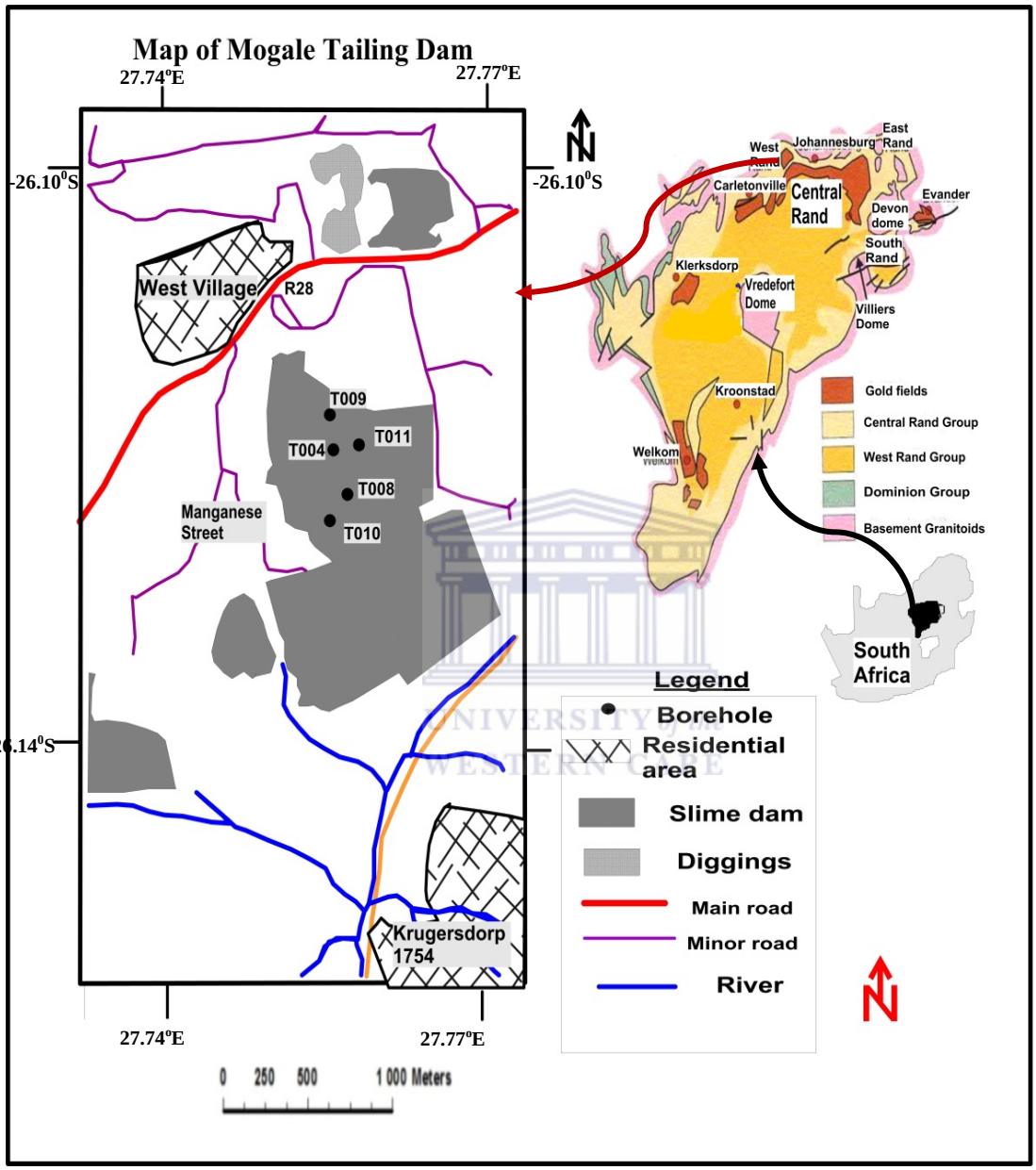

Figure 15: The location map of the boreholes sampled

5.2.1 State of the tailing dam sampled

Visibly, it could be observed that the tailings dam surface has been leached due to the present of whitish fine sand particles on its surface and the gully part made by precipitation agent such as water from rainfall draining from the top of the tailing dam, through its sides downward.

The Witwatersrand's tailing dams are characterized by its greyish colour on its initial deposit. These tailings are of finely grounded materials with large surface area and contain sulphides and buffering materials. The surface of the tailing dam contained fine dry material but as we go deeper, its moisture content increases and becomes sticky. The texture and colour of the Witwatersrand tailings is well known. The tailings are fine materials about <75µm in size because it has been grounded to extract gold before been pumped into the dam.

During site investigation, dust pollution was observed whenever there is strong wind. This could also be a major way in which metallic contaminants and radioactive elements are transported.

A view from the top of the tailing dam visibly showed a whitish coloration (Plate 1), which moved away from the tailing dam through the base to its nearest environment, which is because of, salts (susceptibly gypsum dominated), deposited along the seepage pathway.

Load of sand suspected to be gypsum leached downward from the top of the tailings dam surface from the base of the dam

Plate 1: The base of the tailing dam sampled.

On the side of the tailings dam lays the erosion pathway made by leaching caused by rainfall and surface oxidation from the top of the tailing dam downward (Plate 2).

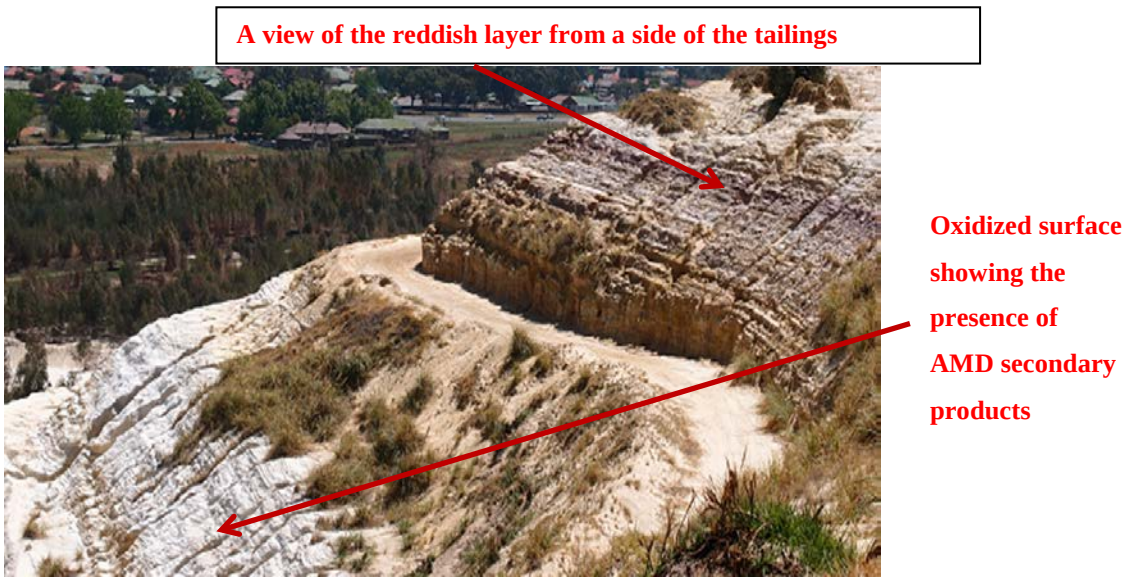

Plate 2: Side view of the tailing dam sampled displaying the effect of erosion

Plate 3: The eroded backside of the tailing displaying an overview of the tailing dam sampled and the drilling auger

5.2.2 Description of drilled hole T004

T004 hole was drilled through a depth of 10.2 meters (Figure 16) within the vegetated-covered part of the tailing dam. At the base of this hole was a dark grey–grey coloured fine tailings trend between 10.2 to 7.8m and was overlaid by reddish coloured fine tailings. This overlying layer was between 7.8m to 7.2m. Then follow by a grey layer in between 7.2m-4.6m with a very fine texture.

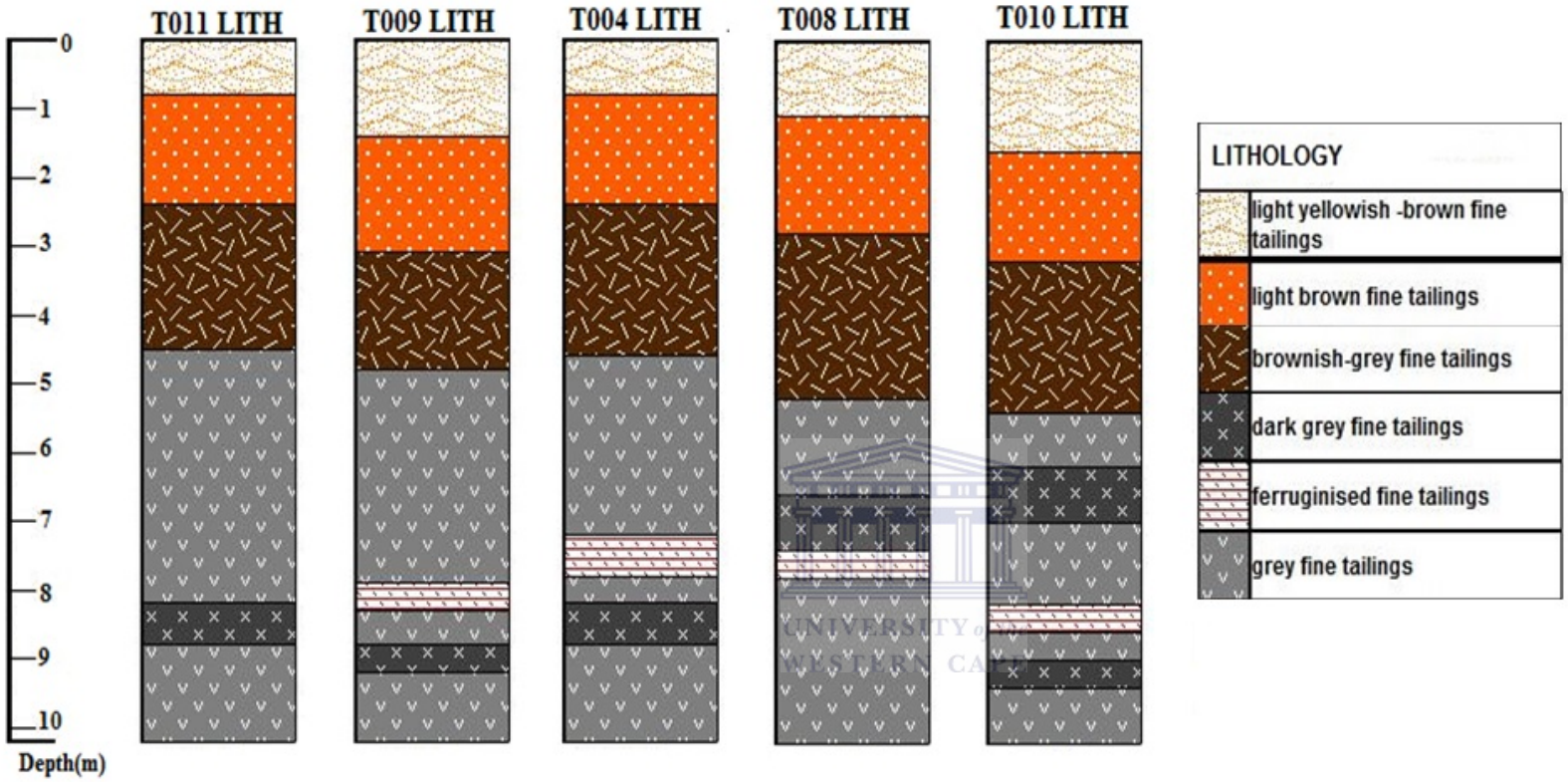

Figure 16: Description of the five drilled holes down depth

A brownish-grey layer overlaid the grey layer at a depth of 4.6m to 2.4m and from 2.4m to the surface of the tailings was variations in colouration showing a complete loss of grey colouration. Also from 2.4m to 0.8m, it becomes light brown fine tailings. After 0.8meter to top of the tailings, it changed to yellowish brown fine tailings. This layer is more sandy, coarse and loose.

5.2.3 Description of borehole T011

T011 was drilled through a non-vegetated covered part of the tailing dam. From the base of the tailings dam, 10.2m to 4.5m, the tailings were greyish and high moisture content (Figure 16).In between the grey coloured layer is a moist dark grey layer (8.2-8.8m). At depth 4.5m-2.4m, it becomes brownish grey. The moisture content increases (the moisture content increases with depth). This is the only drilled hole that does not have the reddish layer. The light brown tailings layer overlaid the brownish grey layer from 2.4m to 0.8m. It eventually changed to yellowish brown up to the surface of the drilled hole.

5.2.4 Description of borehole T009

T009 was drilled through the vegetation-covered surface of the tailings dam to a 10.2m depth. From 10.2m to 8.3m (Figure 16), the layer observed contained greyish fine tailings of increased moisture content. The reddish tailings layer overlaid the grey layer between 8.3-8.0m. Tailings from this layer were moist and fine. From the depth of 8.0m to 4.8m, the colour change to grey with variation in its moisture content. The lower part was moist. On top of the grey tailings layer lies the brownish grey found between 4.8 to 3.1m. From 3.1m to 1.4m, the tailings colour changes to light brown. After 1.4m to the surface, it changes to brownish yellow. This contained some whitish material at the surface and the tailings in this layer were more coarse.

5.2.5 Description of borehole T008

T008 was drilled through the vegetation-covered surface of the tailing dam to a depth of 10.2m. From 10.2m to 7.6m (Figure 16), the layer observed contained moist grey fine tailings. Just below this layer lies the reddish tailings layer between 7.6m -7.4m. From 7.4m to 5.2m, the tailings colouration changes to dark grey. The layer varies from dark grey- grey tailings. It changed to grey at 6.6m depth. It was moist between 6m- 7m. From 5.2m to a depth of 2.8m, the tailings changes to brownish grey Just after brownish grey layer lies the

light brown tailings layer between 2.8m to 1.1m. From 1.1m to the surface, it changes to more coarse yellowish brown tailings.

5.2.6 Description of borehole T010

T010 was drilled to a depth of 10.2m at the backside of the tailing dam closed to the Manganese mill or mine (Plate 3). The surface area was devoid of vegetation and lower elevation than the other hole drilled. It was also along the leaching pathway, with a flat surface of about 50m in length. From observation, the layer is exposed to erosion, and eroded materials will be deposited along this layer and washed away from time to time.

From the bottom layer 10 to 8.6m (Figure 16), grey coloured fine tailings were observed. Between 8.3 to 8.6m, the red tailings layer overlaid the grey tailings layer. From 8.3 to 4.3m, the fine-grained tailings changes to grey (from 6m to 7m, the tailings were moist and dark grey). From 5.2m to 2.5m, the greyish colour changed to brownish grey colour fine tailings. From 2.5m-1.4m, it changes to light brown colour material and from 1.4m to surface of the hole, the tailing colour changes to brownish yellow.

5.2.7 Overall setting of the tailing dam layers

Generally, the tailings are very fine material with high clay content. The five holes drilled (T004, T008, T009, T010, and T011) can be summarised in four distinct layers.

Layer 1 is described as whitish yellow–yellowish brown–light brown colouration. The thickness of this layer ranges from 0m to a maximum depth of 3.2m.

Layer 2 is described by its brownish grey coloured tailings. It ranges in thickness from 2.4m to 5.2m.

Layer 3 is described by its reddish colouration and it is only found in all boreholes except T011 and in-between layer 4. From observation, this red layer thin out from the centre of the tailing towards the side of the tailing dam. It ranges between 7.2-8.6m.

Layer 4 is described by a grey to dark grey colouration. It ranges between 4.5m to 10m. The greyish tailings indicate its initial composition on deposition through pipes into the built tailing dam.

There is much more increase in the retention capacity of tailings compared to waste rock, because of the increase content of clayey mineral. This accounted for increased moisture

content in the tailings dam sampled from 4m downward. This is peculiar to depth btw 3m to 7m and after 9m downward. It might be because of this layers acting as water canopy. In addition, the topmost layers for all boreholes are looser, compared to other depth. Therefore, the loose layer 1m to 3m will allow water to drain out easily, since it not more compacted compared to samples in other layers and it initial composition has been altered due to oxidation. It will not be surprising if the silica oxide in the first 3metres is higher. Colour changes are observed in variation from surface to 4m or 5m in boreholes, afterwards changes to grey.

5.3 Mineralogy of the tailing dam layers

From the five holes drilled with the use of a hand auger to a depth of 10meters measured constantly (as auger moved down) with a strong metallic meter rule. The holes are T004, T008, T009, T010, and T011. The abundance of minerals in the XRD spectral diagram was estimated based on the addition of all the peak counts in percentage wise of a specific mineral. The minerals detected by the XRD results are quartz, pyrophyllite, muscovite, gypsum, delhayellite, clinochlore, pyrite, hematite and jarosite in variable proportion (Figure 18). These minerals can be grouped into major, minor and trace minerals the peaks present. The major minerals are quartz, pyrophyllite, muscovite, and clinochlore, minor minerals are pyrite, delhayellite while trace minerals are gypsum, hematite, jarosite. The four distinctive layers can be classified as, the oxidised zone, un-oxidised and transition zone, and the red layer.

The tailings are predominately quartz and have increased amount of pyrophyllite. Quartz is a primary mineral and since it is not easily weathered, this account for slight variation, which could be because of the total compositional value of other minerals found in the tailings.

Despite the fact that quartz remained the principal gangue material from gold ore and conglomerate after gold extraction has been done. Its high resistance to weathering is responsible for its relative abundance compared to relatively easily-weathered minerals.

The next abundant mineral phase is pyrophyllite ($Al_2Si_4O_{10}(OH)_2$) accompanied with other primary mineral phases found within the tailings such as muscovite ($KAl_3Si_3O_{10}(OH)_2$), clinochlor ($Mg_5Al(Si,Al)_4O_{10}(OH)_8$), and delhayellite? ($(K,Na)_{10}Ca_5Al_6Si_{32}O_{80}Cl_6 \bullet 18H_2O$). Muscovite is a mica and primary mineral that is associated to the Witwatersrand basin deposit.

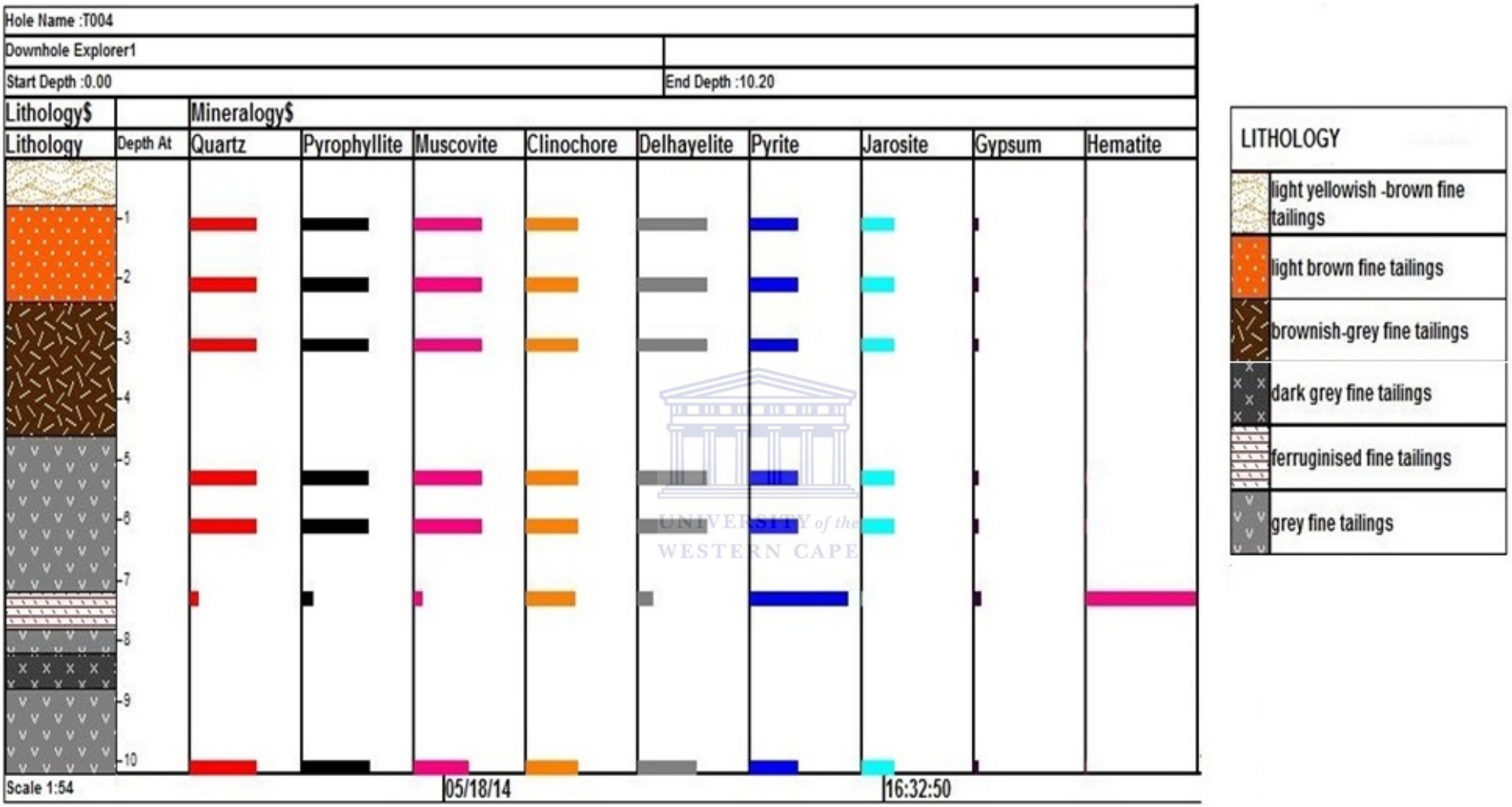

Figure 17 :Downhole distribution of minerals in hole T004

Pyrophyllite is a metamorphic clay mineral that mostly occurs in phyllites and slate in the absence of albite and potassium feldspar and a common mineral associated with hydrothermal alteration assemblages, which is a characteristic of the formation of the Witwatersrand basin.

The presence of hematite is responsible for the red colour of the sample. It is usually found in an oxidizing environment and might have been deposited since the tailing dam was deposited (settled down to form a specific layer). This is suspected to be a clay-sized hematite crystal.

The presence of delhayellite has never been reported observed in any mineralogical assessment of the Witwatersrand gold ore and tailings, except for this study and remains questionable. This mineral might have been negligible in the initial mineralogy of gold deposit in the Witwatersrand.

Gypsum is a secondary product of AMD, and could also be responsible for the neutralization with sulphuric acid generated. Its presence is more prominent on surfaced samples than beneath. The tailing dam contained buffer elements but not enough to neutralise potential acid generated. However, most of the tailings sampled in Witwatersrand have higher AP than NP, which is not enough to prevent oxidation process.

Generally, the layers in the borehole are characterized by its whitish yellow – brownish yellow –light brown- brownish grey- grey colour trend.

The legend for the mineralogy chart is depicted as follows: D- Delhayelite – ($(K,Na)_{10}Ca_5Al_6Si_{32}O_{80}Cl_6 \cdot 18H_2O$); M- Muscovite – ($KAl_3Si_3O_{10}(OH)_2$); G- Gypsum,syn – ($CaSO_4 \cdot 2H_2O$); C- Clinochlore-1MIIb-4 - $Mg_5Al(Si,Al)_4O_{10}(OH)_8$; P- Pyrophyllite-2M - $Al_2Si_4O_{10}(OH)_2$; Q- Quartz, syn - SiO_2; py- Pyrite - FeS_2; H- Hematite, syn - Fe_2O_3; J- Jarosite, hydronian syn –($(K,H_3O)Fe_3(SO_4)_2(OH)_6$

5.3.1 Mineralogical description of Layer 1

Layer 1 has a general mineral composition of quartz, pyrophyllite, muscovite, gypsum, delhayellite, clinochlore, pyrite and jarosite (Figure 18). The thickness of this layer is from 0m to 3.2m. The whitish yellow – yellowish brown –light brown layer summarises the layer as shown in Figure 17. This is based on the percentage peak analysis and not in 100 percentages. In this layer, quartz is the most prominent mineral and ranges from 50%-54.51%. Samples from the first meter have lower percentage of quartz. Though pyrophyllite

is a primary mineral, it ranges from 4.17% 4.55%. Except from samples 001 and 002 that has no pyrite, others have considerable amount that ranges from 0.97% to 1.06%. Samples 021, 021-1, 029, 030,032, 038, 038-1,039-1 have the same the percentage peak for quartz, pyrophyllite, clinochlore, muscovite, gypsum, delhayellite and pyrite. Sample 001 and 020 has similar minerals peak analysis, except that sample 020 has 0.97% of pyrite. The layer has low gypsum except for sample 010 with 1.74% signaling more of the whitish material in the tailing mixture. This layer varies in constituent away from the dam, and this might be the pathway of transport of materials within the tailings. This layer can be classified as the oxidised zone.

Plate 4: Tailings sample of the yellowish brown layer

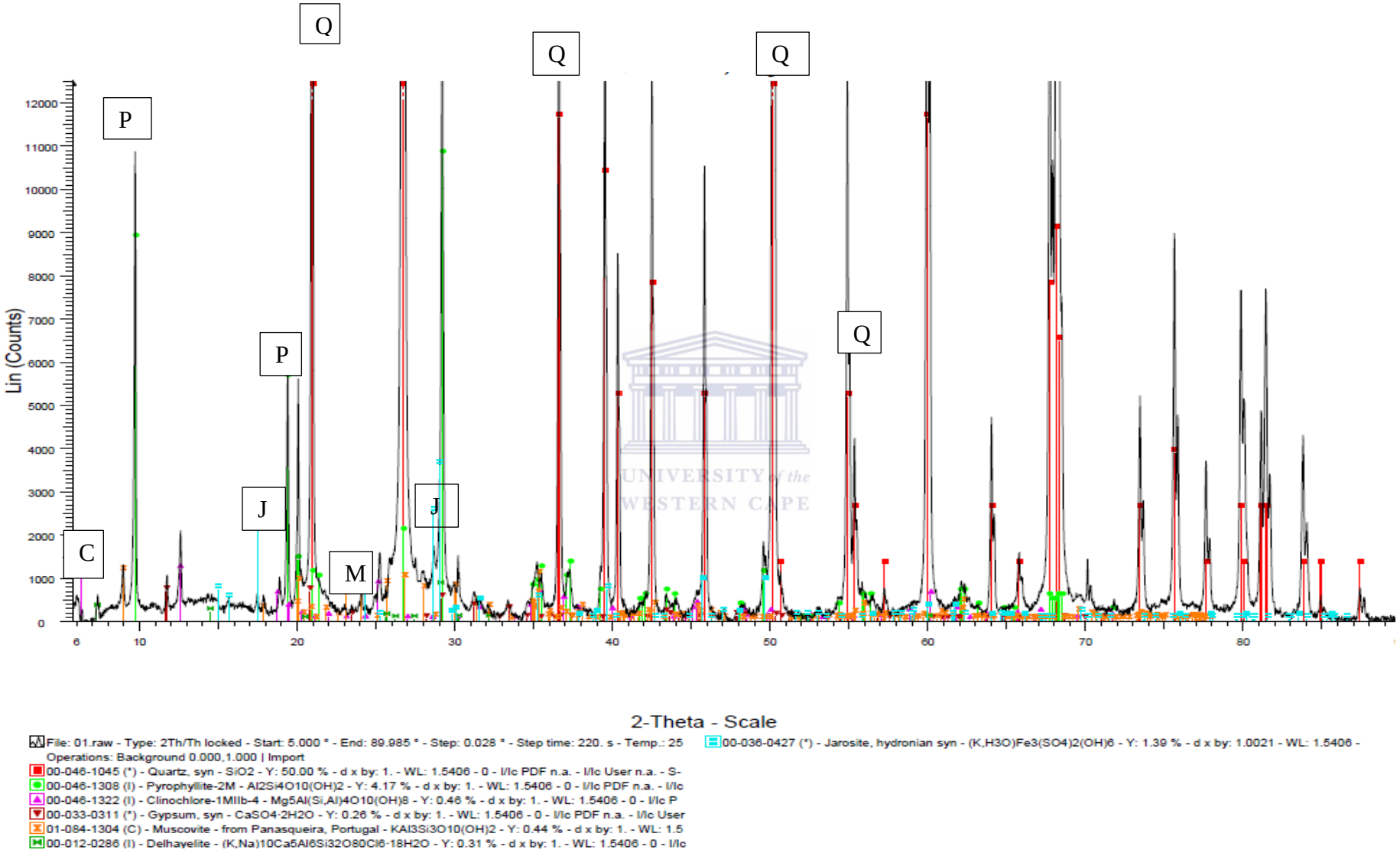

Figure 18: The mineralogical results of sample 001 typical of layer 1

5.3.2 Mineralogical composition of layer 2

Layer 2 is characterized by its brownish grey coloured tailings. It ranges in thickness from 2.4m to 5.2m. It has a general mineral composition of quartz, pyrophyllite, muscovite, gypsum, delhayellite, clinochlore, pyrite and jarosite (Figure 19). Q (54.56%), Pyro(4.55%), Cli(0.50%), Mus(0.48%), Gyp(0.22%), Del(0.34%), Py(1.06%), Ja(0.44%). This layer is more compacted compared to the layer 1. Though very fine sand materials are found, it looks more clayey.

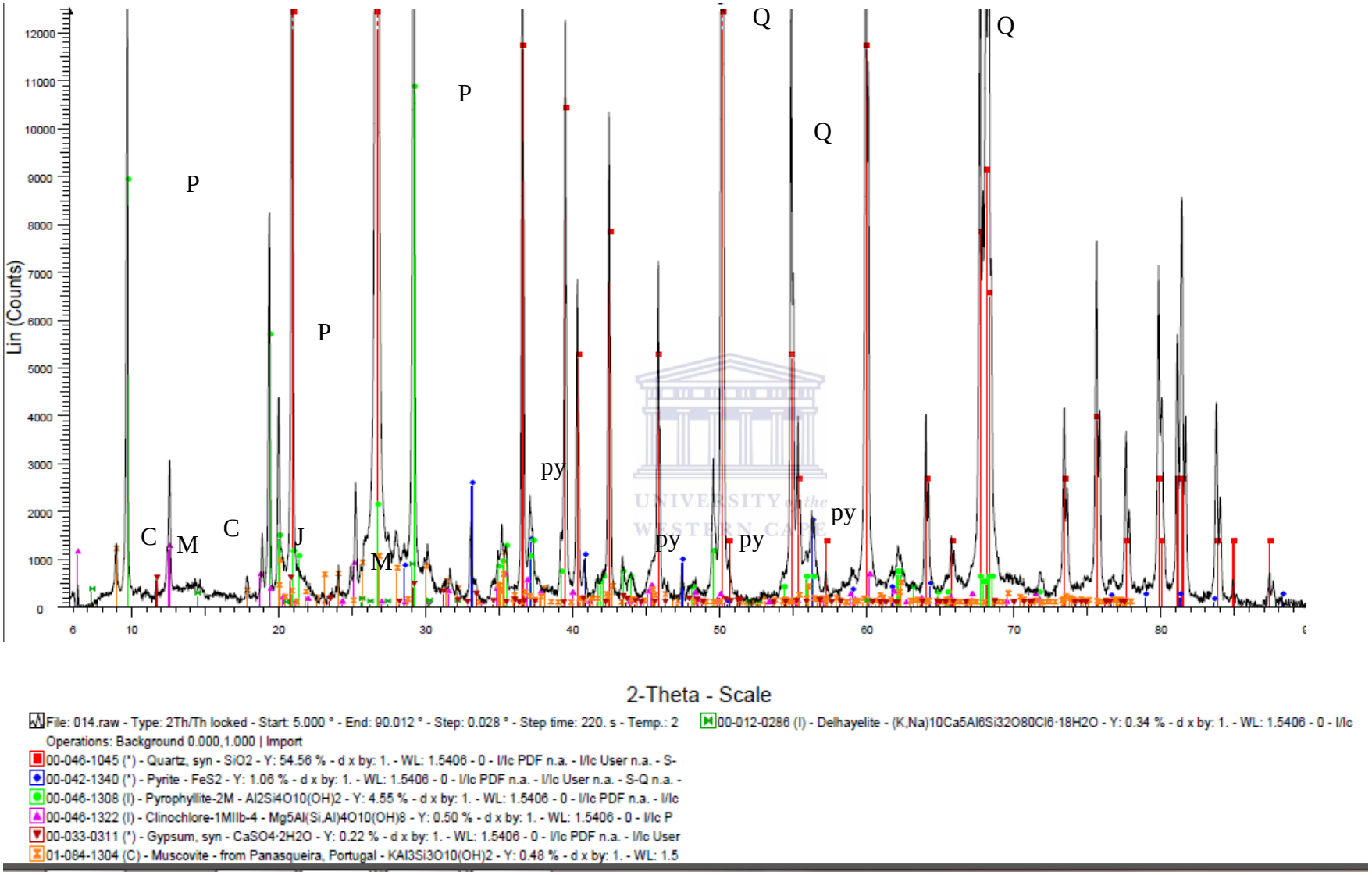

Figure 19: The mineralogical results of sample 021-1 typical of layer 2

5.3.3 Mineralogical composition of layer 3

Layer 3 is the only layer that has a unique mineral composition, which is 50% of quartz, 4.17% of pyrophyllite, 0.48% of muscovite, 0.22% of gypsum, 0.34% of delhayellite, 0.46% of clinochlore, 2.12% of pyrite and 2.08% of hematite in terms of the wavelength count (Figure 20). This is the only layer that does not have jarosite in its composition and has the highest value in pyrite. This shows that the layer is the most preserved since the presence of hematite could inhibit the easy generation of acidic solution from metallic sulphides for a little longer. This layer can also serve has an indicator for acid generation because from laboratory observation, the outer surface of the reddish layer changes after a while to brown on exposure. This layer is found between 7.2m to 8.6m in boreholes (all combined) except T011. Borehole T004 has the largest thickness from 7.2m to 7.8m, T008 is from 7.4m to 7.6m, T009 is from 8.0m to 8.3m and T010 is from 8.3m to 8.6m. This layer 3 is brick red in colour (Plate 5) and shows high iron content than other layers because of the presence of pyrite and hematite (both accumulating a 4.2% peak value. The hematite mineral accounts for the presence of the red colouration and mostly found in an oxidizing environment.

Plate 5: Tailings sample from the reddish layer

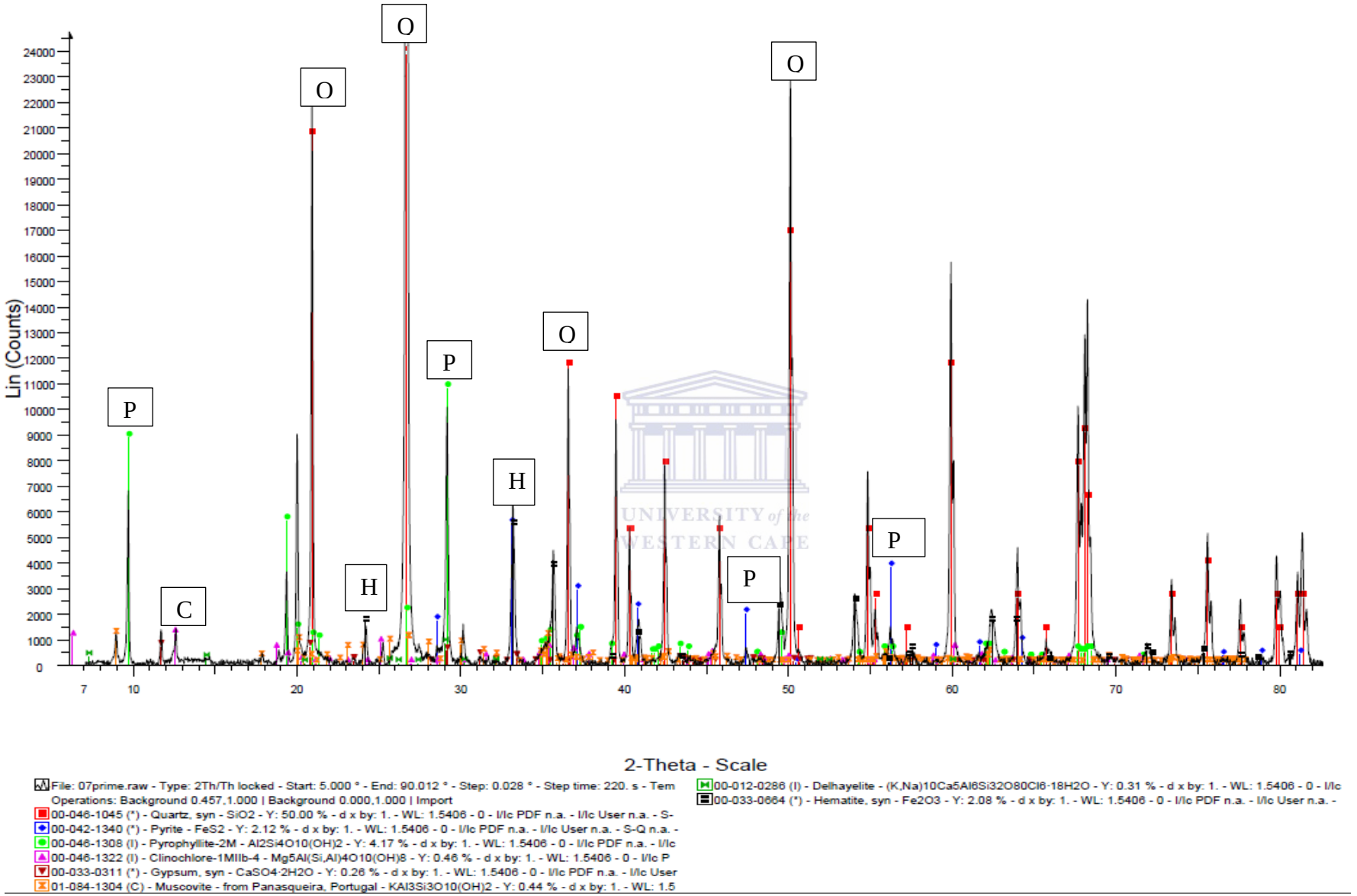

Figure 20: The mineralogical results of sample 027 prime typical of layer 3

5.3.4 Mineralogical composition of layer 4

Layer 4 is found in between layer 2 and 3 and after layer 3. This classified into a specific layer because of its similarity in colour, texture, and mineralogical composition. This layer is characterized by its grey to dark grey colouration (Plate 6&7). The moisture content in this layer is more than every other layer. Layer 4 has a general mineral composition of quartz, pyrophyllite, muscovite, gypsum, delhayellite, clinochlore, pyrite and jarosite(Figure 21). It is found between 3.8 to 10m in T004, 4.5m to 10m in T011, 4.8m to 10m in T009, 5.2m to 10m in T008, and 4.3m to 10m in T010 respectively. This layer has the tendency to easily be oxidized, but presently remain un-oxidized because of not been exposed to precipitation and oxygen.

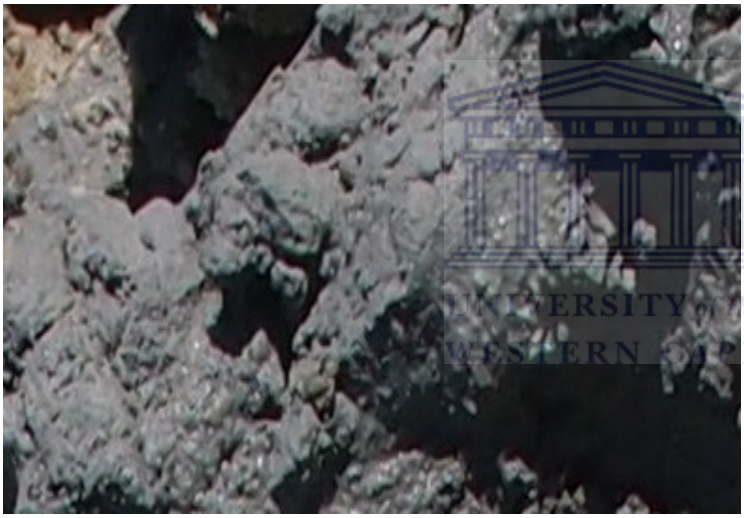

Plate 6: Sample of tailings from the grey layer (some parts are darker)

Plate 7: Sample of tailings from the grey layer

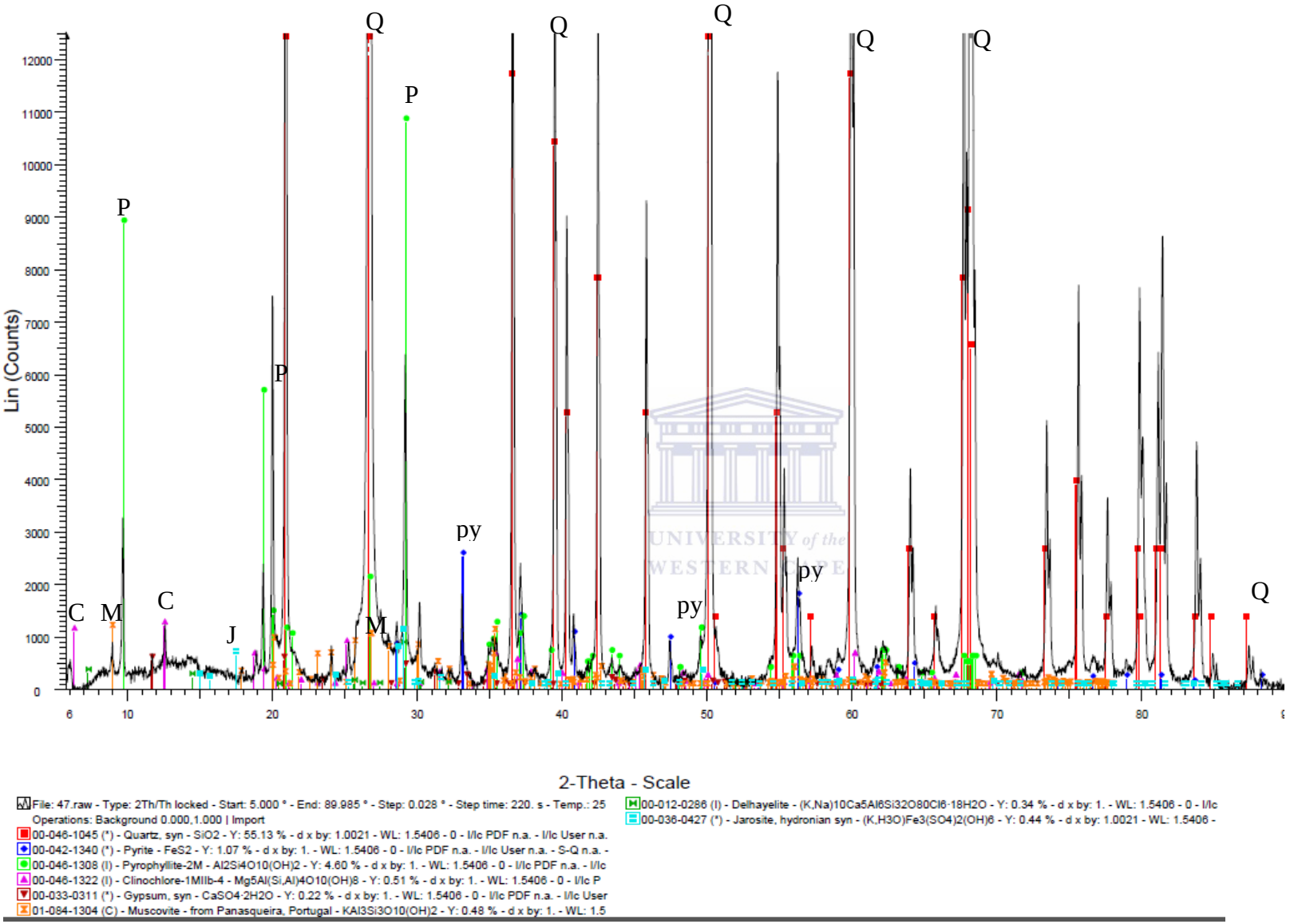

Figure 21: The mineralogy result of sample 047 typical of layer

5.3.5 Summary of XRD results

From these results, quartz, Muscovite, pyropyllite, gypsum, jarosite, delhayelite, hematite and clinochore are present but vary in each sample. The results affirm the presence of quartz in abundance in every sample's result followed by pyropyllite. Quartz, pyrophlite, delhayelite, muscovite and clinochlore and primary minerals, gypsum, jarosite are secondary minerals related to pyrite. Primary quartz in rocks is unchanged and highly stable.

The presence of pyrite shows the acid potential of the tailing dam. It was observed that jarosite is dominant only in samples on or closely beneath the tailing surface where there is no pyrite. As we move down the tailings, pyrite surfaced (transition) and at a depth of an average 5m below, it became prominent (un-oxidized). The reddish samples contain hematite, which accounted for their coloration and can be easily oxidized. Thus, hematite was discovered as the cause of reddish layer found around 7.2m to 8.6m and does not represent oxidation but rather has been deposited from the onset formation of the tailing dam showing the richness of the tailing dam in iron and its associated elements.

In addition, most of the samples contain gypsum, a secondary mineral responsible for the neutralization with sulphuric acid generated. Its presence is more prominent on surfaced samples than beneath. The tailing dam contained buffer elements but not enough to neutralise potential acid generated. However, most of the tailings sampled in Witwatersrand have higher AP than NP and this is not enough to prevent oxidation process.

Gypsum was found throughout the sample but was more profound in the first 2 to 3 meters. Delhayellite can be traced to have been present since the start of the tailing dam and because of its unreactive nature but has never be reported. MT007-1, MT017, MT027-1 and MT044 samples are described by their reddish colour indicating the presence of hematite and this might accounted for the high value for Fe_2O_3 and decreased value for SiO_2 in the geochemical data since quartz.

CHAPTER 6: Geochemistry

6.0 Introduction

The knowledge of geochemistry of mine wastes remains an integral part AMD studies. Based on petrographic studies in chapter 5, the tailings dam lithology can be subdivided into four distinct layers. The whitish yellow – yellowish brown –light brown trend described layer 1 therefore, termed as the oxidised zone. Layer 2 is characterized by its brownish grey coloured tailings, which indicates a transition zone. Layer 3 is characterised by the reddish colouration. Layer 4 is characterised by grey to dark grey colouration. The greyish tailings represent its initial composition on deposition, thus, regarded as the least weathered zone (Bezuidenhout & Rousseau, 2006).

In this study, 51 samples were analysed for 34 elements (including major oxides) from 5 drilled holes in Mogale's tailings dam (site description in chapter 5, section 5.2) namely T004, T008, T009, T010, and T011. The whole analytical data are presented in Appendix A

The knowledge of tailings geochemistry is important in determining the potential threat posed on the geo-ecosystems. The tailings could host a high level of toxic elements concentration, which also may be of economic value. Therefore, geochemical analysis is normally implemented in researches on mine wastes to determine their current and potential long-term effects on the ecosystem and the economy. In this regards, some of the objectives of this study, in this chapter, are as follows:

- To evaluate the tailings geochemical composition to determine the extent of oxidation and link between each zones (oxidized, transition and un-oxidized).
- To use multivariate statistical analysis tool assess the potential leachable heavy metals loads and the risk of heavy metals load present in the tailings dam, its associations and inter-relationships.
- To map the distribution pattern of elements using GIS spatial interpolation and geochemical mass balance
- To predict the possible source of AMD pollution loads, temporal AMD load from the tailing dam sampled and its effect on the environment using a geochemical mass balance and other prediction techniques.

In achieving the objectives stated above, a specific approach was followed and described below:

Data Summary: This gives a general overview of all geochemical dataset in terms of magnitude, range and other descriptive analysis (such as minimum, maximum, mean, median, and standard deviation) as shown in Table X. This assisted in comparing datasets, to summarise the results obtained and eased subsequent interpretation (Khalil, et al., 2013).

Inter-relationships: This underpins on the interrelationship between major oxides and other elements in respect to their concentration in the tailing dam with the use of multivariate statistics. It shows how each element varies (its distribution) down hole and the association found within elements. To determine this relationship, the correlation coefficient analysis was done. The relationship results are shown in Tables 6-7 and Figure 4 to 15.

Element Association: This aspect focuses on the distribution of elements within layers, and the characteristics of its compositional variation within each layer. This assisted in determining the properties of each layer and highlighting the possible factors responsible for the variation within each layer. The multivariate statistical analysis (cluster analysis and Factor Analysis) as shown in Table 8-11 and the effect of total sulphur present highlight relationships and association (Figure 24-25).

Modelling: The use of Geochemical Mass Balance for prediction and GIS for spatial distribution model of elements based on the factor analysis were employed. It determined the alteration of elements (with time) within layers, which relates the gains and losses of elements in relation to its geochemistry and created the distribution model of elements based on the statistical results. This helped in predicting the loads of AMD generated.

6.1 Data Summary

The summary of the geochemical data gives a general overview of what to expect and how the data is distributed. The use of descriptive statistics such as mean, range and standard deviation was employed in this study. The mean of a dataset is a basic statistical parameter, which was calculated as arithmetic mean (A.mean), and geometric mean (G.mean) (Yang, et al., 2011).

In this study, the geometric mean was used because of the high content of some elements plus the fact that the dataset and the dataset are not normally distributed. The standard deviation gives the degree of dispersion or variation distribution (Yang, et al., 2011). Table 5 presents the arithmetic and geometric mean, range and standard deviation of elements contents in the layers and the entire dataset.

Table 5: The summary of the geometric mean, arithmetic mean, standard deviation and range for the entire geochemical data, and its corresponding layers respectively as described by the petrographic studies.

	Entire Analysed Data					Oxidised layer		Transition layer		Reddish layer		Un-oxidised layer	
Variables	Min	Max	G.Mean	A.Mean	Std. D	Std. D	G.Mean	Std. D	G.Mean	Std. D	G.Mean	Std. D	G.Mean
MajorElements													
LOI	1.72	7.26	3.28	3.44	1.12	0.92	2.82	1.06	3.37	0.65	4	1.27	3.36
SiO_2	70.7	90.3	84.24	84.34	4.11	2.17	87.32	2.57	84.48	4.09	76.39	3.81	84.09
Al_2O_3	3.06	9.85	6.25	6.45	1.6	1.32	5.43	1.64	6.35	1.75	6.56	1.63	6.57
Fe_2O_3	0.86	9.31	2.64	3.03	1.93	0.66	1.75	0.59	2.64	0.22	9.03	0.79	2.6
CaO	0.06	2.75	0.43	0.52	0.44	0.25	0.34	0.18	0.41	0.53	0.74	0.57	0.44
MgO	0.09	0.86	0.35	0.4	0.18	0.19	0.25	0.22	0.41	0.1	0.45	0.16	0.37
Na_2O	0.02	0.28	0.07	0.09	0.06	0.06	0.06	0.07	0.07	0.04	0.09	0.06	0.08
K_2O	0.17	0.65	0.32	0.34	0.1	0.08	0.33	0.11	0.33	0.15	0.33	0.11	0.31
MnO	0.01	0.65	0.02	0.06	0.14	0.01	0.01	0.01	0.01	0.21	0.06	0.18	0.03
TiO_2	0.18	0.35	0.24	0.24	0.04	0.03	0.23	0.04	0.25	0.03	0.24	0.04	0.24
P_2O_5	0.01	0.05	0.02	0.03	0.01	0.01	0.02	0.01	0.02	0.01	0.03	0.01	0.03
Cr_2O_3	0.03	0.08	0.04	0.04	0.01	0.02	0.04	0.01	0.04	0.01	0.04	0.01	0.04
Leco A.													
TOT/C	0.01	0.22	0.05	0.07	0.05	0.06	0.04	0.04	0.05	0.1	0.1	0.05	0.05
TOT/S	0.26	2.19	1	1.14	0.51	0.29	0.48	0.38	1.13	0.18	1.52	0.46	1.23
Trace elements													
Ba	29	264	58.59	67.02	45.96	13.97	52.25	18.02	52.08	58.84	73.51	60.91	63.59
Co	0.9	125.9	23.99	38.06	29.36	8.85	4.71	17.19	27.09	16.36	105.74	20.11	37.7
Cs	0.3	3	1.04	1.13	0.52	0.28	0.87	0.34	0.98	0.97	1.37	0.56	1.12
Th	3.6	54.1	8.61	10.08	8.07	1.15	4.89	2.95	8.71	5.76	10.43	10.8	10.84
U	4	655.5	25.53	45.48	90.46	2.42	6.88	173.47	34.71	10.95	38.62	21.54	37.4
Zr	92.7	233.8	122.8	125.14	26.69	15.61	112.26	34.49	121.05	15.65	152.81	24.65	124.41
Mo	1.2	6.4	3.57	3.86	1.39	1.4	3.74	1.45	3.31	1.38	4.45	1.38	3.5
Cu	3.8	308.8	35.43	51.29	58.7	11.11	13.2	69.87	36.24	19.53	65.05	65.37	50.47
Pb	15.4	150.2	42.91	49.66	29.26	29.11	46.7	14.84	41.69	31.42	52.67	35.54	40.41
Zn	4	817	73.02	129.31	143.5	27.06	19.69	213.33	88.87	77.83	142.55	118.98	108.88
Ni	3.8	274.1	69.31	99.79	71.17	32.06	19.85	69.23	77.44	48.54	164.88	66.31	101.83
As	15.3	471.4	105.28	123.12	75.47	55.36	61.63	24.28	97.99	64.75	167.39	91.29	130.68
Au	58.1	1417.5	189.19	248.43	227.93	156.27	154.6	123.36	226.48	501.67	625.72	117.23	152.87
Sb	0.4	2.3	0.73	0.79	0.38	0.21	0.55	0.13	0.66	0.3	1.86	0.2	0.75
Bi	0.7	3.6	1.43	1.55	0.63	0.62	1.27	0.31	1.38	0.61	2.65	0.6	1.39
Hg	0.05	2.51	0.21	0.35	0.47	0.57	0.24	0.66	0.21	0.07	0.13	0.31	0.21
Static test													
Paste pH	2.61	8.69	4.28	4.5	1.52	0.97	3.85	1.57	4.2	1.87	3.82	1.62	4.64
EC (mS/cm)	0.43	3.99	1.09	1.27	0.79	0.82	0.92	1.01	1.15	0.59	1.79	0.64	1.06

6.1.1 Major elements

Major elements constitute the geochemical bulk composition of the tailings dam samples; it is paramount to understand the major elements distribution and their relative abundance. From the results in Table 5, the range of major elements results are LOI (1.72 – 7.26%), SiO_2 (70.7 – 90.3%), Al_2O_3(3.06 – 9.85%), Fe_2O_3 (0.86 -9.31%), CaO (0.06 – 2.75%), MgO (0.09 - 0.86%), Na_2O (0.02 – 0.28%), K_2O (0.17 – 0.65%), MnO (0.01 – 0.65%), TiO_2 (0.18 - 0.35%), P_2O_5 (0.01 – 0.05%), and Cr_2O_3 (0.025 – 0.084%).

Based on the geometric mean, SiO_2(84.24%), Al_2O_3(6.25%), Fe_2O_3(2.64%) and LOI(3.28%), in all samples accounted for about 97.05% of the whole sample concentration, while other major oxides are found in less concentration.

These major elements can be classified into four groups based on their geometric mean as described below.

Group 1 are oxides within contents >10%: Only SiO_2 (84.24%) falls in this group and are associated with high standard deviation (4.13) and this indicates a wide fluctuation in values for SiO_2 (70.7- 90.3%) in the samples. The high content in SiO_2 corresponds to the high content of quartz in the mineralogical results and corroborates with the general composition of Witwatersrand's tailings by (Rosner, 2000; Nengovhela, et al., 2006) of 70% to 90% of SiO_2, which contains the primary and secondary silica oxide.

Group II consists of oxides with contents between that falls within 1-10%: Al_2O_3 (6.25%), Fe_2O_3 (2.64%) and LOI (3.28%) falls into this group, despite having a peak value of 9.85%, 7.26%, 9.31% respectively and their standard deviation is greater than 1.

Group III are oxides and minor elements that fall within 0.1-1%. These oxides are CaO (0.43%), K_2O (0.32%), MgO (0.35%) and TiO_2 (0.24%). The standard deviation for every major elements in this group is <1

Group IV are minor elements with percentage concentration <0.1%: The group consist of Na_2O (0.07%), Cr_2O_3 (0.04%), MnO (0.02%), and P_2O_5 (0.02%). These elements show low standard deviation for every oxide, which is greater than 1.

The four distinct layers show variation in contents and are described below as shown in table 5 as follows.

The oxidised layer (layer 1) contains the highest average content of SiO_2 (87.32%), coupled with the lowest in Al_2O_3 (5.43%), LOI (2.82%), Fe_2O_3 (1.75%), CaO (0.34%), and MgO (0.25%) content when compared to other layers. Therefore, the oxidised layer shows enrichment in SiO_2 and a low content in other major oxides and LOI.

The transition layer shows a considerable high percentage concentration in SiO_2, which is second only to the oxidised layer. Also, it has the highest value in TiO_2 (0.25%) and is also has lower content (second only to the oxidised layer) in Al_2O_3 (6.35%),CaO(0.41%), MgO (0.41%), K_2O(0.07%) as compared to other layers. In this layer, only LOI (1.06), SiO_2 (2.57) and Al_2O_3 (1.64) have standard deviation greater than 1.

Layer 3 is a ferruginised layer (brick red layer) due to the presence of hematite and shows the lowest contents of SiO_2 (76.39%), and is most enriched in Fe_2O_3 (9.03%), CaO (0.74%), LOI (4.09%), MgO (0.45%), Na_2O (0.09%). It is also second to the un-oxidised layer in terms of Al_2O_3 grade (6.56%). The standard deviation for SiO_2 (4.09) and Al_2O_3 (1.75) is greater than 1.

The least altered layer shows lowest contents for SiO_2 (84.09%) as compared to the oxidised and transition layer. It is most enriched in Al_2O_3 (6.57%). The LOI (3.36%) is only greater than the content found in the oxidised layer.

6.1.2 Trace Element distribution and enrichment

In Table 5, a summary of the trace elements is displayed based on their minimum, maximum, geometric mean, arithmetic mean and standard deviation values for the entire dataset and tailing dam layers.

Also, the standard deviation and geometric mean values of trace elements in respect to the 4 distinct layers present while Appendix B showed the arithmetic mean, maximum and minimum values of trace elements for the individual drilled holes.

From the Appendix B, maximum concentration of Co, Pb, Zn, Ni, As, Sb, Bi is found in Drilled hole T008, maximum concentration of U and Hg is found in borehole T009, and maximum concentration of Mo and Cu is found in Drilled hole T010.

Drilled hole T010 has the lowest concentration in Co, U, Pb, Zn, Ni, Au, Bi. Also observed is that some trace elements such as As, Zn, Ni and Co have low concentration at the first two

meters. Drilled hole T004 has the minimum concentration in Zr, Cu while Th and As is found in lowest concentration in T011

6.1.2.1 Trace elements categories

Based on their geometric mean, the trace elements can be grouped into four groups in respect to their magnitude as shown in Table 5. Group 1 with trace element contents (>100ppm), group 2 (50-100ppm), group 3(10-50ppm), group 4(<10). Based on this, Zr, As and Au (though Au is in ppb but grouped for convenience) falls in group 1: Zn, Ba, Ni falls into group 2 while Co, U, Cu and Pb falls in group 3. Other remaining trace elements are Sb (0.73ppm), Bi, Cs, Hg, Th, and Mo fall into group 4.

In summary, the geometric mean for this trace elements above can be represented in terms of their relative abundance as Zr>As>Zn>Ni>Ba>Pb>Cu>U>Th>Mo>Bi>Cs>Sb>Hg(excluding Au). Noteworthy is that the maximum values for Zn, U, Cu, As, Ni, Au, and Ba are extremely high, but their geometric mean was low.

The standard deviation shows extremely high values in Au, As, Ni, Zn, Zr, Pb, Cu, Ba, and U indicating a wide variation and distribution of these trace elements in this tailings dam.

6.1.2.2 Distribution of trace element in layers

From table 5, the trace element concentration of each layer is described as follows:

The oxidised layer show the lowest content in Au(154.6ppb), Zr(112.26ppm), As(61.63ppm), Ni(19.85), Zn(19.69ppm), Cu(13.2ppm), U(6.88ppm), Th(4.89ppm), Co(4.71ppm), and highest concentration in Hg(0.24ppm). From a general point of view, most trace elements are depleted in concentration in this layer. The standard deviation for all trace elements in this layer except Sb (0.38 ppm), Bi (0.63 ppm) and Hg (0.47 ppm) is >1.

Based on the geometric mean, the transition layer trace element content is higher than the oxidised layer only for Zr(121.05 ppm), As(97.99 ppm), Zn(88.87 ppm), Ni(77.44 ppm), Pb(41.69 ppm), Cu(36.24 ppm), U(34.71 ppm), Co(27.09 ppm), Th(8.71 ppm), Bi(1.38 ppm), Cs(0.98 ppm) and Sb(0.66 ppm). The layer is the least enriched in Ba(53.08 ppm) and Mo(3.31ppm).

The ferruginised layer contain highest content in Au(625.72), As(167.36ppm), Ni(164.88 ppm), Zr (152.81 ppm), Zn(142.55 ppm), Co(105.74 ppm), Ba(73.51 ppm), Pb(52.67 ppm), Cu(38.62 ppm), U(38.62 ppm), Th(10.43 ppm), Mo(4.45 ppm), Cs(1.37 ppm).

The least altered layer is second only to the reddish layer in enrichment of Au(152.87 ppb), As(130.68 ppm), Zr (124.41 ppm), Zn(108.88 ppm), Ni(101.83 ppm), Ba(63.59 ppm), Cu(50.47 ppm), Co(37.7 ppm), U (37.4 ppm), Mo(3.5 ppm), Bi(1.39 ppm),Sb(0.75 ppm).

This layer is most enriched in Th (10.84 ppm). Comparatively, most chalcophiles except Pb and Mo show increasing value from the oxidised layer to the least oxidised layer.

6.1.2.3 Distribution of some selected trace elements

From the whole dataset in Appendix B and in relation to Table 5, the trace elements discussed below was considered because of its high mobility and association with sulphide containing minerals, acid mine drainage, and can pose great environmental risk.

- **Molybdenum (Mo)**

Mo has been a major chalcophile of concern if found above found in concentrations above the permissible level. Layer 1 has a considerably low concentration with an increasing trend as it approaches Layer 2. Every other layer has a considerably high value of Mo. There is no specific trend of Mo concentration across the layers.

- **Cobalt (Co)**

The concentration of Cobalt in T004, T008, T009, T010,and T011 ranges from 7-89.7ppm, 2.9-97.1ppm, 4.4- 114ppm, 0.9-125.9ppm, and 10.5-37.9ppm respectively.

The concentration of Co found in layer 1 is generally low, and T010 has the lowest concentration of 7ppm. The depletion of cobalt in the first layers might be because of leaching or oxidation effects.

From layer 1, the content of Co increases in layer 2 (T011 generally has low value in Co). In layer 2, T010 still have depleted concentration of Co, while other boreholes have an increased concentration (increasing down hole). In boreholes T004, T008, T009 and T010, layer 3 shows the highest enrichment in Co of 125.9, 97.1, 114, and 89.7ppm respectively, compared to all layers.

Generally, Layer 4 has a considerably high concentration of Co. Overall; there is an increasing trend in the concentration of Co down hole. There is an increasing trend in concentration of Co down depth and the third layer contains the highest value Co.

- **Uranium (U)**

Uranium is a well-known radioactive element associated to the uraniferous gold tailings of the Witwatersrand. U concentration varies in layers from each borehole. It ranges from 7.3-57.6, 7-100.9, 6.8- 655.5, 4- 40, and 7.5- 106.5ppm in T004, T008, T009, T010, T011 respectively.

In all boreholes, a significant low concentration of U was found in the layer 1.This gradually increases down hole from layer 2 - layer 3- layer 4.

The highest concentration of U was found in the fifth meter of the borehole T009 of 655.5ppm indicating a highly concentrated zone of uranium. Uranium also has an approximately increasing trend down hole in all drilled holes. It might be has a result of its tendency to be mobile and leached in the upper zones.

- **Lead (Pb)**

There is no major enrichment or depletion trend for Pb from layer 1 to layer 4. The concentration of Pb ranges from 23.5-150.2, 24.8- 96.1, 17.9-51.9, 16.2-72.5, 15.4-83.2 ppm in T008, T009, T010, T011, and T004 respectively.
Therefore, Pb can be said to be evenly distributed in layers and does not show a specific trend. This might account for its stability.

- **Zinc (Zn)**

The concentration of zinc in boreholes shows a specific trend. It ranges from15-817, 24-538, 4- 136, 8-169, 14-346ppm in T008, T009, T010, T011, and T004 respectively. Except for T011, layer 1 shows a significant depletion in other borehole, which increases downward as it proceed into layer 2.

In T009, T004 and T010, Layer 2 still has a depleted concentration of Zn while other boreholes show a significant increase.

Generally, T010 has the lowest overall enrichment in Zn, except for its layer 3 that is characterised with 136ppm, while T008 has the maximum enrichment in Zn (with a maximum concentration of 817ppm found in the fifth meter).

Layer 3 and 4 have significant value of Zn but more prominent in the latter. T004 shows high value of Zn in layer 2 and 4 respectively and diminishes as it moves into layer 3.

- **Copper (Cu)**

Copper ranges from11.7-282.5, 21-55.5, 3.8- 308.8, 32.5-51, 16.9-52.1 ppm in drilled holes T008, T009, T010, T011, and T004 respectively.

It was observed in layer 1 of all drilled holes show relatively lower content of Cu with a similar trend to Zn.

In borehole T004, T010, T009, Cu increases downward in a linear trend, while T008 and T011 does not show a peculiar trend. In T010, Cu has a depleted concentration between layer 1 and layer 2 and increases from layer 3 to layer 4. In T011 and T009, the concentration of Cu could be said to be evenly distributed in all layers. In T010, layer 2 has a significantly high value of Cu of 306ppm.

- **Nickel (Ni)**

Nickel ranges from 11.2- 274.1, 9- 229.4, 3.8- 154.7, 35.7- 153.8, 16.6- 246.3 ppm in borehole T008, T009, T010, T011, and T004 respectively.

Just like Cu, it increases down hole. It is observed that in all boreholes, layer 1 has a low concentration of nickel except for the second meter in T011. This low concentration extends to layer 2 in T010, while it increases in other boreholes steadily.

Layer 3 in T008, T009, T010, T004 show optimum enrichment in Ni. Layer 4 shows an evenly distributed concentration of Ni in all boreholes.

- **Arsenic (As)**

Arsenic is known for its detrimental effect on the ecosystem and man. Generally, arsenic is significantly present in all layers. It ranges from 23.3-471.4, 61.5-192.7, 15.3-185.1, 47.8-118.4, 81.2-137.1 ppm in borehole T008, T009, T010, T011, and T004 respectively.

In all the boreholes, there is no specific linear trend except zigzag trend down hole. In layer 1, borehole T008 has a depleted concentration of As. T004 and T010 have an increasing trend of As in layer 1, while others have a considerably high concentration.

In layer 2, a similar concentration trend of As in T008, T004, and T010. In layer 3, As is found in substantially high concentration in borehole T004, T008, T009, and T010. In layer 4, As is present in a cumulatively high concentrations.

- **Gold (Au)**

Gold in the tailings are remnant of the gold extraction, because the extraction method used did not remove all the gold present. In the study, Au is analysed for in ppb as compared to other trace elements in ppm. It ranges from 84-1417.5, 84.2-532.9, 58.1-831.5, 63.5-576.5, and 125.9-403.9 ppb in drilled holes T008, T009, T010, T011, and T004 respectively.

Except for drilled hole T010, that has considerably lower amount of Au in layer 1 and layer 2. Other boreholes have considerably high concentration, which is mostly greater than 200ppb in layer 1 and layer 2.

It was observed in layer 3, which is the iron rich zone, has the highest concentration of Au in all boreholes except T011 (because layer 3 is not found in T011), thus showing its association with the ferruginised layer.

6.1.3 Distribution of Total Sulphur and Total Carbon within the geochemical data

The total percentage sulphur and carbon present in the tailing samples were determined by leco analysis, as described earlier in chapter 4 in section 4.4.4.

From the results in Table 5 above, the total percentage carbon which represents the total organic material present in the samples, and the values ranged from <0.02 to 0.22%.

In addition, the total percentage sulphur signifies the total percentage of sulphides present and the values ranged from 0.26 to 2.75% in all samples. The geometric mean for total sulphur and total carbon are 1.00% and 0.05% respectively. The oxidised layer shows the lowest value of total sulphur (0.48%) and carbon (0.04%). The contents of the total sulphur and total carbon in the transition layer are 1.13% and 0.05% respectively

The ferruginised layer has the highest value of total sulphur (1.52%) and total carbon (1%). The contents of the total sulphur and total carbon in the least altered layer are 1.23% and 0.05%. The relative abundance for the concentration of total sulphur in the layers is as follows: ferruginised layer (1.52%)> least altered layer (1.23%)> transition layer (1.13%) > oxidised layer (0.48%).

The relative abundance for the concentration of total carbon in the layers is as follows: ferruginised (0.1)> un-oxidized layer (0.05%) = transition layer (0.05%) > oxidised layer (0.04%).The standard deviation for both Total sulphur and carbon is less than one.

6.1.4 Paste pH and EC

From table 4, the paste pH and EC were done for 51 samples (spread over five boreholes) and their values ranged from 2.61 – 8.69 and 0.43 – 3.99 mS/cm respectively.

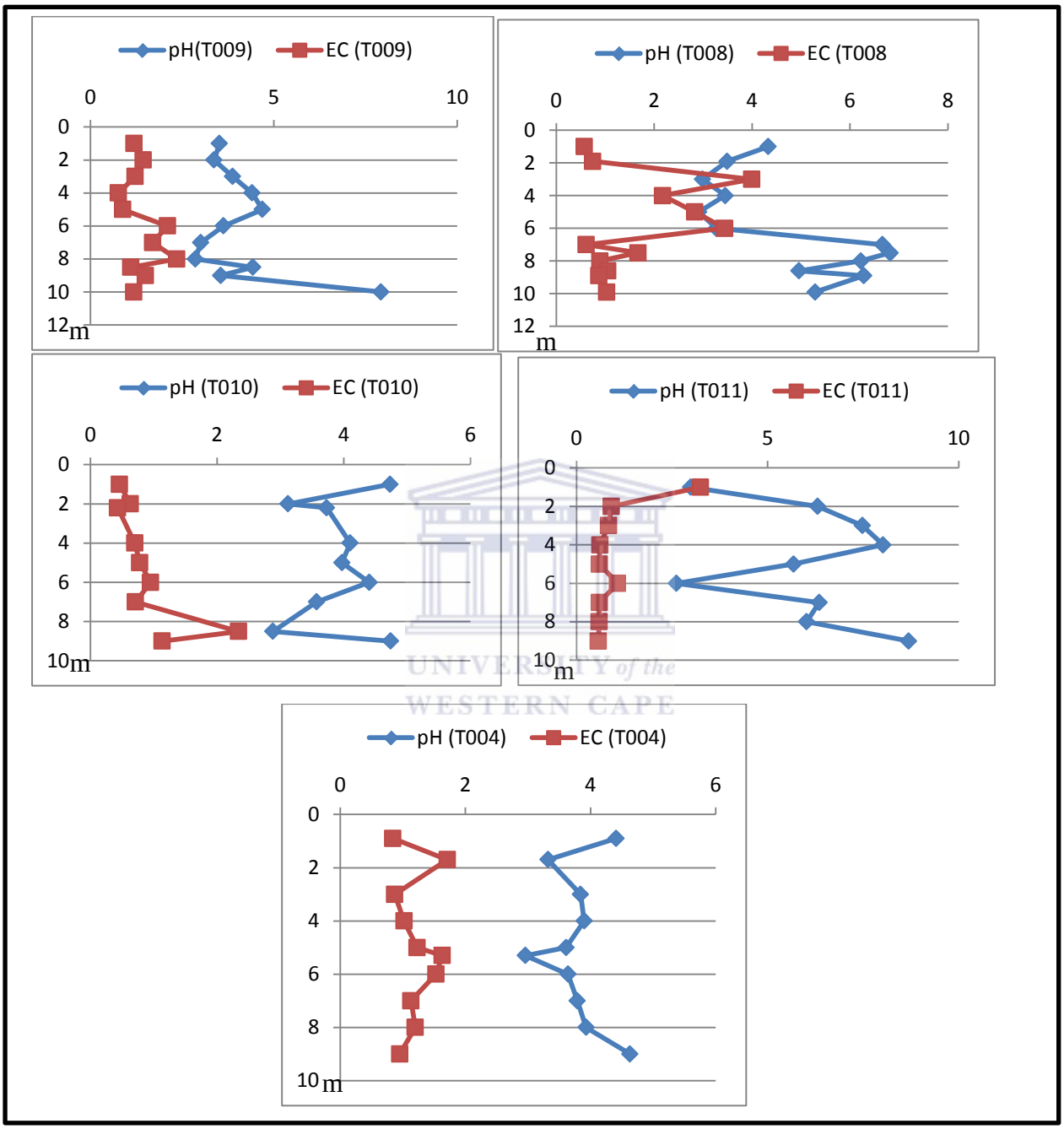

Figure 22: Graphical representation of the paste pH and EC distribution down hole for all the boreholes

The geometric mean for pH and EC was 4.28 and 1.09 mS/cm respectively. The general low pH indicates an acidic environment. The pH of the tailing dam shows these trends in layers on average: least altered layer (4.64) > transition layer (4.2) > oxidized layer (3.82) > ferruginised layer (3.85).

The EC of the tailing show this trend: ferruginised layer (1.79 mS/cm) >transition layer (1.15 mS/cm)> least altered layer (1.06 mS/cm) > oxidized layer (0.92 mS/cm). From Figure 22, as pH increases, EC decreases (vice-versa) because during oxidation process, as pH is lowered, ions (such as SO_4^{2-}) (Saria, et al., 2006)are generated, leading to the increase in the tailings electrical conductivity (EC). The first few meters show low pH and high EC, which is a characteristic peculiar to the presence of AMD. At depth between 6-8m, show increase in pH and lowering of EC indicating that oxidation process is slower.

6.2 Inter-relationship

6.2.1 Correlation Coefficient Analysis

Correlation coefficient analysis was done to establish elements interrelationship in within tailing dam. Pearson correlation coefficient of the major oxides, LOI (volatiles), Tot/S, Tot/C, Ba, Co, Cs, Th, U, Zr, Mo, Cu, Pb, Zn, Ag, Ni, As, Au, Cd, Bi, Hg, and Sb was done. The test of significance shows elements that are highly correlated. The significance level used and considered is r=0.01 which is flagged two tailed and significance level r=0.05 is one –tailed.

6.2.1.1 Correlation Coefficient of Major oxides

From the results as shown table 6 below, SiO_2 shows a negative correlation to all major oxides (except TiO_2 and Cr_2O_3) including LOI and Tot/S. Large percentage of SiO_2 is found in the tailings as quartz. SiO_2, though negatively correlated to all major elements, but is highly negative correlated to LOI, Fe_2O_3, CaO, MnO, P_2O_5. Al_2O_3, K_2O, Na_2O, P_2O_5 are positively correlated to one another.

Fe_2O_3 is slightly correlated to MgO but highly positive correlated with Tot/S and Tot/C. TiO_2 shows no correlation with no major elements showing that it has a different mineralised origin to other major elements. Tot/S is positively correlated with MnO, CaO, P_2O_5. LOI is positively correlated with Al_2O_3, CaO, MgO, MnO, P_2O_5, Tot/S and Tot/C and highest negative correlation with SiO_2.

6.2.1.2 Correlation Coefficient of selected heavy metals

From the Pearson correlation results (Table 7) of Ba, Co, Cs, Th, U, Zr, Mo, Cu, Pb, Zn, Ag, Ni, As, Au, Cd, Bi, Hg, Sb, TOT/C, TOT/S in the table below, notable correlation was observed. Mo is negatively correlated only with Zn and shows no correlation with other elements.

Table 6: Pearson Correlation Coefficient results for the Major Oxides including LOI, Tot/S and Tot/C

Correlations

	LOI	**SiO_2**	**Al_2O_3**	**Fe_2O_3**	**CaO**	**MgO**	**Na_2O**	**K_2O**	**MnO**	**TiO_2**	**P_2O_5**	**Cr_2O_3**	**TOT/C**	**TOT/S**
LOI	1													
SiO_2	**-.800****	1												
Al_2O_3	**.441****	**-.641****	1											
Fe_2O_3	.352*	**-.663****	.016	1										
CaO	**.692****	**-.674****	.285*	.275	1									
MgO	**.368****	**-.364****	.024	.314*	.173	1								
Na_2O	.209	**-.372****	**.712****	-.060	.169	-.280*	1							
K_2O	.275	**-.446****	**.791****	-.058	.202	-.052	**.781****	1						
MnO	**.576****	**-.592****	.227	.239	**.844****	.233	.134	.096	1					
TiO_2	.013	-.217	.327*	.019	.035	.128	.342*	.204	.182	1				
P_2O_5	**.590****	**-.612****	**.645****	.126	**.462****	.125	**.571****	**.527****	**.408****	.071	1			
Cr_2O_3	.171	-.138	.191	.042	.092	-.069	.350*	**.415****	.075	.076	.339*	1		
TOT/C	**.574****	**-.615****	.171	**.460****	**.652****	.278*	.056	.200	**.631****	.054	.352*	.309*	1	
TOT/S	**.552****	**-.532****	.035	**.530****	**.401****	**.413****	-.113	-.266	**.433****	.017	**.365****	-.136	.289*	1

****. Correlation is significant at the 0.01 level (2-tailed).**

***. Correlation is significant at the 0.05 level (2-tailed).**

Table 7: Pearson Correlation Coefficient results for the selected heavy metals including Tot/S and Tot/C

Correlations

	Ba	Co	Cs	Th	U	Zr	Mo	Cu	Pb	Zn	Ag	Ni	As	Au	Cd	Bi	Hg	Sb	TOT/C	TOT/S
Ba	1																			
Co	.334*	1																		
Cs	**.898****	.355*	1																	
Th	**.817****	**.409****	**.774****	1																
U	.035	.164	.082	.075	1															
Zr	.006	.279*	-.069	.044	-.039	1														
Mo	-.162	-.087	-.235	-.133	-.290*	.346*	1													
Cu	.092	.193	.144	.299*	.034	-.029	-.037	1												
Pb	**.657****	.219	**.617****	**.650****	.066	-.247	-.337*	-.035	1											
Zn	.249	**.553****	.312*	.275	.203	-.151	**-.374****	.049	.193	1										
Ag	**.777****	**.445****	**.743****	**.685****	.205	.095	-.125	.045	**.781****	.289	1									
Ni	**.368****	**.828****	**.398****	**.471****	.234	.050	-.324*	.163	.272	**.822****	**.443****	1								
As	**.765****	**.475****	**.729****	**.860****	.015	.182	-.121	.196	**.605****	.211	**.745****	**.425****	1							
Au	.115	**.458****	.264	.047	.019	.096	-.093	.088	.276*	.118	.368*	.295*	.201	1						
Cd	.128	-.015	.189	.119	-.024	-.160	.187	-.067	.112	.020	-.004	-.034	.049	.044	1					
Bi	**.398****	**.472****	**.513****	**.472****	.034	-.051	-.117	.001	**.736****	.137	**.666****	.320*	**.548****	**.557****	.075	1				
Hg	-.094	-.304*	-.182	-.120	-.166	.349*	.205	-.008	-.133	-.268	-.025	-.355*	-.057	.062	-.070	-.157	1			
Sb	.184	**.713****	.312*	.180	-.026	.277*	.065	.117	.127	.141	.364*	**.406****	**.381****	**.690****	.043	**.551****	-.028	1		
TOT/C	**.623****	**.486****	**.521****	**.430****	.013	-.004	-.144	-.028	**.486****	.296*	**.588****	**.400****	**.506****	**.412****	.201	**.449****	.035	**.516****	1	
TOT/S	.241	**.748****	.226	**.457****	.176	.350*	-.157	.265	.137	**.492****	.373*	**.750****	**.537****	.238	-.027	.279*	-.217	**.500****	.289*	1

***. Correlation is significant at the 0.05 level (2-tailed).**

****. Correlation is significant at the 0.01 level (2-tailed).**

U shows no correlation with any of the element and this is because it has it source from the radioactive elements within the initial ore before extraction.

Ba is positively correlated with Cs, Th, Pb, Ag, Ni, As, Bi and Tot/C indicating a related source. Co, Th, Zn, Ni, Ag, As, Au, Bi, Sb, Tot/C and Tot/C suggesting a similarity in their properties as related to Au and Tot/S.

Zn, Co, Th, Ni, As, and Sb show highly positive correlation with Tot/S, therefore, indicating the presence of their sulphides (except Th). They can also be traced to a mafic origin and are the seat of Acid mine drainage generation upon oxidation.

6.2.2 Clustering Analysis of the geochemical data

Clustering analysis is used to group the objects or units present in the analysis into categories (known as cluster) depending on their similarities, to find the best grouping for objects within each cluster in terms of similarity (Santos, et al., 2005; Alkarkhi, et al., 2009).

In this study, Hierarchical-clustering analysis was done to show a sequential cluster formation. Ward's method of clustering measured at an interval of squared Euclidean distance.

The most similar objects (samples) are initially considered, grouped and linked to one another, thus, depending on their similarities. As the similarities decreases, the objects or cases are finally grouped into a single cluster that has many clusters displayed as a tree diagram or dendrogram. HCA helps to identify the clusters of similar cases within the five boreholes sampled as shown in the Figure 23.

The dendrogram is presented in Figure 23, summarised in Table 9, and shows the distribution of samples into four clusters. Two main clusters were observed in which each cluster could be grouped into two sub-clusters each. The analysis was extracted based on SiO_2 (accounted 88.2% of original grouped cases correctly classified) and Al_2O_3 (accounted 49% of original grouped cases correctly classified).

Main Cluster 1 has cluster 1a and cluster 1b as sub-clusters indicating that they both have a generic composition. Main cluster 2 has sub cluster 2a and 2b showing a common or similar source. For SiO_2, main cluster 1 are samples rich in SiO_2 while main cluster 2 is characterised with depletion in SiO_2, defines the main clusters.

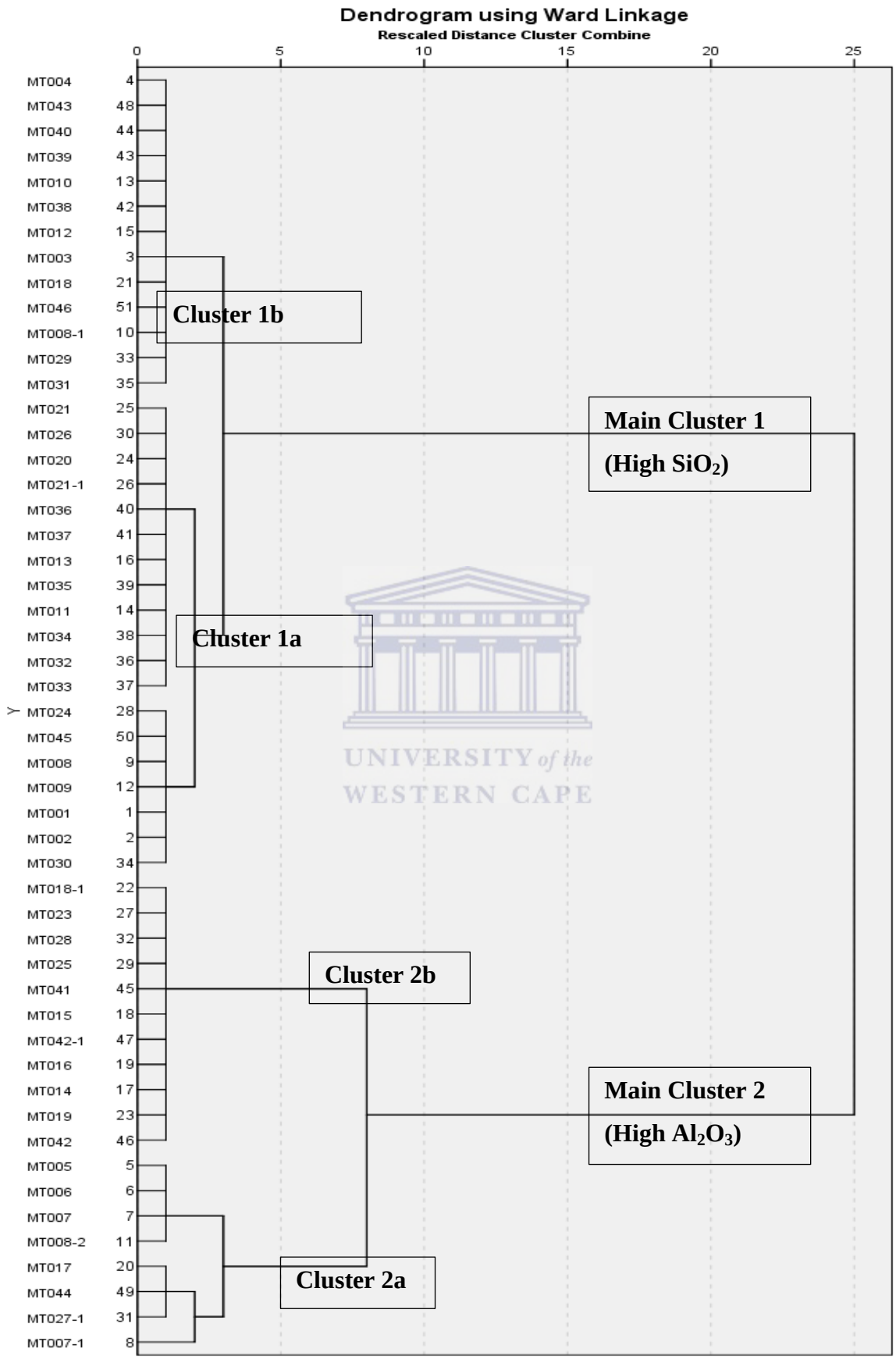

Figure 23: Dendrogram for Hierchical Clustering analysis of the five drilled holes

Table 8: Structure matrix (discriminant analysis) defining the clusters Summary of the clusters based on samples.

Ward Method					
Cluster		**Frequency**	**Percent**	**Valid Percent**	**Cumulative Percent**
	1	**19**	**37.3**	**37.3**	**37.3**
	2	**13**	**25.5**	**25.5**	**62.7**
Valid	**3**	**8**	**15.7**	**15.7**	**78.4**
	4	**11**	**21.6**	**21.6**	**100**
	Total	**51**	**100**	**100**	

Standardized Canonical Discriminant Function Coefficients		
	Function	
	1	2
SiO_2	1.106	0.336
Al_2O_3	0.264	1.125

Structure Matrix		
	Function	
	1	2
SiO_2	.974*	-0.228
CaO^b	-.434*	-0.026
LOI^b	-.398*	-0.019
MnO^b	-.357*	0.033
$TOTC^b$	-.236*	-0.223
$TiO_2{}^b$	.122*	0.054
Al_2O_3	-0.291	.957*
K_2O^b	-0.208	.665*
$Fe_2O_3{}^b$	-0.3	-.570*
Na_2O^b	-0.071	.565*
$TOTS^b$	-0.334	-.403*
$P_2O_5{}^b$	-0.286	.387*
MgO^b	-0.048	-.341*
$Cr_2O_3{}^b$	0.078	.114*

100.0% of original grouped cases correctly classified.

Pooled within-groups correlations between discriminating variables and standardized canonical discriminant functions

Variables ordered by absolute size of correlation within function.

*. Largest absolute correlation between each variable and any discriminant function

b. This variable not used in the analysis.

Table 9: Cluster analysis result reflecting how samples are grouped into the four clusters.

Cluster1	depth (m)	Cluster2	depth (m)	Cluster3	depth (m)	Cluster4	depth (m)
MT001	1	MT003	3	MT005	5	MT014	5
MT002	2	MT004	4	MT006	6	MT015	6
MT008	8	MT008-1	8.5	MT007	7	MT016	7
MT009	10	MT010	1	MT007-1	7.5	MT018-1	9
MT011	2	MT012	3	MT008-2	9	MT019	10
MT013	4	MT018	8.5	MT017	8	MT023	4
MT020	1	MT029	1	MT027-1	8.5	MT025	6
MT021	2	MT031	3	MT044	7	MT028	9
MT021-1	2.4	MT038	1			MT041	4
MT024	5	MT039	2			MT042	5
MT026	7	MT040	3			MT042-1	5.4
MT030	2	MT043	6				
MT032	4	MT046	9				
MT033	5		5				
MT034	6						
MT035	7						
MT036	8						
MT037	9						
MT045	8						

Therefore, there are four clusters showing variation in respect to SiO_2 and Al_2O_3 classification in which the cluster analysis was based on. Based on the discriminant analysis, cluster 1a, 1b, 2a and 2b define 37.3%, 25.5%, 15.7% and 21.6% of the samples analysed respectively.

Based on the predicted membership group for the clusters structure matrix and dendrogram, given by the result in Table 8-9 and Figure 23, each cluster can be classified as follows:

Cluster 1 is defined by high value of SiO_2 and lower enrichment in sulphide-related elements. This indicates that silica oxide is not positively associated with other elements. Cluster I have similar relationship with cluster 2 in terms of SiO_2 but more rich in SiO_2 than cluster 2.
Cluster 1b show a group of cases of cluster depleted in other heavy metals but high values in SiO_2 (compared to cluster 3 and 4). The first few layers for each borehole are found in the group, confirming the geochemical properties of the tailings.
Cluster 3 is characterized by significant concentration in LOI, Fe_2O_3, CaO, MnO, Tot/S, Tot/C and very low concentration of SiO_2. Cluster 2b shows elements that have high values in Fe_2O_3, Au and heavy metals that are sulphide-related and this confirms the petrography and mineralogical results that characterized the third layer (reddish layer).

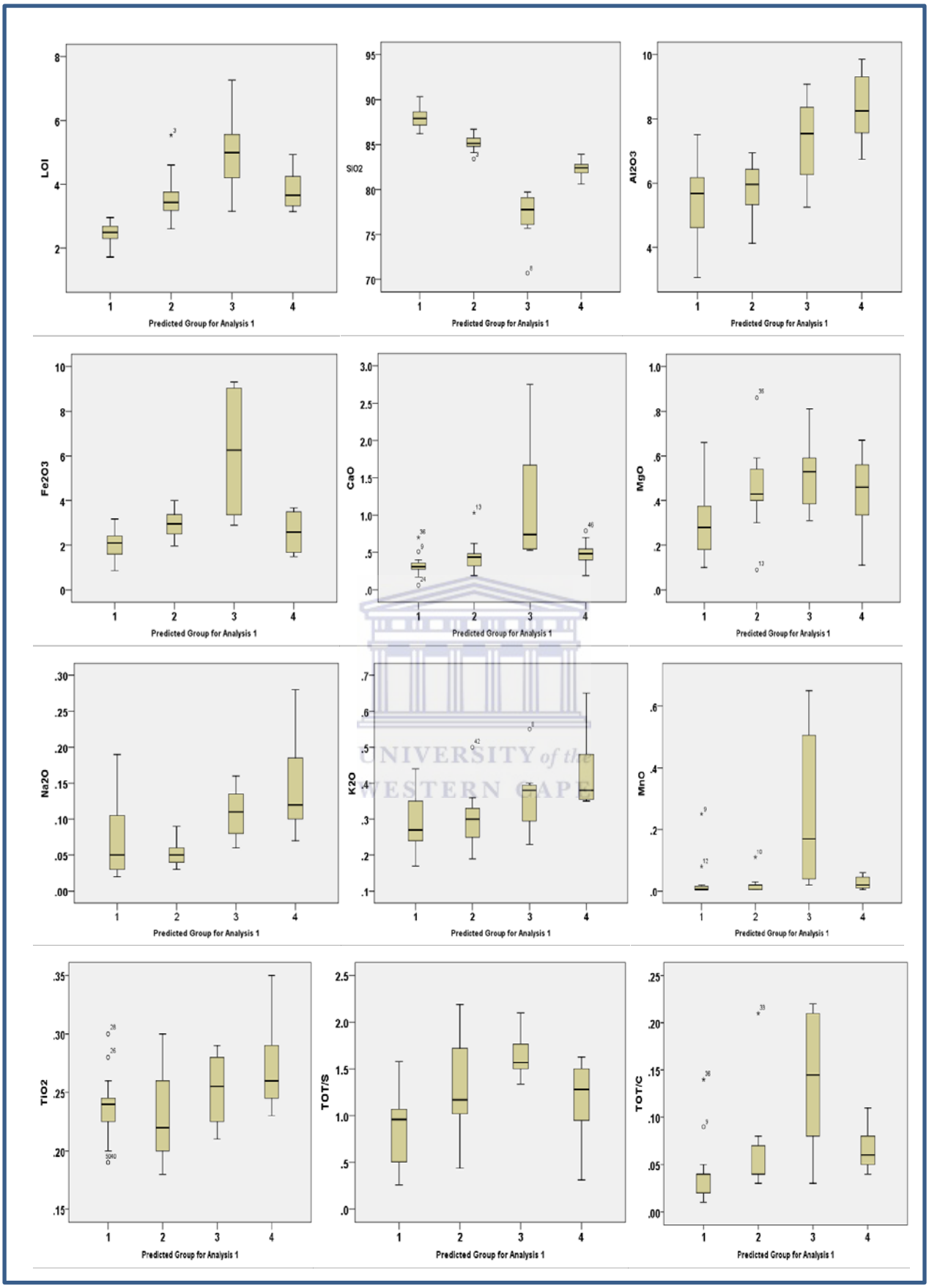

Figure 24: Distribution of elements within the four clusters using predicted group for analysis

Cluster 2b is described by the high presence of Al_2O_3, Na_2O, K_2O, TiO_2, P_2O_5. These show that samples characterized by cluster 4 are rich in clayey materials

Samples that fall within each cluster are grouped in Table 9. The box plot represents the graphical representation of each cluster as regards each major element. Boxplot 1, 2, 3, 4 signifies cluster 1a, 1b, 2a and 2b respectively (Figure 24).

The box plot (Figure 24) for the major elements shows that the content SiO_2 is highest in cluster 1a samples and lowest in cluster 2a samples. Tot/S, Fe_2O_3, Tot/C, MgO, CaO, and LOI show a similar concentration trend in which cluster 2a has the highest content and cluster 1a has the lowest content. This implies that Cluster 2a and cluster 1a samples contains the highest and lowest content in LOI, Fe_2O_3, CaO, MnO, Tot/S, Tot/C respectively

In addition, Al_2O_3, Na_2O and K_2O show a similar trend in content. The highest contents of Al_2O_3, Na_2O, K_2O, TiO_2 was found in cluster 2b samples and lowest contents of Al_2O_3, Na_2O, K_2O was found in cluster 1a samples. The content of TiO_2 is lowest in cluster 1b and highest in cluster 2b

In conclusion, most of the samples described by cluster 1a and 1b dominated the first few layers, which entails the oxidized layer while Cluster 2a samples are found in the reddish color layer and in samples closed to this layer. Most samples in cluster 2b are from the bottom samples.

Based on the discriminant analysis, the relative abundance of SiO_2 in each cluster is defined as follows: cluster 1a> cluster 1b> cluster 2b> cluster 2a while the relative abundance of Al_2O_3 is defined as cluster 2b> cluster 2a> cluster 1b> cluster 1a. The box plot also reflects this.

6.3 Elemental Association

6.3.1 Factor Analysis

Factor analysis was done on the data using LOI, SiO_2, Al_2O_3, Na_2O, K_2O, MgO, Fe_2O_3, MnO, P_2O_5, Cr_2O_3, TiO_2 and Tot/S as variables to determine the major factors that determine the compositional patterns of major element and heavy metals present within the samples and layers.

The principal component method was used based on eigen value greater than 1. A varimax rotation method and suppressing small coefficient greater than 0.1 was used. An eigen value is the measure of the significance of each factor.

From the results below (as shown in table 10 and table 11), four factors were extracted based on the analysis.

A histogram was plotted for each borehole based on each factor. This factor explains about 100% variance within the data.

Factor 1 = 37.25%
Factor 2 = 25.49%
Factor 3 = 15.69%
Factor 4 = 21.57%

6.3.1.1 Description of factor analysis results

The factors analyzed (Table 10) for can be classified into four groups, and are described below:

Factor 1 accounted for 37.25% of the total variance and was positively correlated with Al_2O_3, Na_2O, K_2O, P_2O_5, Cr_2O_3, Cs (which define this group) and negatively correlated to SiO_2 indicating rich presence of clayey materials (clayey rich).

Factor 2 accounted for 25.49% of the total variance and was positively correlated LOI volatile, CaO, MnO, P_2O_5, TOT/C, TOT/S, Ba, Co ,Cs, Th, Pb, Ag, Ni, As, Bi and negatively correlated with SiO_2 indicating the carbonates zone generated as a result of additives such as lime (calcium-rich).

Factor 3 accounted for 15.69% of the total variance and was positively correlated. LOI, Fe_2O_3, MgO, Tot/S, Co, Zn, Ni, Au, Sb, EC and negative correlated to SiO_2. This indicates the presence of a ferruginised zone.

Factor 4 accounted for 21.57% of the total variance and was positively correlated to TiO_2 and negatively correlated to Mo. This is the only factor that does not show any correlation to SiO_2 (indicating a moderate level of SiO_2). The factor represents samples that is enrich in TiO_2 and its related element (titanium-rich).

In general, factor 3 is most negatively correlated to SiO_2, indicating a high depletion of SiO_2 than other factors. Factor 2 and 3 has positive correlations in LOI, TOT/S, Co, Ni. Factor 3 is highly positively correlated in Tot/S, Co, Ni than factor 2 while factor 2 is highly positively correlated in LOI than factor 3.

Table 10: The results of factor analysis done by principal component analysis method of extraction.

Component Transformation Matrix				
Component	**1**	**2**	**3**	**4**
1	**0.62**	**0.643**	**0.435**	**0.118**
2	**0.724**	**-0.324**	**-0.592**	**0.144**
3	**0.023**	**-0.475**	**0.469**	**0.744**
4	**-0.303**	**0.506**	**-0.491**	**0.642**

Rotated Component Matrix[a]				
	Component			
	1	**2**	**3**	**4**
K_2O	**0.908**			**0.127**
Na_2O	**0.85**	**0.108**	**-0.185**	**0.227**
Al_2O_3	**0.813**	**0.222**		**0.316**
P_2O_5	**0.678**	**0.446**	**0.208**	
Cr_2O_3	**0.597**			**-0.334**
CaO	**0.146**	**0.921**	**0.146**	
MnO		**0.905**	**0.136**	**0.135**
LOI	**0.335**	**0.659**	**0.476**	**-0.101**
Fe_2O_3			**0.825**	
MgO	**-0.13**		**0.705**	**0.206**
TOT/S	**-0.148**	**0.446**	**0.692**	
SiO_2	**-0.487**	**-0.533**	**-0.629**	**-0.123**
TiO_2	**0.198**			**0.883**

Extraction Method: Principal Component Analysis.

Rotation Method: Varimax with Kaiser Normalization.[a]

a. Rotation converged in 6 iterations. 4 components extracted

Table 11: Pearson correlation of the four factors with all the variables in the analysis

	REGR factor score 1	REGR factor score 2	REGR factor score 3	REGR factor score 4
LOI	.335*	**.659****	**.476****	-.101
SiO_2	**-.487****	**-.533****	**-.629****	-.123
Al_2O_3	**.813****	.222	.070	.316*
Fe_2O_3	.038	.085	**.825****	-.100
CaO	.146	**.921****	.146	-.033
MgO	-.130	.086	**.705****	.206
Na_2O	**.850****	.108	-.185	.227
K_2O	**.908****	.049	-.095	.127
MnO	.042	**.905****	.136	.135
TiO_2	.198	.004	.068	**.883****
P_2O_5	**.678****	**.446****	.208	-.089
Cr_2O_3	**.597****	-.063	.007	-.334*
TOT/C	.194	**.540****	**.355***	-.112
TOT/S	-.148	**.446****	**.692****	-.028
Ba	.346*	**.856****	.002	.143
Co	.036	**.366****	**.819****	.007
Cs	**.429****	**.782****	.033	.157
Th	.140	**.885****	.036	-.089
U	.022	.035	.212	.261
Zr	-.223	.034	.163	.238
Mo	.056	-.247	-.148	**-.375****
Cu	.335*	.045	.177	-.286*
Pb	-.128	**.722****	.045	-.057
Zn	.088	**.306***	**.491****	.211
Ag	.006	**.789****	.135	-.010
Ni	.037	**.462****	**.708****	.151
As	.079	**.872****	.125	-.129
Au	.083	.104	**.494****	-.026
Cd	.197	.086	-.065	-.156
Sb	.162	.166	**.677****	-.223
Bi	-.136	**.512****	.299*	-.204
Hg	.188	-.124	-.252	-.064
Se	.023	-.057	.399*	.185
pH	-.203	.240	-.083	.122
EC	.113	.027	**.609****	-.143

It could show that factor 2 is related to the product of oxidation while factor 3 is related to the initial sulphides present than has not be oxidized.

In conclusion, four major factors determine the state of the tailing dam sample and are peculiar to specific layer within the tailings. These factors has to do with the oxidation state of the tailing (that a certain part of the tailing has been oxidized and undergoing oxidation), the enrichment of gold and sulphides presenting the tailing that could be of interest and the enrichment of clayey materials responsible for the fineness of certain layers.

6.4 Geochemical characteristics and significance of total sulphur

The total percentage S signifies the total percentage of sulphides present and ranges from 0.26- 2.75% in all samples. In this study, more attention is given to the total sulphur because of its potential for the generation of acid mine drainage from tailings.

Oxidation of sulphides of pyrite to produce acid, and effectively lowering the pH of the drainage, water pathway and other water bodies affected. , which then enters the ground water regime beneath the dumps. This acidic water is believed to be entering streams along the Witwatersrand (Naicker, et al., 2003).

Based on assumption, the values of the total %S in samples can be used to calculated the Acid Base Accounting parameters for the tailings. The Acid base Accounting is a generally utilised static test for the estimation and quantification of the acid generating potential of mine wastes. Acid Base Accounting (ABA) analyses conducted by PHD, 2002, on various Witwatersrand gold tailings samples showed AP: NP ratios from 1:0.5 to 1:2.78. Measured S concentrations varied between 0.17% and 0.45 % S, thus placing the tailings within the uncertain range, with its potential to generate AMD.

From the geochemical data, the total %S is assumed to be synonymous to the total amount of sulphide present in the tailings that can be oxidized and thus generating acidic leachates. Therefore, this is used to calculated the maximum potential acidic as follows. Assuming that, 100% of the sulphur present is available to produce acid, this reaction below will be considered.

Table 12: The acidic potential, neutralisation potential and the maximum potential acidity of the samples in all drilled holes

	T008			T009			T010			T011			T004	
S. No	**C.NP/MPA**	**NP/MPA**	**S.No**	**C.NP/MPA**	**NP/MPA**	**S. No**	**C.NP/MPA**	**NP/MPA**	**S. No**	**C.NP/MPA**	**NP/MPA**	**S. No**	**C.NP/MPA**	**NP/MPA**
MT001	1.70	0.44	**MT010**	0.73	0.63	**MT020**	0.40	0.09	**MT029**	0.78	0.28	**MT038**	1.52	0.57
MT002	1.36	0.47	**MT011**	0.59	0.24	**MT021**	0.62	0.34	**MT030**	0.62	0.11	**MT039**	0.50	0.16
MT003	0.26	0.05	**MT012**	0.55	0.17	**MT021-1**	0.70	0.42	**MT031**	0.85	0.20	**MT040**	0.50	0.13
MT004	0.47	0.09	**MT013**	0.37	0.11	**MT023**	0.73	0.50	**MT032**	0.50	0.30	**MT041**	0.47	0.15
MT005	0.42	0.13	**MT014**	0.57	0.17	**MT024**	0.15	0.06	**MT033**	0.31	0.18	**MT042**	0.66	0.25
MT006	0.65	0.23	**MT015**	0.44	0.14	**MT025**	0.38	0.17	**MT034**	0.28	0.13	**MT042-1**	0.49	0.19
MT007	0.66	0.40	**MT016**	0.39	0.14	**MT026**	0.27	0.09	**MT035**	0.47	0.12	**MT043**	0.42	0.14
MT007-1	0.64	0.38	**MT017**	0.36	0.15	**MT027-1**	0.39	0.14	**MT036**	0.47	0.13	**MT044**	0.42	0.19
MT008	0.50	0.22	**MT018**	0.26	0.10	**MT028**	0.39	0.18	**MT037**	0.50	0.10	**MT045**	0.20	0.07
MT008-1	0.14	0.04	**MT018-1**	1.28	0.25							**MT046**	0.30	0.11
MT008-2	0.65	0.53	**MT019**	0.33	0.10									
MT009	0.43	0.17												

$$FeS_2 + 15/4O_2 + 7/2H_2O \longrightarrow Fe(OH)_3 + 2H_2SO_4$$

From the balance stoichiometry reaction above, the mass of 1% pyrite translates to 30.6Kg of H_2SO_4 per tonne of materials (kgH_2SO_4/t). From this, the maximum potential acidic is calculated as the product of the weight of the total sulphur (in %) by 30.6.

In addition, since calcium carbonate ($CaCO_3$) reacts to neutralise H_2SO_4 generated on a 2:1 stoichiometric ratio, the comparative acid neutralising capacity is a function of the amount of CaO content present, which is expressed in the weight of H_2SO_4.

$$2CaCO_3 + 2H_2SO_4 \longrightarrow 2CaSO_4 + 2H_2O + 2CO_3$$

From the above equation, to express %CaO in respect to %S, a conversion factor is required. This is because the molecular weight of CaO is 56, which is greater than S (32), and in this study, 0.57 is used has the conversion factor. From the %CaO, the neutralisation potential (NP) of the tailings can be calculated by assuming that % CaO is responsible for the neutralisation process in the tailings. This is then calculated as % CaO, multiply by 30.6Kg of H_2SO_4 per tonne of materials and the conversion factor.

Another method is used in this study to calculate the NP, since the MgO is substantial, undergoes the same reaction as CaO and can also be involved in the neutralisation process. Therefore, the summation of all the material that can be responsible for neutralisation is calculated as follows:

(%CaO x 30.6 x conversion factor for CaO(0.57) + %MgO x 30.6 x conversion factor for MgO (0.8)) = Cumulative Neutralisation Potential (C.NP).

Therefore, from this, we can calculate the Net Acid Producing Potential separately as NAPP and Cumulative NAPP, which is calculated as NP/MPA and C. NP/MPA respectively. Table 12 shows the results.

If NAPP or C.NAPP is less than 1, indicates that it is acid generating, if it is greater than one indicates that is has the potential to be acidic, if it is greater than 2, means it is not acid generating. Tailings that contain sulfides and insufficient buffering minerals are particularly susceptible to acid generation because the finely ground material has a large accessible reactive surface area.

From Table 12, the NAPP is less than 1 for all samples, indicating that it is acid generating at all layers. Most samples that falls within layer 1 have values greater than 0.5, while other samples show low value of NAPP.

For the Cumulative NAPP, all samples are less than 1 except MT001, MT002, MT018-1 and MT038 which are greater than 1 but less than 2. Except for MT018-1, all others are topmost layers.

As regards C.NAPP, it implies that if both CaO and MgO present in the tailings as a buffer, it could only neutralize AMD generated in the layer 1. There is no specific trend for the tailing dam neutralization potential but a generalized effect. Samples that fall within cluster 1 show the highest NAPP and C.NAPP values, while samples from cluster 3 reflect the lowest values.

6.5 Modelling

6.5.1 GIS Inverse Distance Weighed (IDW) Analysis results

Based on statistical analysis, elements from similar origin are known and grouped as factors. Generally, SiO_2 shows a significant negative correlation with each factor. Factor 1 is clayey rich, factor is calcium rich, strongly related to the carbonates, factor 3 are iron/sulphide-rich, and strongly related to gold and factor 4 is titanium-rich.

Table 13: Percentiles values of elements used in IDW analysis as intervals for the map display

Percentiles	SiO_2(%)	Al_2O_3(%)	Fe_2O_3(%)	CaO(%)	TOT/S(%)	U(ppm)	Au(ppb)
25%	**82.3**	**5.33**	**1.97**	**0.3**	**0.83**	**10**	**106**
50%	**85.1**	**6.28**	**2.59**	**0.4**	**1.09**	**32.4**	**186.7**
75%	**87.2**	**7.51**	**3.4**	**0.54**	**1.53**	**43.1**	**322**
Minimum (0%)	**70.7**	**3.06**	**0.86**	**0.06**	**0.26**	**4**	**58.1**
Maximum (100%)	**90.3**	**9.85**	**9.31**	**2.75**	**2.19**	**655.5**	**1417.5**

Using the IDW analysis, the spatial distribution of elements with similar trend down depth was observed (Setianto & Triandini, 2013). Elements in each factor show a peculiar trend and are described below. Also, the variation pattern of SiO_2 could also serve a basis for the four factors. For each element, the quartile values of the element in the whole data are used to

reflect an unbiased distribution pattern. Based on its quantile percentages, the analysis was done as shown in Table 13

6.5.1.1 Distribution pattern of SiO_2

The range of values for SiO_2 is 70.7-82.3% (R1), 82.3-85.2% (R2), 85.2-87.2% (R3) and 87.2-90.3% (R4) (Figure 25). The first two meters show high concentration of SiO_2. The area containing the highest content of SiO_2 (R4) increases in a south-north trend from the first meter to the second meter of the tailings dam. This decreases drastically at the third meter to values in R3. From the third meter to the fourth meter, the concentration of SiO_2 decreases and drifted the southeast to the southwest.

At the fifth meter, very low values of SiO_2 is observed at the southeast of the tailing dam and this low concentration spread out towards the southwest at the sixth meter. The lowest concentration range R1 spread out towards the northwest at the seventh meter. At this depth (7m), values from R1 filled a large area of the tailings. From 7m to 9m depth, the concentration of SiO_2 increases swiftly.

In general, the overall distribution of SiO_2 depicts a decreasing trend down depth to the 7^{th} meter and increases from the 7^{th} meter downward. In addition, the first two meters show the highest concentration in SiO_2.

6.5.1.2 Distribution pattern of Al_2O_3 (clay-origin group)

The range of values for Al_2O_3 is 3.06-5.33 % (R1), 5.33-6.28% (R2), 6.28-7.51% (R3) and 7.51-9.85% (R4) (Figure 26). The distribution pattern of Al_2O_3 is different from the SiO_2. The eastern part of tailing dam stretching northward and southward contains the lowest concentration range R1 of Al_2O_3 at the depth of 1m.

This trend becomes prominent at the depth of 2m, occupying a large area of the tailing dam. At the third meter, the content of Al_2O_3 increased to values of R2. Tailings around drill hole T011 show concentration in R1. At the fourth meter, the concentration of Al_2O_3 increases to R4 in the west and southwest part of the tailing dam.

This high concentration drifts towards southern part of the tailing dam form the fourth meter to the seventh meter depth. As compared to SiO_2, btw 4m to 7m, concentration of SiO_2 decreases while Al_2O_3 decreases.

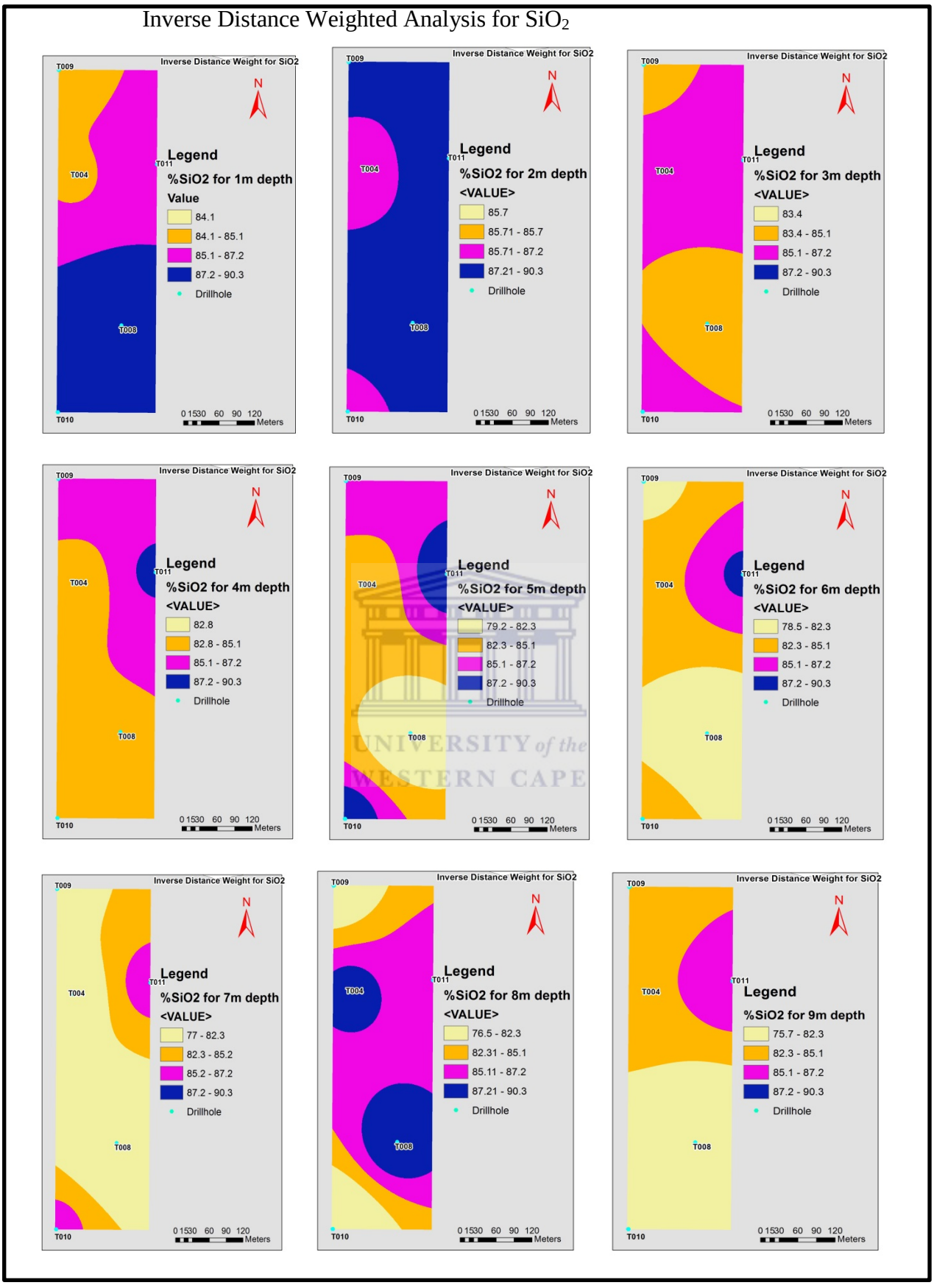

Figure 25: Distribution pattern of SiO_2 down depth

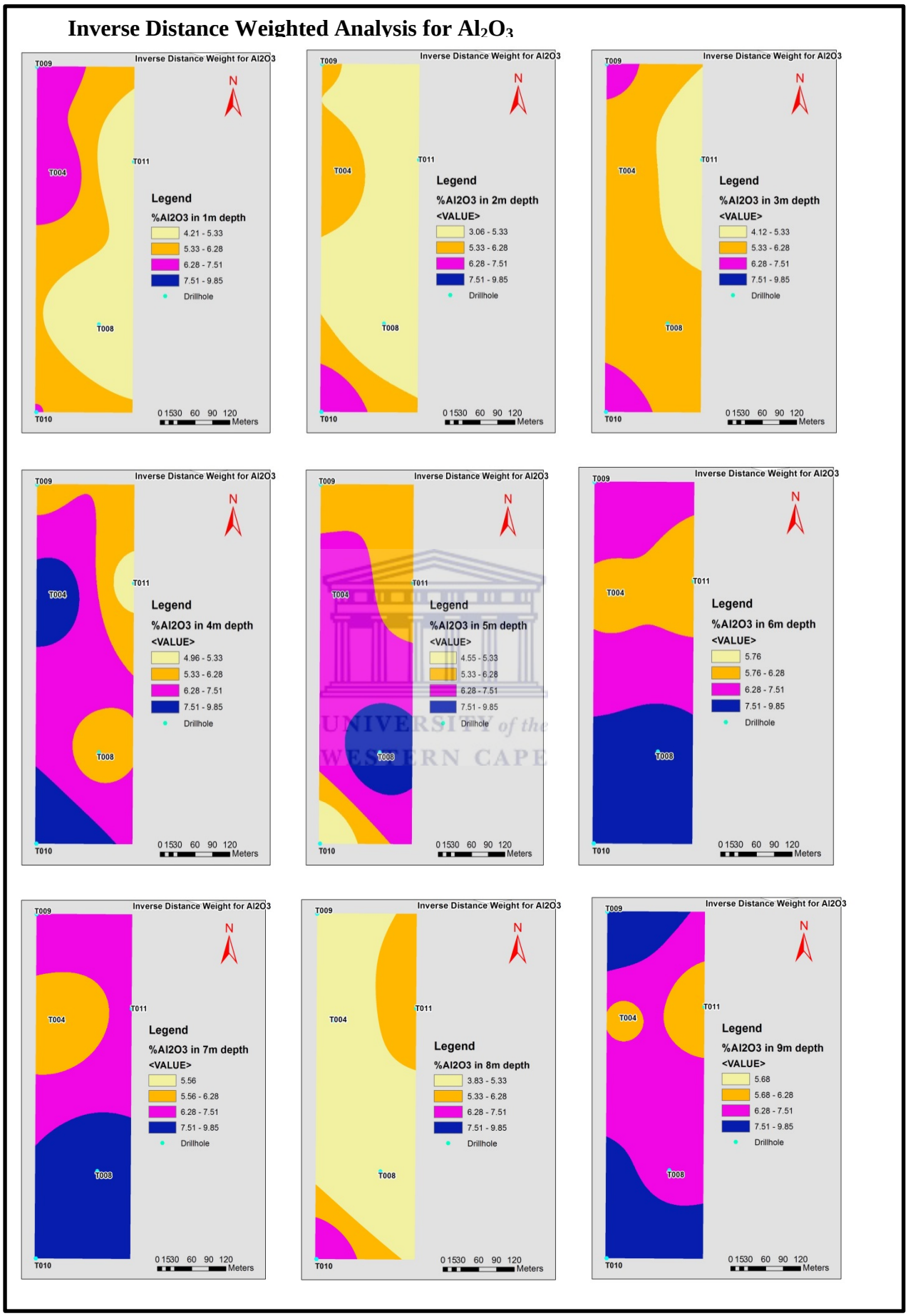

Figure 26: Distribution pattern of Al_2O_3 down depth

At 8m depth, the concentration of Al_2O_3 decreases drastically from the northwest through the southeast of the tailing dam. At 9m depth, the concentration of Al_2O_3 increases and high values spread through the depth.

6.5.1.3 Distribution pattern of CaO (carbonates)

The range of values for CaO is 0.06-0.30 %(R1), 0.3-0.4%(R2), 0.4-0.54%(R3) and 0.54-2.75%(R4) (Figure 27). The CaO represents the carbonates group. At the first meter, the northern part of the tailing dam contains high content of CaO in R4. The concentration of CaO in this depth decreases from the north to the south. At 2m depth, the larger area of the tailing dam contains concentration of CaO that falls within R2.

At the third meter depth, the concentration of CaO increases around the northern part of the tailing dam and decreases in the southern part of the tailing dam. At the fourth meter, the highest concentration R4 values around the northeast of the dam (around T011) and drifted towards the northwest at 5m depth. The high content of CaO (R4) drifts towards the southeast of the tailing dam at 6m depth.

At 7m depth, large area of the tailings dam, that is, from the northwest through southeast, contains the highest content R4 of CaO. This indicates that at 7m depth, the concentration of CaO is generally high as compared to all depth. At 8m depth, the concentration of CaO reduces drastically and increases again at the 9m depth.

6.5.1.4 Distribution of total sulphur (sulphide-group trend)

The total sulphur concentration shows a significant trend down depth that depicts leaching pattern of sulphides (Figure 28). The range of values for Tot/S is 0.26-0.83 %(R1), 0.83-1.09%(R2), 1.09-1.53%(R3) and 1.53-2.19%(R4).

At 1m depth, tot/S concentration through this depth fall within R1, indicating a highly depleted surface. That is, the total area of the tailings at this depth contained the lowest concentration R1. At 2m depth, through the northwest to northeast of the tailing dam, the concentration of tot/S increases, and falls within R2, while other part of the tailings dam still contain values from R1 concentration range.

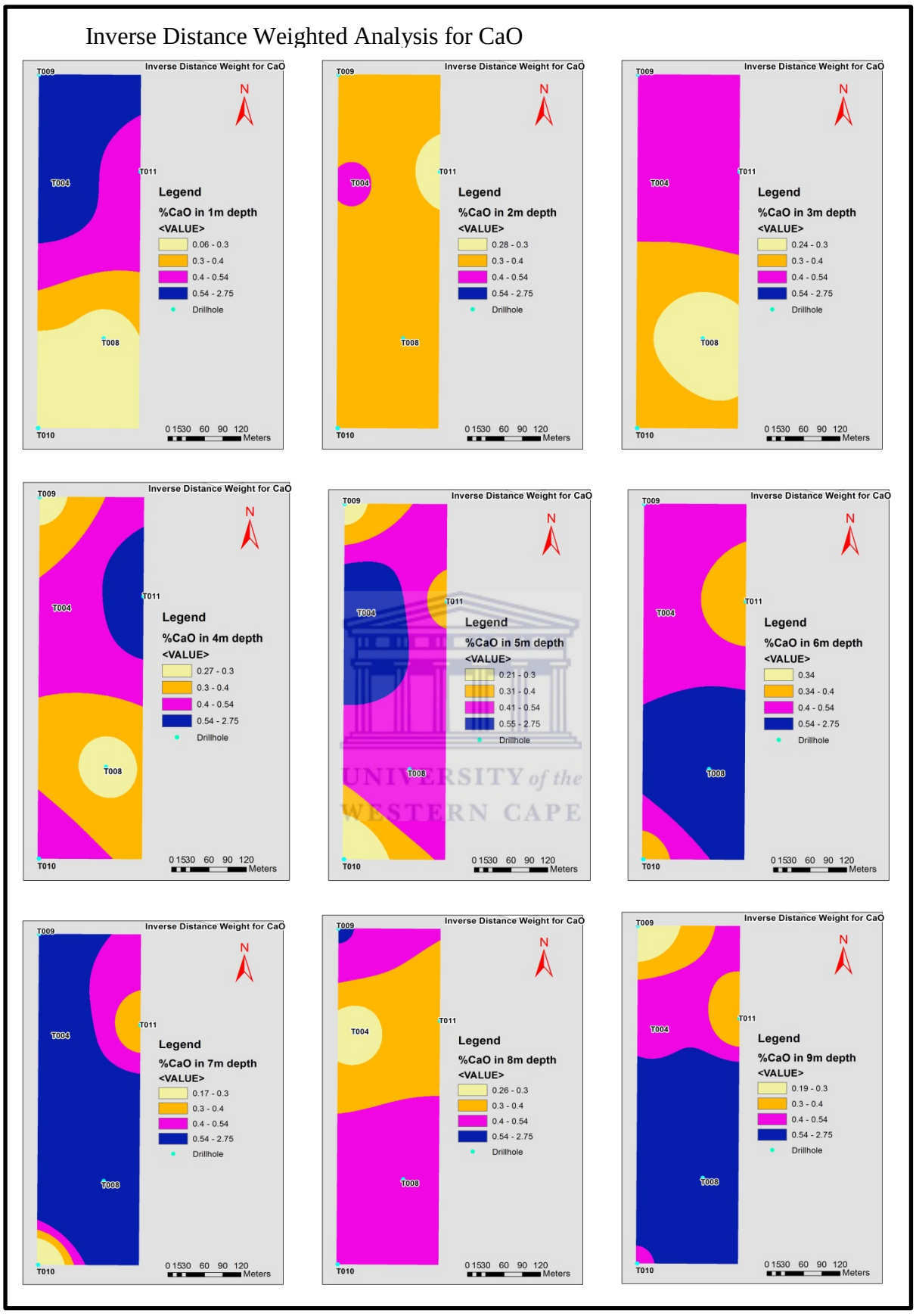

Figure 27: Distribution pattern of CaO down depth

Inverse Distance Weighted Analysis for Tot/S

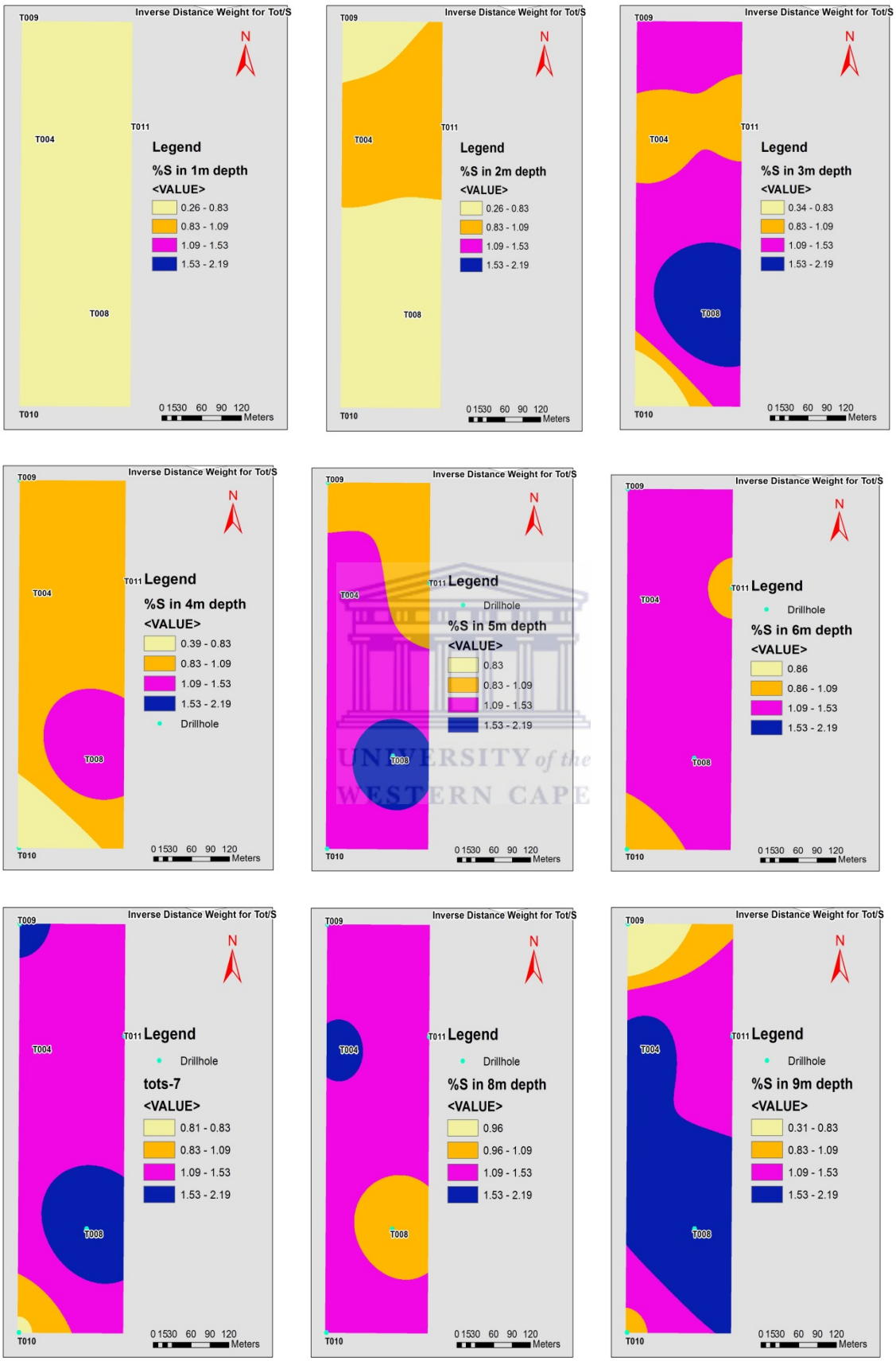

Figure 28: Distribution pattern of Tot/S down depth

At 3m depth, the concentration of tot/S increases around drilled hole T008(southeast) to R4 and around T010, the concentration remained very low (R1). Larger area of the tailings dam at 3m depth is filled with R3 concentration range. At 4m depth, the concentration of tot/S reduces to mostly R2 concentration range.

At 5m depth, the concentration increases to R3 and this covers a large area of the tailings dam. Around the drilled hole T008, high concentration R4 of tot/S is observed, while the concentration in the north to northeast still falls within R2.

At 6m depth, the content of the total sulphur increases, in which larger area of the tailings dam falls within R3. At 7m depth, the concentration of tot/S increases around T008 and T009 to R3, while other parts are mainly filled with R3 concentration range. At 8m depth, large area of the tailing contains concentration of tot/S of R3. At 9m depth, the concentration of tot/S increases to R4 through west to southeast of the tailings dam, and decreases northward and southward.

6.5.1.5 Distribution pattern of Uranium (U) (a mobile radioactive element)

Uranium shows a specific distribution trend similar to tot/S, but shows no association in terms of factor analysis. This shows that both undergo the same leaching trend (Figure 29). The range of values for U is 4-10ppm (R1), 10-32.4ppm (R2), 32.4-43.1ppm (R3) and 43.1-655.5ppm (R4).

The first meter shows complete depleted layer of U with the minimum concentration values R1. At 2m depth, the concentration of U increases to R2 from the upper northwest to northeast. This increases steadily at the 3m depth. Larger area of the tailings dam at this depth still maintains the R2 concentration range, as it drifts towards the south.

From the south east, the R4 concentration range surfaced through the west. This trend continues and expands through a larger area at 4m depth and show a decreasing trend northward and southward. Between 5m and 6m depth, the area covered by R4 diminishes towards the southwest of the tailings dam.

At 7m depth, the concentration of U increases from the southeast through the north, with R4 concentration range. This occupies a large area of the tailings dam at this depth. At 8m depth, the area containing R4 reduces and fills with values of R3 concentration range. At 9m depth, the area containing R4 increases and forms a similar pattern to its distribution at 7m depth.

Inverse Distance Weighted Analysis for U

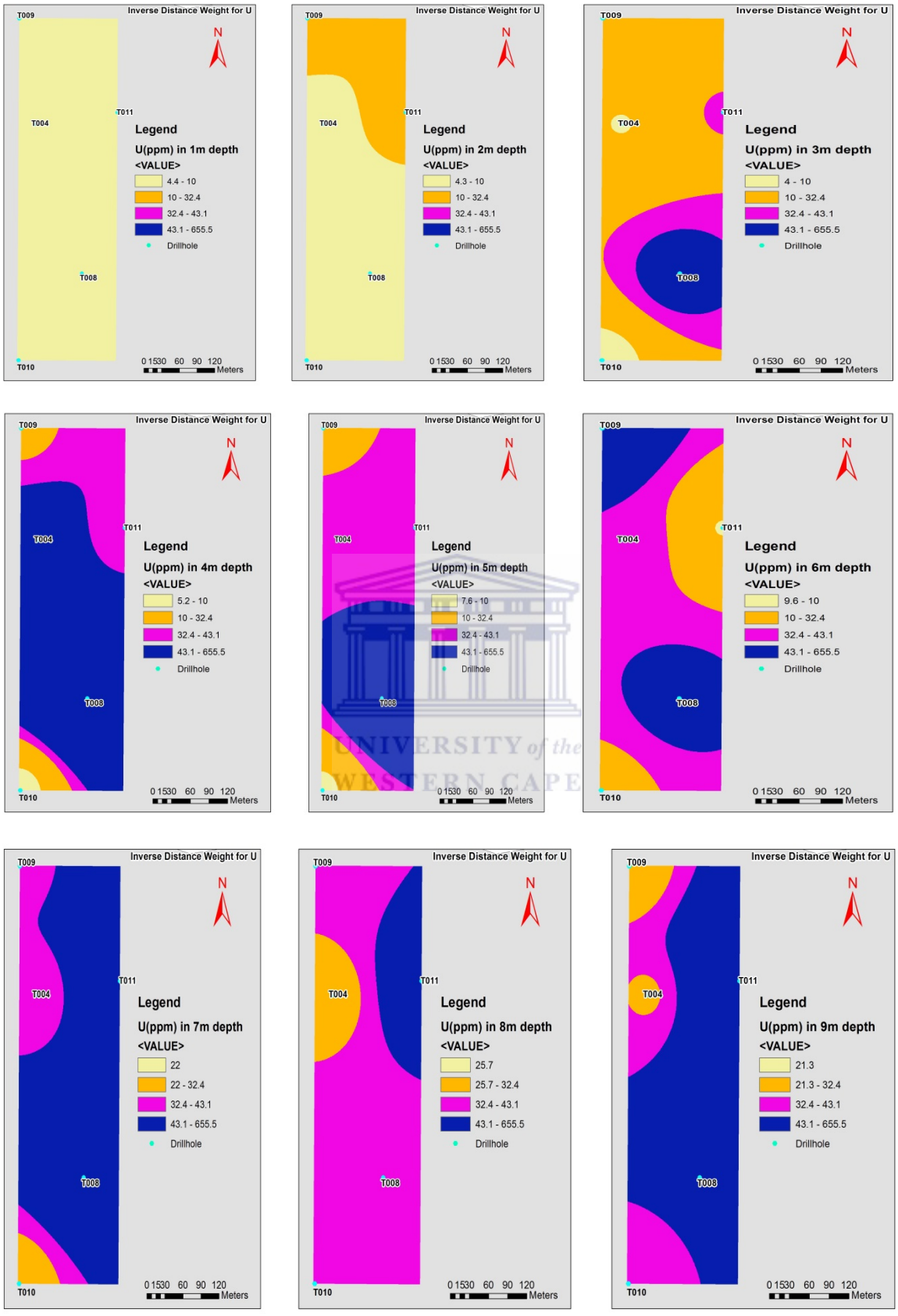

Figure 29: Distribution pattern of U down depth

Inverse Distance Weighted Analysis for Au

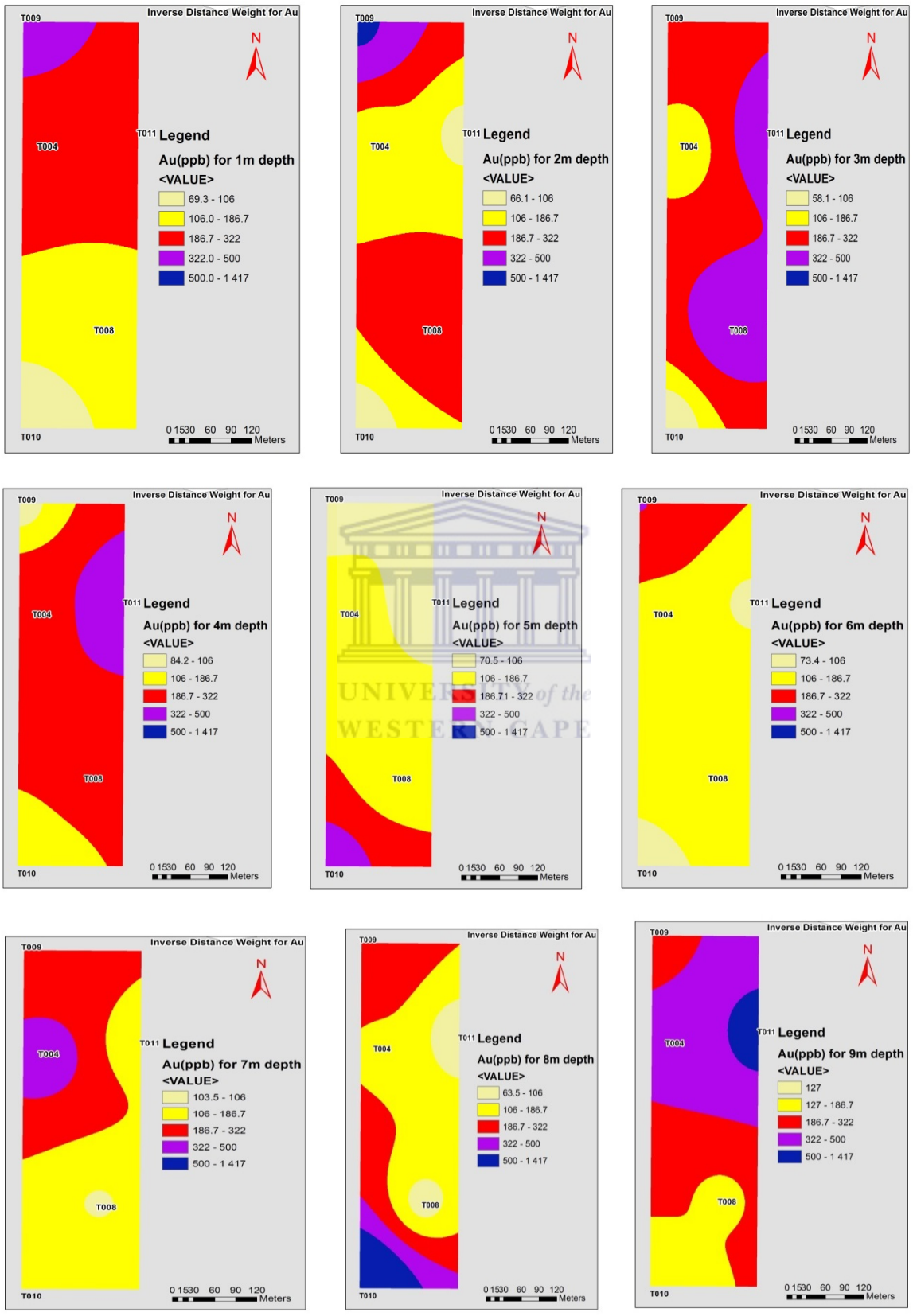

Figure 30: Distribution pattern of Au down depth

6.5.1.6 Distribution pattern of Gold (Au)

Gold, though associated with sulphides, shows a no specific distribution trend similar to tot/S, but shows no association in terms of factor analysis. From Figure 31, the range of values for Au is 58.1-106ppb (R1), 106-186.7ppb (R2), 186.7-322ppb (R3), 322-500ppb (R4) and 500-1417ppb (R5). Since the standard deviation of Au is high, R5 was given so as to determine how economical is the Au present.

The first meter shows a decreasing trend of Au from T009 to T010 with the minimum concentration values R1 (from R4 to R1) at T010 but no R5 concentration range. At 2m depth, the concentration of Au increases slightly to R5 at T009 the upper northwest. This decreases downward to R2 at the middle of the drilled holes and later increases to R4 before a downward decreasing trend to R1. At the 3m depth, the tailing dam generally show enrichment in Au as compared to the first two meters.

Larger area of the tailings dam at this depth still maintains the R3 concentration range, followed by R4, which outline west towards T008. This trend at 4m depth but R4 diminishes as R3 increases towards the southeast. Between 5m and 6m depth, the concentration of Au in the tailings dam decreases generally (as compare to other layer) in an opposite trend. At 7m depth, the concentration of Au increases from the northeast through the north to the south generally with an increase Au concentration as compared to 5 and 6m.

At 8m depth, the area containing R5 and R4 increases from south to south east and north to northeast. At 9m depth, the area containing R4 increases. In addition, the depth (9m) show high concentration of Au compared to other depths.

6.5.2 Geochemical Mass Balance

The estimation of geochemical mass balance in determining the alteration processes in rock materials is done in numerous ways, in which ISOCON method of mass balance is most widely used. This is because of its simplicity, in terms of its flexibility and its graphical approach (Mukherjee & Gupta, 2008).

This slope of the best-fit ISOCON line may differ within the scope of slopes well defined by specific conserved elements plots far from the origin. If identical weight/slope is given to all elements (as used in this study), irrespective of their concentration level, the mean of slopes of the immobile elements, (which implies the ratio of the concentration in altered to unaltered

elements) may offer a better estimation for reference frame without option to graphical plot, ISOCON solution and mass balance numerical results (Mukherjee & Gupta, 2008).

Table 14: Summary of the mass balance results for layers

ISOCON	Layer 1	Layer 2	Layer 3	Layer 4
	Gain/Loss in wt.% or ppm	Gain/Loss in wt.% or ppm	Gain/Loss in wt.% or ppm	Gain/Loss in wt.% or ppm
Major Elements	**ΔCi**	**ΔCi**	**ΔCi**	**ΔCi**
LOI	**-0.04**	**0.23**	**1.02**	**0.03**
SiO_2	**2.72**	**0.03**	**-8.35**	**0.12**
Al_2O_3	**-1.31**	**-0.45**	**-0.07**	**-0.43**
Fe_2O_3	**-0.61**	**-0.16**	**6.53**	**0.14**
CaO	**0**	**-0.01**	**0.44**	**-0.03**
MgO	**-0.07**	**0.02**	**0.06**	**-0.03**
Na_2O	**-0.04**	**-0.03**	**-0.01**	**-0.02**
K_2O	**0.01**	**0.02**	**0.03**	**-0.02**
MnO	**-0.02**	**-0.02**	**0.11**	**0.01**
TiO_2	**-0.01**	**0.01**	**0.01**	**0**
P_2O_5	**-0.01**	**0**	**0**	**0**
Cr_2O_3	**0**	**0**	**0**	**0**
TOT/C	**0**	**0**	**0.08**	**-0.01**
TOT/S	**-0.74**	**-0.28**	**0.23**	**0.01**
Trace Elements				
Ba	**-3.09**	**0**	**30.47**	**0.88**
Co	**-26.11**	**-9.32**	**71.86**	**3.52**
Cs	**-0.13**	**0**	**0.52**	**-0.02**
Ga	**-0.84**	**-0.18**	**0**	**-0.3**
Sr	**-6.58**	**-2.84**	**5.66**	**-0.96**
Th	**-4.53**	**-0.57**	**1.79**	**0.18**
U	**-41.12**	**-14.62**	**-8.99**	**-7.18**
V	**-0.49**	**2.03**	**2.82**	**2.37**
Zr	**-3.95**	**2.98**	**39.37**	**10.74**
La	**-6.13**	**-3.79**	**2.48**	**-0.38**
Ce	**-12.57**	**-8.17**	**6.28**	**-1.03**
Mo	**0.23**	**0.06**	**1.03**	**0.32**
Cu	**-28.62**	**10.21**	**20.2**	**22.64**
Pb	**13.82**	**-1.29**	**13.16**	**-6.87**
Zn	**-88.81**	**-28.97**	**34.57**	**17.07**
Ni	**-63.49**	**-18.24**	**74.99**	**9.92**
As	**-27.44**	**-22.21**	**61.13**	**13.19**
Au	**-64.6**	**-29.95**	**463.61**	**-104.27**
Sb	**-0.32**	**-0.28**	**0.96**	**-0.15**
Bi	**0**	**-0.06**	**1.23**	**-0.14**
Hg	**0.23**	**-0.04**	**-0.13**	**-0.04**
pH	**-2.27**	**-1.68**	**-2.15**	**-1.32**
EC (µ/cm)	**0.21**	**0.29**	**0.91**	**0.1**

In this study, the mass balance calculation was based on the Gain/Loss relative to C_i^0, represented as $\Delta C_i/C_i^0$. Where ($_i$) stands for the element analysed for, (^{0}) represents original value, C_i represents the average value of element ($_i$) in the specific layer, C_i^0 is the average value of element ($_i$) in the bottom samples, ΔC_i represents (C_i - C_i^0), and when ΔC_i is +ve, there is gain /enrichment, when –ve, there is loss/depletion (Figure 31).

The average values of all major oxides and elements found in the each layer as described by the petrography was used to calculate the mass balance in respect to the bottom samples (which is assumed to be the least altered sample) (Table 14).

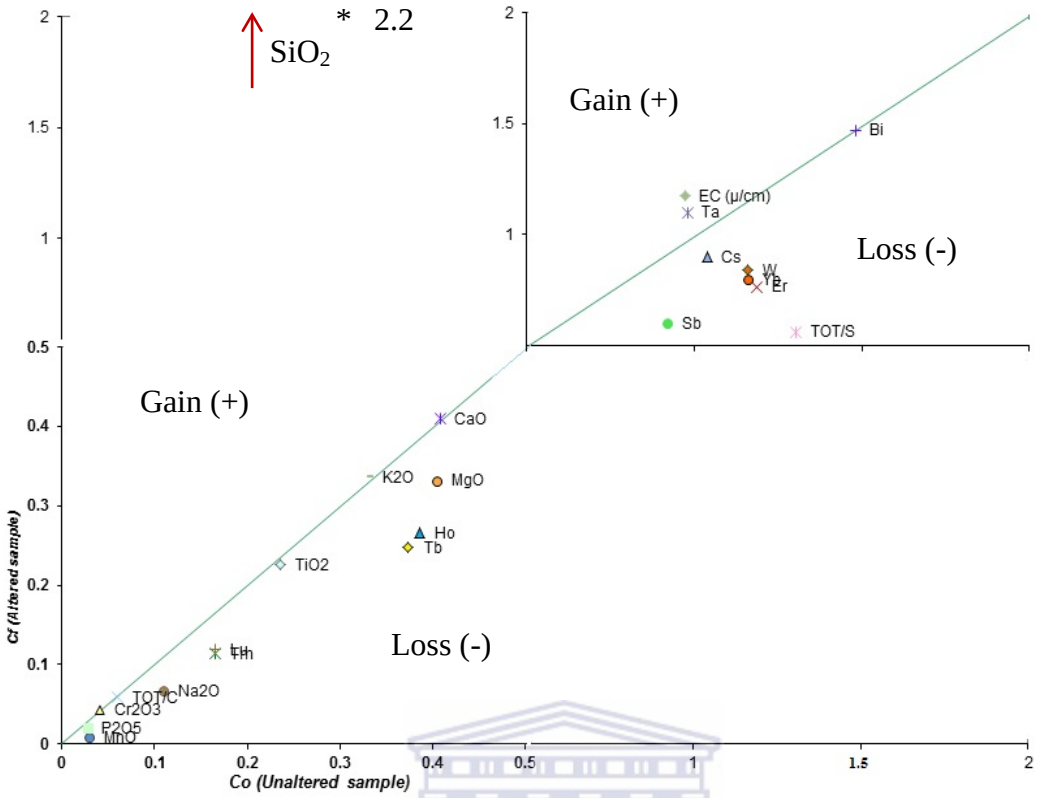

Figure 31: Isocon diagram for layer 1 (the elements gain and loss in respect to ΔCi)

6.5.2.1 Mass balance results for the major elements

It should be noted from the previous study that the boreholes characterized consist of four distinct layers based on the petrography. The mass balance numerical results show notable variations in gain or enrichment and loss of constituents present. The major oxides reflect the framework of the tailings and noticeable variation will give useful information based of the processes that might have occurred within the tailings.

The average values of all major oxides and elements found in the each layer as described by the petrography was used to calculate the mass balance. The mass balance results for major elements and trace elements are shown are Figure 32-35.

Oxidised layer (layer 1)

From the result of the mass balance of layer 1 and the average bottom samples values (for all boreholes combined) Layer 1 is characterised, as shown is the Figure 33, by significant loss in Fe_2O_3, Na_2O, MnO, LOI (volatiles), Tot/S, P_2O_5, Al_2O_3, MgO and TiO_2 and gain in SiO_2, K_2O, and CaO.

This layer shows depletion in sulphide related elements/total sulphur, and Fe_2O_3 but enrichment in silica, which suggests significant leaching of elements from the layer. Loss in Al_2O_3 shows why samples from this layer are more coarse than all other layers

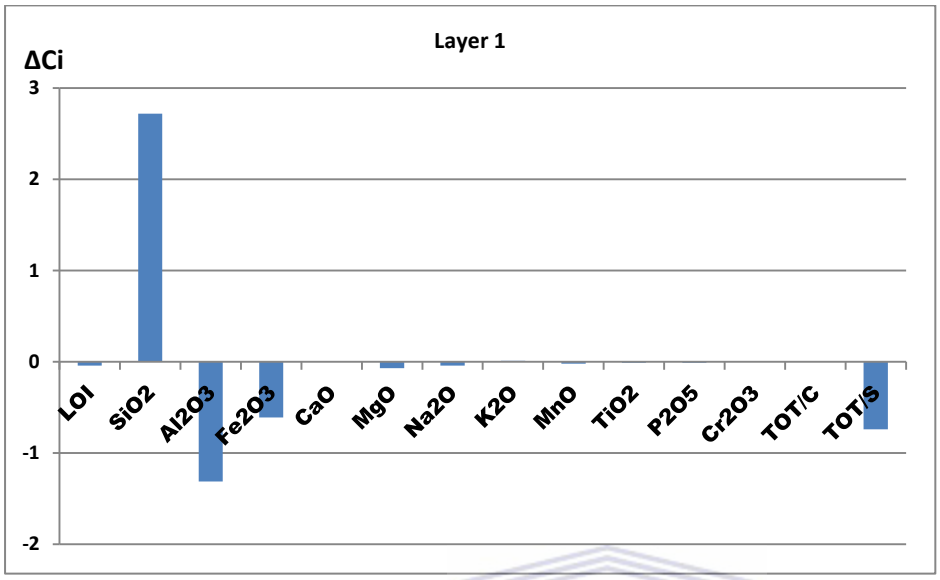

Figure 32: Graphical representation of the mass balance results for major elements, LOI, Tot/S and Tot/C in layer 1

Transition Layer (layer 2)

Layer 2 shows (Figure 33) an appreciable difference from layer 1, though most elements losses in layer 1 are observed in layer 2. The amount of element loss diminishes and the amount of element gain increases except for CaO, which shows slight loss.

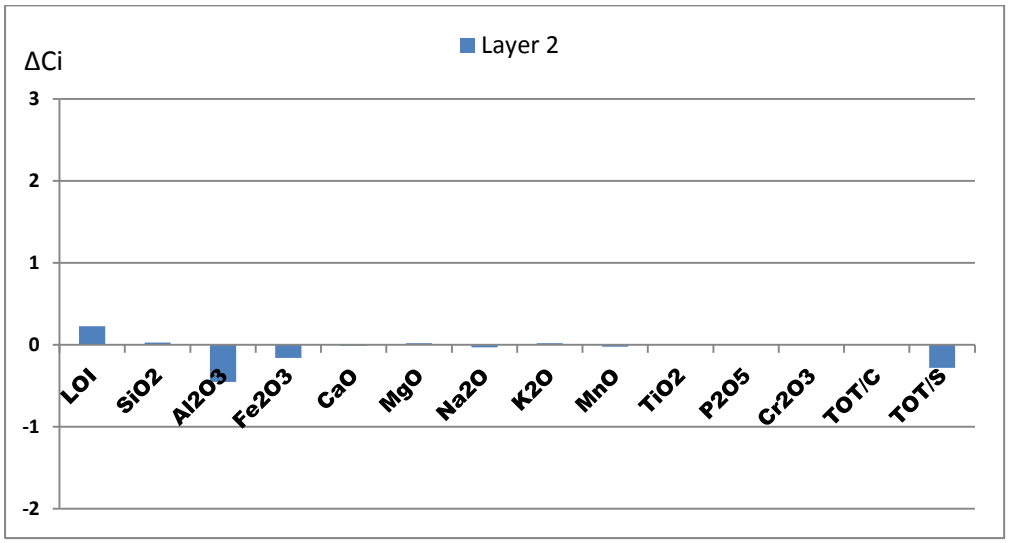

Figure 33: Graphical representation of the mass balance results for major elements, LOI, Tot/S and Tot/C in layer 2

Therefore, in layer 2, LOI, MgO, and K_2O are gained while Fe_2O_3, Na_2O, MnO, P_2O_5, Al_2O_3, CaO and TiO_2 show a loss though not as significant as layer 1. Silica remained unchanged with an approximately zero mass balance result thus suggesting no pronounced gain or loss.

Au-Fe (reddish) rich layer (layer 3)

Layer 3 shows enrichment in LOI (volatiles), K_2O, CaO, Fe_2O_3, Tot/S and MgO, while SiO_2 and Na_2O are loss and oxides of Al and P remain constant (Figure 35).

In this layer, there is prominent or significant enrichment in oxides of Ca, Fe and Mn. The enrichment in Fe confirms the presence of hematite as it is the only layer that hematite can be found. Also, the shows that the layer is a ferruginised layer with high presence Fe_2O_3 than any other layer. The enrichment in S shows the tendency of enrichment of this layer in sulphides.

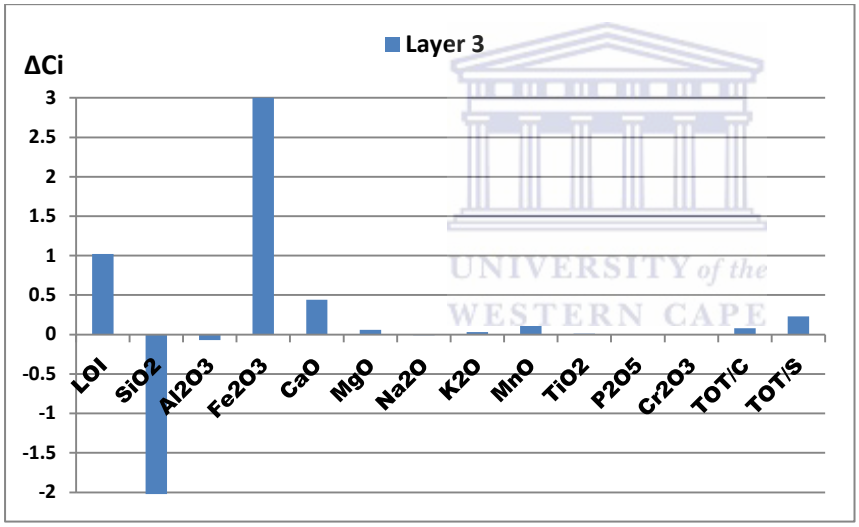

Figure 34: Graphical representation of the mass balance results for major elements, LOI, Tot/S and Tot/C in layer 3

The enrichment of CaO shows the presence of carbonates such as $CaSO_4$ or $CaCO_3$, possibly due to addition of additives to the tailings.

Un-oxidized Layer (layer 4)

Finally, Layer 4 shows a very slight gain and loss (Figure 36)as compare to the bottom samples indicating similarity in their constituent except for a slight gain in Si and loss in Al which could indicate and confirm that the bottom layers are least altered.

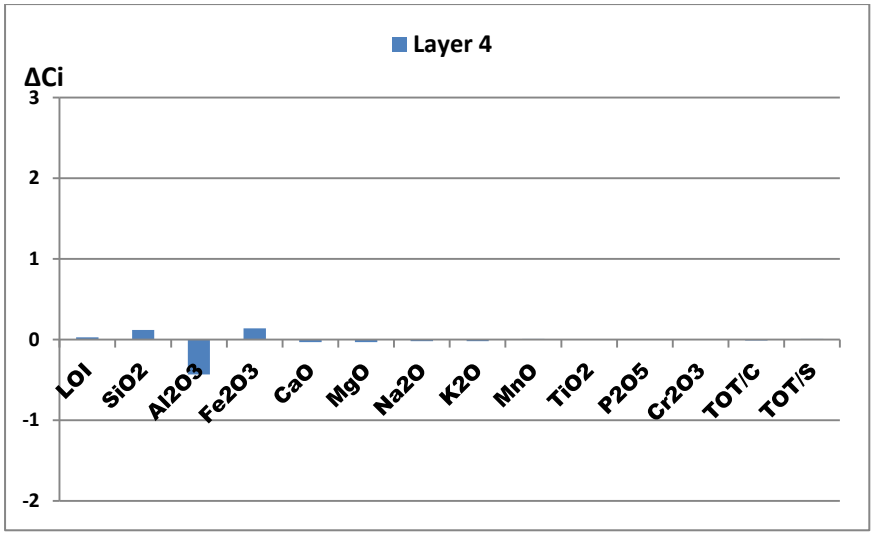

Figure 35: Graphical representation of the mass balance results for major elements, LOI, Tot/S and Tot/C in layer 4

6.5.2.2 Mass balance results for trace elements

Out of all elements analysed for, Ba, Co, U, Mo, Cu, Pb, Zn, Ni, As, Au, Sb, C and Bi are selected because they are chalcophiles or of significant importance.

As observed from each layer (Figure 36), there exists a distinct variation in their mass balance results. In layer 1, the entire elements listed above (Ba, Co, U, Cu, Zn, Ni, As, Au, Sb, C and Bi) except Pb and Mo, shows loss in values. Mass balance results of Co, Cu, Zn, Ni, and As suggest the depletion of sulphides and the oxidised state of layer 1 as compare to other layers.

In layer 2, Co, U, Pb, Zn, Ni,As, Au, Sb, C and Bi show a loss but not as significant as layer 1 (Figure 37). Layer 1 has a maximum value of about over -29.95 to about -0.40 for most elements loss, as compared to layer 2 that has ΔCi of -29.95 as the maximum. In layer 2, Mo, Cu, are gained and Ba remains unchanged. This layer relatively reflects an oxidising zone just like layer 1.

Layer 1 show substantial loss in pH and gain in EC indicating an oxidising environment in which heavy metals such Co, U, Zn, Ni, As, Sb, and Bi are leached. The gain in Pb could be as a result of the presence of its sulphide (unreactive), because as other elements are loss its concentration increases.

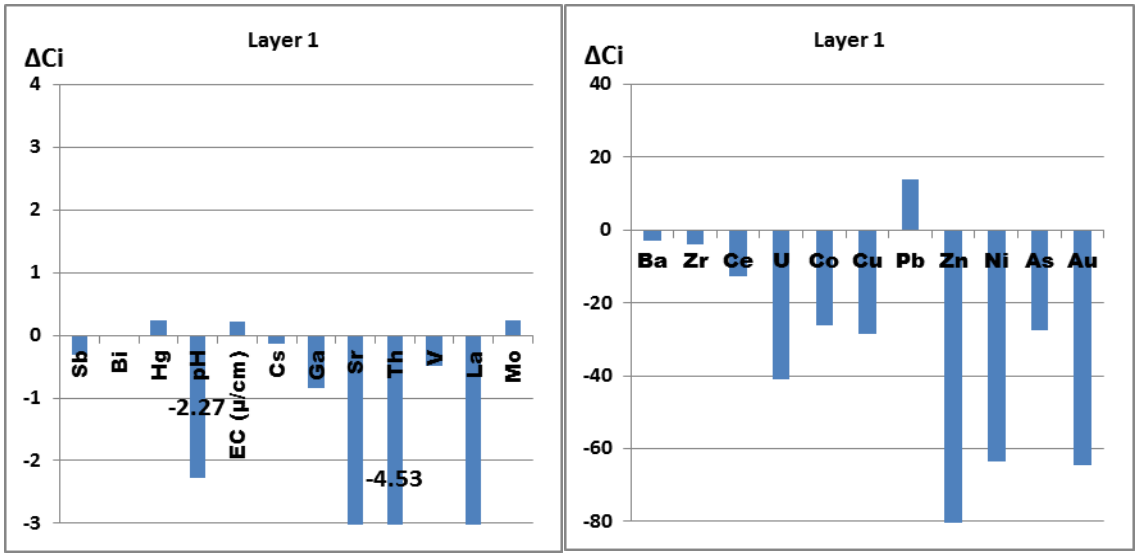

Figure 36: Graphical representation of the mass balance results for selected trace elements in layer

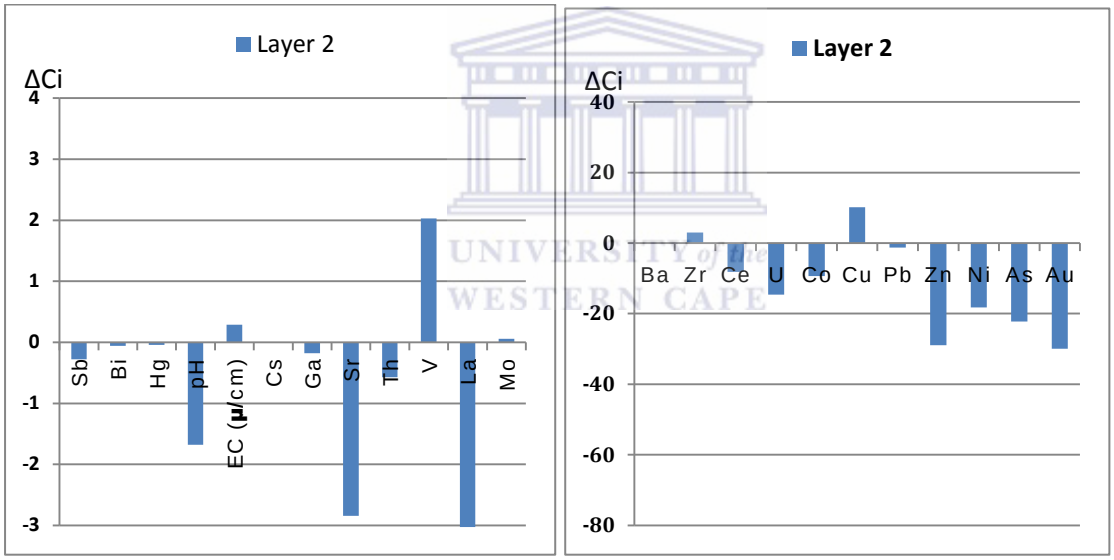

Figure 37: Graphical representation of the mass balance results for selected trace elements in layer 2

In the case of layer 3 (Figure 38), Ba, Co, Mo, Cu, Pb, Zn, Ni, As, Au, Sb, C and Bi show significant enrichment, while U only shows loss. This layer shows high enrichment in Co, Au and C, which makes this, layer a good target for gold mining. From the statistical result, Co relates to gold and this is accounted for because of the high enrichment of Au and Co, and because of a similar trend in composition.

As observed that this layer shows loss in SiO_2, this might account for the enrichment of this layer.

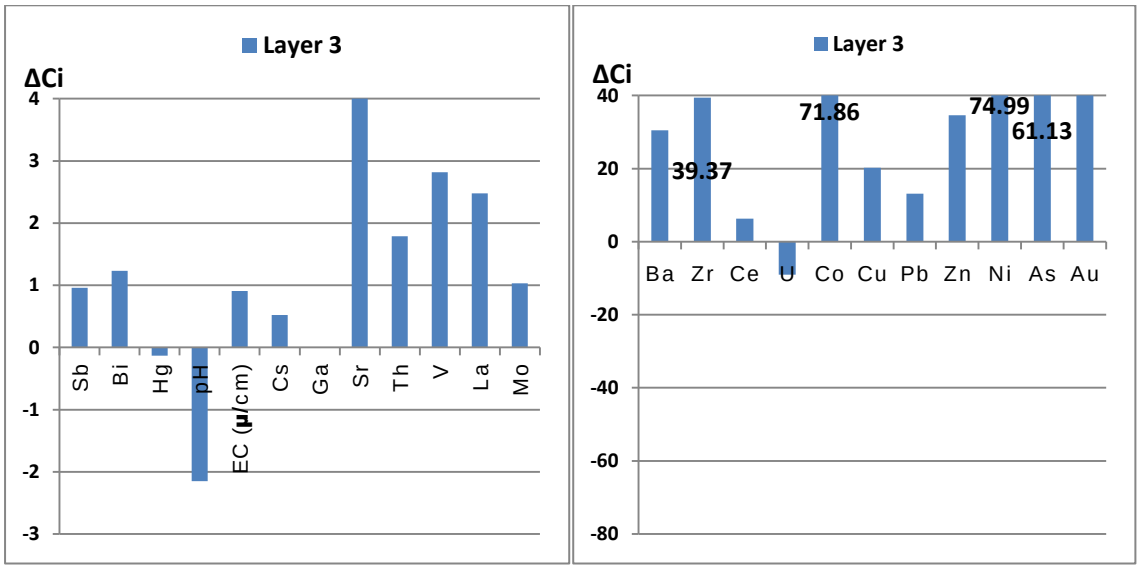

Figure 38: Graphical representation of the mass balance results for selected trace elements, pH and EC in layer 3

Finally, layer 4 shows an usual variation, in which some elements are loss and some gain. Co, Mo, Cu, Zn, Ni, As are gained (Cu was significantly gained) while U, C, Pb, and Au were loss and Ba remain constant (Figure 39).

Since most of these elements have high values in ppm, changes in layer 4 and the bottom samples, show less variation, which can be easily accounted for as normal variance.

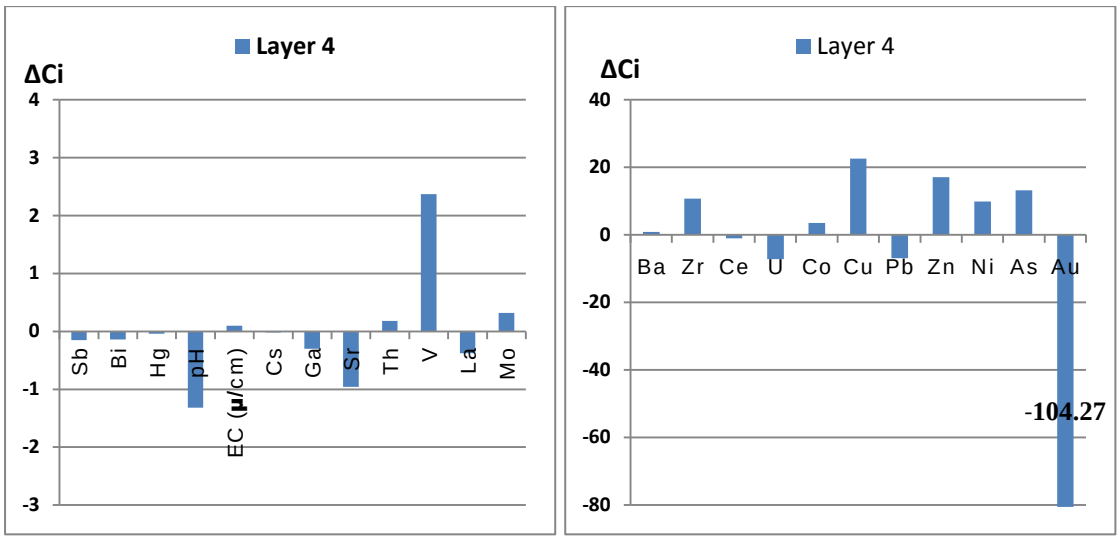

Figure 39: Graphical representation of the mass balance results for selected trace elements in layer 4

In summary, Layer 1 shows significant depletion in chalcophiles and other elements except silica compared to layer 2. A diminishing trend in depletion was observed in layer 2. Layer 3 shows the high or significant enrichment of chalcophile elements, hematite and sulphides.

The % overall mass change for layers is highest in layer 1, indicating that it is the most altered layer (overall mass change 0.60%), next to it is layer 3 (overall mass change 0.43%), which shows high enrichment. Afterward, then layer 2 (overall mass change 0.18%) shows why it is the transition zone and layer 4 (overall mass change 0.07%), showing a slight difference as expected.

6.5.3 The Geochemical Mass Balance (GMB) prediction model

The GMB prediction model was used to predict the rate of AMD generated over the period of the tailings dam existence.

The formula used was Culmulative rate = $\Sigma^{i}_{n}\ \Delta Ci/T$ in which ΔCi is the loss or gain for element i, T is the time of existence in years and n is the number of element analysed for and i is the element analysed for.

Afterward the average of the culmulative rate is done to give the actual rate of depletion or enrichment in layers.

From the result in Table 15, 0.122% of elements in layer 1 are loss yearly while 0.042% of elements in layer 2 are loss.

Table 15: Rate of AMD generated in respect to time

Analysis	Layer 1	Layer2	Layer 3	Layer 4
Cul. Rate (kg/tonne/yr)	**-6.321**	**-2.195**	**13.872**	**-1.228**
Max	**-6.610**	**-2.467**	**-0.293**	**-2.976**
Min	**0.289**	**0.272**	**14.165**	**1.748**
Av. Rate(kg/tonne/yr)	**-0.122**	**-0.042**	**0.267**	**-0.024**
Proportional loss **stoich. Rate**	**5.146** **5.000**	**1.787** **2.000**	**-11.294** **11.000**	**1.000** **1.000**

Layer 3 shows a noticeable enrichment that indicates that certain portion of elements leached from layer 1 and 2 are trapped within the Layer 3. Therefore, it could be said that 0.164% (±0.02%) of the tailings dam's bulk composition is leached yearly.

6.6 Summary of results

The results given above based on cluster analysis, factor analysis and geochemical mass balance can be summarised as follows:

From the cluster analysis, samples are grouped into four clusters defined based on their enrichment in siliceous materials and clay-rich materials.

The relative abundance of SiO_2 for the cluster is defined as follows: Cluster 1a> Cluster 1b> Cluster 2b> Cluster 2a (as defined by the discriminant analysis) while the relative abundance of Al_2O_3 is defined as Cluster 2b> Cluster 2a> Cluster 1b> Cluster 1a

Most of the samples characterized by cluster 1a and 1b dominated the first few layers, which entails the oxidized layer. Cluster 2a characterized the reddish layer and samples closed to this layer. Most samples in cluster 2b falls within the un-oxidized layer.

Borehole T011 shows an absolute different representation of samples in clusters as compared to others because all samples present in T011 are classified by Cluster 1a and 1b (this indicates a compositional variation to other drilled holes).

Four major factors are responsible or determine the compositional properties of the boreholes and layers. Factor 1 accounted for 37.25% of the total variance and is defined by Al_2O_3, Na_2O, K_2O, P_2O_5, Cr_2O_3, Cs indicating the rich presence of clayey materials

Factor 2 accounted for 25.49% of the total variance and is defined by LOI (volatiles), CaO, MnO, P_2O_5, TOT/C, TOT/S, Ba, Co, Cs, Th, Pb, Ag, Ni, As, Bi and indicating the carbonate-rich zone in an oxidizing or a potential oxidizing environment.

Factor 3 accounted for 15.69% of the total variance, defined by LOI, Fe_2O_3, MgO, TOT/S, Co, Zn, Ni, Au, Sb, EC, and is most depleted in SiO_2. This indicates the presence of ultra-mafic minerals and gold in high presence.

Factor 4 accounted for 21.57% of the total variance and defined by TiO_2 and loss in Mo.This is the only factor that does not show any correlation to SiO_2.

Therefore, it could be said that the relative abundance SiO_2 in the factors is determined based on how negatively correlated the factors are defined as follow: Factor 4>factor 1>factor2>factor3. It should be noted that this is in regards to the association of factors with SiO_2.

From the geochemical mass balance results, the oxidized layer (layer1) shows significant depletion in chalcophiles and other elements except silica.

In the transition layer (layer 2), LOI (volatiles), MgO, and K_2O are gained while Fe_2O_3, Na_2O, MnO, P_2O_5, Al_2O_3, MgO, CaO and TiO_2 show a loss though not as significant as layer 1. Silica content remained unchanged as the mass balance result was approx. zero. This indicates that oxidation process as started within this layer.

Layer 3 is Au/Fe rich and shows the high or significant enrichment of chalcophile elements than the other.

The least altered layer (layer 4) shows only slight gain and loss of elements and oxides as compare to the bottom samples indicating similarity.

The % overall mass change for layers is highest in layer 1, indicating that it is the most altered layer (overall mass change 0.60%), next to it is layer 3 (overall mass change 0.43%), which shows high enrichment. Afterward, then layer 2 (overall mass change 0.18%) shows that the oxidation process has started (that is why it is the transition zone) and layer 4 (overall mass change 0.07%), showing a slight difference as expected.

The IDW interpolation analysis shows that leachable sulphides and uranium are depleted because of their mobility in the top layer of the tailing dam.

In addition, at 7m depth, enrichment of elements is observed and the first two meters show high enrichment in SiO_2.

CHAPTER 7 Discussions and Conclusion

7.1 Discussions

This chapter discussed the results from chapter five (petrography) and six (geochemistry) in conformity with the aims and objectives of the study and attempted to answer the research questions (Section 1.3).

Multivariate statistical evaluation of data comprising of major elements and heavy metals present in the tailing dam selected and spatial analysis by GIS as well as geochemical mass balance techniques were utilised to achieve the aim and objectives of the study as follows:

- To evaluate the mineralogical and geochemical composition of the tailing dam to understand the geological characteristics of and link between each zone (oxidized, transition and un-oxidized).
- To use multivariate statistical analysis tool to assess the potential leachable heavy metals loads and the risk of heavy metals load present in the tailings dam, its associations and inter-relationships.
- To map the distribution of elements using GIS spatial interpolation and geochemical mass balance
- To predict the possible source of AMD pollution loads, temporary AMD load from the tailing dam sampled and its effect on the environment using a geochemical mass balance and other prediction techniques.

The knowledge of the mineralogical and geochemical composition of the tailing sampled is significant because it reflect the behaviour of minerals and elements within the various zones.

The petrography (as described in Chapter 5) was able to characterize the tailing dam into four distinct layers. This differs from other reports of three layers. This indicated that the third layer is only peculiar to the Mogale gold tailing. The main layers that characterized gold tailing are the oxidized layer, transition layer and un-oxidized layer (Bezuidenhout & Rousseau, 2006 ; Nengovhela, et al., 2006). In regards to the Mogale gold tailings, the presence of a ferruginised layer was observed in-between the least altered/un-oxidized layer.

From the results in Section 5.2, chapter 5, the five drilled holes (T004, T008, T009, T010, and T011) sampled can be classified into four distinct layers. Nengovhela, et al., (2006) classified some selected tailings dams into three zones, which are the oxidized, transition and reduced zone (otherwise known as least altered/un-oxidized zone), except for the third layer

(ferruginised zone) which may be peculiar to Mogale tailing dam. Tailings dams in the Witwatersrand was said to have been oxidized to a depth 2m by Oelofse, et al., (2007), while to 3.5m by Nengovhela, et al., (2006) and the transition zone lies between the oxidized and un-oxidized zone. The oxidised layer varied from 2.4m to 3.2m from the results within all five boreholes.

Generally, Witwatersrand gold tailings are constrained within a relatively narrow compositional range (similar to the mineralogical composition of the typical Witwatersrand's gold reef). The minerals identified in this study conform to those commonly found in ores and tailing dams of the Witwatersrand basin (Rosner, 2000; Nengovhela, et al., 2006; Tutu, et al., 2008) as shown in Section 5.3, Chapter 5.

The XRD was able to detect a total number of nine different minerals (quartz, muscovite, pyropyllite, gypsum, jarosite, delhayelite, hematite, pyrite and clinochor are present). Quartz is by far the most dominant mineral in all the samples, while pyropyllite was the second in abundance (Rosner, 2000; Nengovhela, et al., 2006). Jarosite, pyrite and gypsum as a product of additives showed variable content in the samples, and their relative proportions are indicators of oxidized state of the tailings and extent of AMD generation (Hobbs & Cobbing, 2007; Oelofse, et al., 2007).

From these results, the actual percentage of minerals present is not known, but their relative abundance has been estimated through the peaks from the XRD charts. The major minerals are quartz, pyrophyllite, muscovite, and clinochlore, minor minerals are pyrite, delhayellite while trace minerals are gypsum, hematite, jarosite. The mineralogy results could corroborate the percentage of minerals in the tailings dam as given in literature but only show their prominence (Rosner, 2000; Bezuidenhout & Rousseau, 2006). The results show the presence of quartz in abundance in every sample result. Samples at the top are unique because of the absence of pyrite, indicating that the first and second meter might have been completely oxidized.

The presence of delhayellite has not been observed in any mineralogical of the Witwatersrand gold ore and tailings, except for this study and therefore questionable. Due to its unreactive nature, delhayellite could have been present ever since the start of the tailing dam but not detected because of its minute concentration in the ore (if present). Delhayelite is known to be an aluminosilicate that can be found within the framework of rhodesite meroplesiotype series (Ferraris & Angela, 2005).

Primarily, the oxidation of sulphide minerals and additives (such as lime) resulted in the production of secondary minerals such as jarosite and gypsum (Rosner, 2000; Vermeulen, 2001). There is a variation in jarosite in respect to pyrite because its peaks become more prominent in the absence of pyrite. It was observed that jarosite is dominant only in samples on or closely beneath the tailing dam surface where there is no or slight trace of pyrite (Nengovhela, et al., 2006). As we move down the tailings, pyrite occurred in samples as from depth of 3m below the surface.

The reddish (ferruginised) layer found around 7.4m to 8.3m does not appear to be part of the oxidized zone. Its formation could be due to the infiltration of weathered tailings contents downward. No literature obtained highlighted the presence of this reddish layer and therefore could be peculiar to Mogale tailing dam.

Furthermore, most of the samples contain gypsum, a secondary mineral that can be suspected to have its origin from dolomite or lime, which was added for neutralisation of AMD. Its presence was more pronounced in surfaced samples than beneath. Gypsum was found throughout the section but was most concentrated in the first 2 to 3 meters.

The major elements contents occurred in the following decreasing order: SiO_2(84.24%)> Al_2O_3(6.25%)> LOI(3.28%)> Fe_2O_3(2.64%) >CaO(0.43%)> MgO(0.35%)> K_2O(0.32%)> TiO_2(0.24%)> Na_2O(0.07)> Cr_2O_3(0.04%)> MnO (0.02%) ≈ P_2O_5(0.02%). The total carbon content of up to 0.2 %wt is indicative of a significant content of organic matter in the mine tailings (Rosner, 2000). These contents and trends are in line with values reported for Witwatersrand tailings by Rosner, (2000). The total sulphur content (Table 5) ranges from 0.26-2.19% and was responsible for the highly significant potential acid generation capacity of the tailings dam (Nengovhela, et al., 2006). Low total sulphur in the uppermost layer (Bezuidenhout & Rousseau, 2006) suggests an extensive depletion in sulphides in the horizon.

Some trace elements (such as U, As, Zn, Ni, Co, and Cu) showed low content in the first few meters and a high content at the base of the dam. This showed that these trace elements are mobile. Some trace elements such as U and Au showed few extremely high values and this accounted for their high standard deviation. The high concentration of trace elements (such as U, As, Co, Cu, Pb, Zn, and Ni) at the least weathered zone could be compliable with the its high content in the Witwatersrand basin (Rosner, 2000) where gold has been mined

The data from this investigation show that the Mogale tailing dam is generally acidic. The low pH may result from percolation of weathering solution (Akcil & Koldas, 2006), acid mine drainage and related heavy metals from the upper levels into the underlying layers (Afriyie- Debrah, 2009). Nengovhela, et al., (2006) observed that the tailings dams in the Witwatersrand are generally acidic in the first 10meters. This implies that the acid potential is greater than the neutralisation potential (Vermeulen, 2001)despite the presence of buffer reactions within upper ten meters of the tailings dam.

In order to assess the distribution pattern of the potential leachable heavy metals loads and the risk of heavy metals load present in the tailings dam, its elemental associations and inter-relationships pattern were determined by multivariate statistical analysis tools (Aucamp & van Schalkwyk, 2003; Heikkinen, et al., 2009). This analysis involved both the cluster and factor analysis.

Two main clusters were observed which further sub-divide into two sub-clusters each. This showed that the samples could be classified into four clusters for clarity sake. Samples in cluster 1 are commonly defined by high content in SiO_2 while those in cluster 2 are low in SiO_2 but enriched in Al_2O_3. The relative abundance of SiO_2 for the cluster was defined as follows: Cluster 1a> Cluster 1b> Cluster 2b> Cluster 2a (as defined by the discriminant analysis). Samples that are classified in cluster 1 are mainly found in the first 3 meters of the tailings.

The factor analysis identified four major controls of elements in the tailing dam. 1) Factor 1 with positive scores for Al_2O_3 Na_2O, K_2O, P_2O_5, Cr_2O_3, Cs (which define this group) and negatively correlated to SiO_2 underpins the enrichment of clays. Al_2O_3 underpins the enrichment of clays (Al_2O_3-rich). 2) Factor 2 displayed positive scores for CaO, LOI (volatiles), MnO, P_2O_5, Tot/C and negatively score for SiO_2 indicating the carbonates zone in an oxidizing environment (calcium-rich). The positive score for CaO reveals the presence of additives products (such as $CaSO_4$) during mineral processing. These additives (mostly lime) are added to buffer acid generating potential of the sulphide minerals before disposing the mine tailings (Naicker, et al., 2003; Hobbs & Cobbing, 2007). 3) Factor 3 showed positive scores for LOI, Fe_2O_3, MgO, Tot/S, and negative scores to SiO_2. The positive score for Fe_2O_3 and total sulphur underpins the presence of sulphides in ore (such as pyrite) responsible for the tailings acid potential generation. 4) Factor 4 shows positive scores for TiO_2, which is

associated with the presence of refractory titanium-rich minerals in ore (Rosner, 2000; Oelofse, et al., 2007).

Heavy metals that mainly affects the ecosystem and man are As, U, Cd, Zn, Co, Mo, Pb, Ni, and Cu (Lee, et al., 2005; Cheng, et al., 2009; Price, 2009; Wright & Welbourn, 2009) (Cheng, et al., 2009; Price, 2009; Lee, et al., 2005; Wright & Welbourn, 2009). From the results in section 6.1.2, Chapter 6, As, Co, Cu, Pb, Zn, Ni of sulphide origin (Aucamp & van Schalkwyk, 2003; Dold, 2005) anomalous and are highly correlated with total sulphur and Fe_2O_3, which in addition to U could be transported into the ecosystem.

Based on the overall potential acidity that can be generated, the total %S (Table 12) is assumed to be synonymous to the total amount of sulphide present in the tailings (INAP, 2009) that can be oxidized, and this determined the amount of acidic leachates generated. From the result in Table 12, the Net Acid Producing Potential (NAPP) is less than 1 for all samples, indicating that it is acid generating at all layers.

For the Cumulative Net Acid Producing Potential (NAPP) (Dold, 2005; INAP, 2009), all samples are less than 1 except MT001, MT002, MT018-1 and MT038 (Table 12) which are greater than 1 but less than 2. Except for MT018-1, all others are topmost layers. This shows that the tailings dam has the potential to generate acid mine drainage if exposed to oxidation, and this could account for the general acidic pH of the tailings dam(implies that the neutralisation potential is lower than the acidic potential) (INAP, 2009). This result above is based on assumption and therefore could not quantify the actual acidic potential because not all sulphides present (such as PbS) could have been oxidised.

The IDW interpolation analysis (Section 6.5.1, Chapter 6) reflects the distribution pattern of elements down depth (Setianto & Triandini, 2013), and their relative behaviour based on the factor analysis. The significance of the knowledge of the elemental distribution pattern assisted in understanding general trend of mobile and non-mobile elements and species in tailing dam sampled. The high concentration of SiO_2 and low concentration of Al_2O_3 and tot/S in the first two meter depicts depletion and this fall within layer 1.

Sulphides and uranium show a distinct depletion trend indicating that the surface has exposed to extensive leaching (Naicker, et al., 2003). The high presence of CaO in the first meter could be because of carbonates formed from neutralisation process and deposited as salts. There is enrichment of sulphides coupled with low SiO_2 at a depth below 7m, which

coincides with the ferruginised layer. This layer is probably a sink for elements emanating from the upper layers. Also, from the IDW interpolation, it could be inferred that tailings from the 3m, 8m and 9m could be economically viable if assessed for U and Au and therefore the tailing should be reclaimed.Therefore, the tailing dam could be said to be uraniferous-gold tailing (Winde, et al., 2004). The concentration of Au indicates that tailings could still be reprocessed for gold.

The geochemical mass balance results show a variable loss and gain in the contents of major oxides and trace elements in each horizon with depth. The results further show that oxide/ trace element loss is highest in the topmost layer where the weathering is most intense and decreases down depth. A gradient occurs between an upper zone with reddish colour (that is, through a brownish zone to a greyish basal zone). The loss and gain of oxides/ trace elements (Appendix F) as quantified can be used to predict a temporal rate of AMD generation, if the actual age of the dam is known (Saria, et al., 2006).

Based on the geochemical mass balance analysis (Table 14), layer 1 shows significant depletion in chalcophiles, but highly enriched in SiO_2. In layer 1, the gain for the major oxides varied from 0-2.72%; while the loss varied from 0-1.31% (loss indicates –ve; gain indicates +ve). In layer 2, the gain for the major oxides varied from 0-0.23%; while the loss varied from 0-0.451%. A diminishing trend in depletion was observed in layer 2.

In layer 3, the gain for the major oxides varied from 0-6.53%; while the loss varied from 0-8.35%. Layer 3 shows the high or significant enrichment than any other layers and could be said to contain more of Au and sulphides. Layer 4 shows slight variation in elemental composition. The mass balance results for the trace elements (except Au) show that the weight loss in ppm followed a trend: layer 1 > layer 2> layer 4> layer 3. Layer 1 shows the greatest loss and layer 3 shows the greatest gain. The total sulphur shows a specific trend in layers as follow: the % of loss of layer 1 > layer 2> layer 4> layer 3.

Therefore, the oxidized zone could be said to vary within the borehole depend on position of the tailings. This ranges from 2.8 -3.2m.

Since the tailing dam was built in 1952 and giving a period of 2 years of depositional time, it was assumed that any prominent oxidation process starts 60 years ago. Researchers speculated on the effect of years a tailing dam is built (Saria, et al., 2006; Nengovhela, et al., 2006), but remain a major factor to consider. From table 16, it shows that layer 1 is the most

leached surface and about 0.122% of the layer is leached yearly. Layer 3 shows high presence of clayey materials and extreme low value in SiO_2 as compared to other layers. This increases its retention capacity leading elements deposition. Elements leached downward are trap within the third layer. This accounted for the highly moisturised layer 4 since leachates cannot drain out easily.

Over time, a large proportional of the tailings have been leached. The AMD leachates have been transported away along pathways (along the slope of the dam). It should be noted the steepness of the tailing determines the efficiency of the transport of AMD leachates.

The tailing dam show a general enrichment in sulphide related materials and U (outside the oxidized zone) (Figure 36-37). Nevertheless, for economic value, the presence of Au, and U is a source of attraction that could bring profit in mining and facilitate reclamation. The reddish layer shows high enrichment in Au (which ranges from 189.19-1417.5 ppb) and a target in which high values of profitable trace element in respect to a tonne of the tailings.

From the IDW interpolation(Section 6.5.1.6), it could be inferred that tailings from the 3,8 and 9m could be economically viable if assessed for Au and U and therefore the tailing should be reclaimed. In addition, U shows an average of about 45ppm, and with a maximum value of 655ppm, and could be worth mined for in the tailings dam.

From the above submission, Au, and U could be of economic value, if this tailing dam is reprocessed.

7.2 Conclusion

This study was set based on assessment and prediction of AMD loads in gold tailings dam, Witwatersrand Basin using Mogale tailings dam as a case study. Various tools and methods were employed to achieve this aim and answer the research questions.

For assessment studies, petrography (physical characteristics and mineralogical studies) and multi-element analysis were used to determine the physical characteristics, and have an overview of minerals and elemental composition of the tailing dam. Also, multivariate statistics was used to characterise the tailing dam based on association, relationship and the compositional patterns of major elements and trace elements present within layers. The IDW interpolation using GIS was able to give an overview of elements spatial distribution with depth in the tailing dam.

For prediction studies, geochemical mass balance was used to predict the extent in which the tailings dam has been oxidised over a period.

The mineralogy highlighted the minerals present in the tailings dam, but not quantified. The mineralogical composition was similar to previous researches done except for the presence of delhayelite and these minerals varied within the samples from zone to zone. If the minerals present were quantified, it would have assisted the assessment studies because minerals could be related directly to the major oxides composition, which serves the framework of the tailings.

The determination of the elemental composition and use of multivariate statistical analysis were effective in the assessment by revealing the various associations and relationships that affected the compositional range of elements present which are responsible and available for oxidation within the tailings dam.

This study showed that the tailings dam has the potential to generate acid mine drainage if exposed to oxidation, and this could account for the general acidic pH of the tailings dam which implies that the neutralisation potential is lower than the acidic potential.

The IDW interpolation gives a bull's eye view of how elements are distributed within the tailing dam, but a more precise model(such as kriging) could be employed in latter studies and create a comparison of models. Since interpolation was based on every meter, samples that fall in-between each meter could also contain relevant information but was not taken into the distribution (interpolation) model.

The prediction based on geochemical mass balance remained questionable because it has not been generally accepted and was based on limited parameters available. Since the prediction was based on the selected element mass alteration, a more precise result could have been attained if prediction is based on the overall elemental alteration (including rare earth elements present) and specific depth intervals. Also, a comparison results of prediction based on geochemical mass balance for various tailings dam could serve as a measure of the degree of oxidation.

Though all the research questions were attempted, the actual acid potential and neutralization potential were not ascertained but was based on assumption that the total sulphur was responsible for acid potential and the presence of CaO and MgO could be responsible for the neutralisation potential of the tailings dam as employed by other prediction researches.

In summary, the application of the tools used in this study to assess and predict AMD loads of other tailings dams, and making comparisons could lead to greater revelations and help to determine which of the tailings dams need urgent remediation action. Further research will be based on this. In addition, the availability of other parameters such as oxygen concentration, moisture content and retention capacity of the tailing dam should be known and considered for latter studies.

7.3 Recommendations

The following recommendation can be given.

The interaction between the oxidized zone and transition zone should be given more attention, to determine the actual extent of damage.

The incorporation of data from other tailings dams in the assessment and prediction using the tools employed in this study will give a comparison of results in which remediation process can be based on.

The mass balance calculation should be done based on individual element since the rate of oxidation and mobility of elements differs.

Data from soil and water surrounding the tailings dam should be incorporated into mass balance calculation, to determine if there is any trend of AMD heavy metals transport and correlation.

Reference

Abzalov, M. 2008, "Quality control of assay data: a review of procedures for measuring and monitoring precision and accuracy", *Exploration and Mining Geology*, vol. 17, no. 3-4, pp. 131-144.

Adler, R.A., Claassen, M., Godfrey, L. & Turton, A.R. 2007, "Water, mining and waste: an historical and economic perspective on conflict management in South Africa", *The Economics of Peace and Security Journal*, vol. 2, no. 2, pp. 32-41.

Afriyie–Debrah, C. 2014, "Acid Mine Drainage: Effect of acid mine drainage on water and soil resources within the Bogoso/Prestea Mine Resource.(Bogoso Concessional Area)", .

Akcil, A. & Koldas, S. 2006, "Acid Mine Drainage (AMD): causes, treatment and case studies", *Journal of Cleaner Production*, vol. 14, no. 12, pp. 1139-1145.

Akpor, O. & Muchie, M. 2010, "Remediation of heavy metals in drinking water and wastewater treatment systems: Processes and applications", *International Journal of Physical Sciences*, vol. 5, no. 12, pp. 1807-1817.

Alkarkhi, A.F., Ismail, N., Ahmed, A. & Mat Easa, A. 2009, "Analysis of heavy metal concentrations in sediments of selected estuaries of Malaysia—a statistical assessment", *Environmental monitoring and assessment*, vol. 153, no. 1-4, pp. 179-185.

Alloway, B.J. & Alloway, B. 1995, "Heavy metals in soils",.

Anglo American 1995. A basic course on slimes dams (South African gold paddock dams) for metallurgists. Tailings unit, Geotechnical section, Civil engineering department, Anglo American Corporation of South Africa.

AngloGold Ashanti. 2004. Case studies. Woodlands Project – good progress being made with phytoremediation project. Environment – AngloGold Ashanti Report to Society.

Aucamp, P. & Van Schalkwyk, A. 2003, "Trace element pollution of soils by abandoned gold mine tailings, near Potchefstroom, South Africa", *Bulletin of Engineering Geology and the Environment*, vol. 62, no. 2, pp. 123-134.

Bezuidenhout, N., & Rousseau, P. D. (2006). *Investigations into the depth and rate of weathering on Witwatersrand gold tailings dam surfaces as key information for long-term*

ARD risk assessments. 7th International Conference on Acid Rock Drainage (ICARD) (pp. 128-139). 3134 Montavesta Road, Lexington, KY 40502: the American Society of Mining and Reclamation (ASMR).

Blowes, D. & Ptacek, C. 1994, "Acid-neutralization mechanisms in inactive mine tailings", *The environmental geochemistry of sulfide mine-wastes, Short course Handbook,* vol. 22, pp. 271-292.

Chen, M. & Ma, L.Q. 2001, "Comparison of three aqua regia digestion methods for twenty Florida soils", *Soil Science Society of America Journal,* vol. 65, no. 2, pp. 491-499.

Cheng, H., Hu, Y., Luo, J., Xu, B. & Zhao, J. 2009, "Geochemical processes controlling fate and transport of arsenic in acid mine drainage (AMD) and natural systems", *Journal of hazardous materials,* vol. 165, no. 1, pp. 13-26.

Chevrel, S., Courant, C., Cottard, F., Coetzee, H., Bourguinon, A. & Ntsume, A. 2003, "Very high resolution remote sensing coupled to GIS-based environmental assessment–East Rand gold field, South Africa", *Report BRGM/RP*, .

Chunhacherdchai, L., Chotpantarat, S. & Tongcumpou, C. 2011, "Investigating of heavy metals in different depths of soil tailings from Akara Gold Mine, Thailand using three-steps modified BCR sequential extraction", *Proceedings of International Conference on Environmental Science and Technology (ICEST 2011).*

Coetzee, H. 1995, "Radioactivity and the leakage of radioactive waste associated with Witwatersrand gold and uranium mining", *Merkel, BJ, Hurst S., Löhnert EP & Struckmeier W.*

Coetzee, H., Winde, F. & Wade, P. 2006, *An Assessment of Sources, Pathways, Mechanisms and Risks of Current and Potential Future Pollution of Water and Sediments in Gold-mining Areas of the Wonderfonteinspruit Catchment: Report to the Water Research Commission,* Water Research Comission.

Dankert, B.T. & Hein, K.A. 2010, "Evaluating the structural character and tectonic history of the Witwatersrand Basin", *Precambrian Research,* vol. 177, no. 1, pp. 1-22.

Dimitrova, R.S. & Yanful, E.K. 2012, "Factors affecting the shear strength of mine tailings/clay mixtures with varying clay content and clay mineralogy", *Engineering Geology*, vol. 125, pp. 11-25.

Dold, B. 2005, "Basic concepts of environmental geochemistry of sulfide mine-waste", *Mineralogía, geoquímica y geomicrobiología para el manejo ambiental de desechos mineros.XXIV Curso Latinoamericano de Metalogenia*, vol. 22, pp. 1-36.

Doye, I. & Duchesne, J. 2003, "Neutralisation of acid mine drainage with alkaline industrial residues: laboratory investigation using batch-leaching tests", *Applied Geochemistry*, vol. 18, no. 8, pp. 1197-1213.

Durand, J. 2012, "The impact of gold mining on the Witwatersrand on the rivers and karst system of Gauteng and North West Province, South Africa", *Journal of African Earth Sciences*, vol. 68, pp. 24-43.

Dyson, L.L. 2009, "Heavy daily-rainfall characteristics over the Gauteng Province", *Water SA*, vol. 35, no. 5.

Eriksson, P., Altermann, W., Catuneanu, O., Van der Merwe, R. & Bumby, A. 2001, "Major influences on the evolution of the 2.67–2.1 Ga Transvaal basin, Kaapvaal craton", *Sedimentary Geology*, vol. 141, pp. 205-231.

Estifanos, S. 2013, "Heavy Metal Pollution Assessment by Partial Geochemical Extraction Technique", *Momona Ethiopian Journal of Science*, vol. 5, no. 1, pp. 71-88.

Expert Team of the Inter-Ministerial Committee 2010, "Mine water management in the Witwatersrand Gold Fields with special emphasis on acid mine drainage", *Report to the Inter-Ministerial Committee on Acid Mine Drainage.Pretoria: Department of Water Affairs*, .

Ferraris, G. & Gula, A. 2005, "Polysomatic aspects of microporous minerals–heterophyllosilicates, palysepioles and rhodesite-related structures", *Reviews in mineralogy and geochemistry*, vol. 57, no. 1, pp. 69-104.

Frimmel, H., Groves, D., Kirk, J., Ruiz, J., Chesley, J. & Minter, W. 2005, "The formation and preservation of the Witwatersrand goldfields, the world's largest gold province", *Economic Geology 100th Anniversary Volume*, , pp. 769-797.

Gaikwad, R. & Gupta, D. 2008, "Review on removal of heavy metals from acid mine drainage", *Applied ecology and environmental research,* vol. 6, no. 3, pp. 81-98.

GDACE, 2007. *GDACE Mining and Environmental Impact Guide Chapter 2: The History and Economic Contribution of Mining,* Johannesburg: DIGBY WELLS AND ASSOCIATES, GROWTH LAB AND THE COUNCIL FOR GEOSCIENCE.

Gold-Bullion-Pro, 2012. *7 Interesting Facts About Gold Mining in South Africa.* [Online] Available at: http://www.goldbullionpro.com/7-interesting-facts-about-gold-mining-in-south-africa/

Günther, D., Quadt, A.v., Wirz, R., Cousin, H. & Dietrich, V.J. 2001, "Elemental analyses using laser ablation-inductively coupled plasma-mass spectrometry (LA-ICP-MS) of geological samples fused with Li2B4O7 and calibrated without matrix-matched standards", *Microchimica Acta,* vol. 136, no. 3-4, pp. 101-107.

Gresens, R.L. 1967, "Composition-volume relationships of metasomatism", *Chemical Geology,* vol. 2, pp. 47-65.

Guillén, M.T., Delgado, J., Albanese, S., Nieto, J.M., Lima, A. & De Vivo, B. 2012, "Heavy metals fractionation and multivariate statistical techniques to evaluate the environmental risk in soils of Huelva Township (SW Iberian Peninsula)", *Journal of Geochemical Exploration,* vol. 119, pp. 32-43.

Günther, D., Quadt, A.v., Wirz, R., Cousin, H. & Dietrich, V.J. 2001, "Elemental analyses using laser ablation-inductively coupled plasma-mass spectrometry (LA-ICP-MS) of geological samples fused with Li2B4O7 and calibrated without matrix-matched standards", *Microchimica Acta,* vol. 136, no. 3-4, pp. 101-107.

Haber, L.T., Allen, B.C. & Kimmel, C.A. 1998, "Non-cancer risk assessment for nickel compounds: issues associated with dose-response modeling of inhalation and oral exposures", *Toxicological Sciences,* vol. 43, no. 2, pp. 213-229.

Heikkinen, P., Räisänen, M. & Johnson, R. 2009, "Geochemical characterisation of seepage and drainage water quality from two sulphide mine tailings impoundments: acid mine drainage versus neutral mine drainage", *Mine Water and the Environment,* vol. 28, no. 1, pp. 30-49.

Hobbs, P. & Cobbing, J. 2007, "Hydrogeological Assessment of Acid Mine Drainage Impacts in the West Rand Basin, Gauteng Province", Rep. no. CSIR/NRE/WR/ER/2007/0097/C. CSIR

Janisch, P.R. 1986, "Gold in South Africa", *Journal of The South African Institute of Mining and Metallurgy*, vol. 86, no. 8, pp. 273-316.

Jolley, S., Freeman, S., Barnicoat, A., Phillips, G., Knipe, R., Pather, A., Fox, N., Strydom, D., Birch, M. & Henderson, I. 2004, "Structural controls on Witwatersrand gold mineralisation", *Journal of Structural Geology*, vol. 26, no. 6, pp. 1067-1086.

Kisser, M.I. 2005, *Digestion of solid matrices Part 1: Digestion with Aqua Regia Report of evaluation study*, .

Kumar, D. 2010, "Emerging Tools and Techniques for Mine Safety and Disaster Management" in *Natural and Anthropogenic Disasters* Springer, , pp. 332-365.

Law, J. & Phillips, G. 2005, "Hydrothermal replacement model for Witwatersrand gold", *Economic Geology 100th Anniversary Volume*, , pp. 799-811.

Lee, P., Kang, M., Choi, S. & Touray, J. 2005, "Sulfide oxidation and the natural attenuation of arsenic and trace metals in the waste rocks of the abandoned Seobo tungsten mine, Korea", *Applied Geochemistry*, vol. 20, no. 9, pp. 1687-1703.

Liefferink, M. 2012, "Environmental Risks and Hazards Pertaining to AMD and Radioactivity within the Witwatersrand Goldfields", *PowerPoint Presentation.Federation for a Sustainable Environment*, .

Longerich, H., Jenner, G., Fryer, B. & Jackson, S. 1990, "Inductively coupled plasma-mass spectrometric analysis of geological samples: a critical evaluation based on case studies", *Chemical Geology*, vol. 83, no. 1, pp. 105-118.

López-Moro, F.J. 2012, "EASYGRESGRANT—A Microsoft Excel spreadsheet to quantify volume changes and to perform mass-balance modeling in metasomatic systems", *Computers & Geosciences*, vol. 39, pp. 191-196.

Marsden, D. 1986, "The current limited impact of Witwatersrand gold-mine residues on water pollution in the Vaal River system", *Journal of The South African Institute of Mining and Metallurgy*, vol. 86, pp. 481-504.

McCarthy, T. & Rubisge, B. 2005, *Story of Earth and Life,* Struik.

Mendelsohn, F. & Potgieter, C.T. 1986, "Guidebook to sites of geological and mining interest on the central Witwatersrand", Geological Society of South Africa, .

Mukherjee, P. & Gupta, P. 2008, "Arbitrary scaling in ISOCON method of geochemical mass balance: An evaluation of the graphical approach", *Geochemical Journal,* vol. 42, no. 3, pp. 247-253.

Naicker, K., Cukrowska, E. & McCarthy, T. 2003, "Acid mine drainage arising from gold mining activity in Johannesburg, South Africa and environs", *Environmental Pollution,* vol. 122, no. 1, pp. 29-40.

Nengovhela, A., Yibas, B. & Ogola, J. 2007, "Characterisation of gold tailings dams of the Witwatersrand Basin with reference to their acid mine drainage potential, Johannesburg, South Africa", *Water SA,* vol. 32, no. 4.

Norman, M., Robinson, P. & Clark, D. 2003, "MAJOR-AND TRACE-ELEMENT ANALYSIS OF SULFIDE ORES BY LASER-ABLATION ICP–MS, SOLUTION ICP–MS, AND XRF: NEW DATA ON INTERNATIONAL REFERENCE MATERIALS", *The Canadian Mineralogist,* vol. 41, no. 2, pp. 293-305.

Norman, N. & Whitfield, G. 2006, *Geological journeys: A traveller's guide to South Africa's rocks and landforms,* Struik.

Norrish, K. & Thompson, G. 1990, "XRS analysis of sulphides by fusion methods", *X-Ray Spectrometry,* vol. 19, no. 2, pp. 67-71.

Oelofse, S., Hobbs, P., Rascher, J. & Cobbing, J. 2007, "The Pollution and Destruction Threat of Gold Mining Waste on the Witwatersrand: A West Rand Case Study", *10th International Symposium on Environmental Issues and Waste management in Energy and Mineral Production (SWEMP, 2007), Bangkok*, pp. 11.

Piercey, S.J. 2014, "Modern Analytical Facilities 2. A Review of Quality Assurance and Quality Control (QA/QC) Procedures for Lithogeochemical Data", *Geoscience Canada,* vol. 41, no. 1, pp. 75-88.

Price, W. 2009, "Prediction Manual for Drainage Chemistry from Sulphidic Geological Materials. MEND Report 1.20. 1", *Natural Resources Canada,* .

Rasmussen, B., Fletcher, I.R., Muhling, J.R., Mueller, A.G. & Hall, G.C. 2007, "Bushveld-aged fluid flow, peak metamorphism, and gold mobilization in the Witwatersrand basin, South Africa: Constraints from in situ SHRIMP U-Pb dating of monazite and xenotime", *Geology*, vol. 35, no. 10, pp. 931-934.

Rasmussen, B. & Muhling, J.R. 2009, "Reactions destroying detrital monazite in greenschist-facies sandstones from the Witwatersrand basin, South Africa", *Chemical Geology*, vol. 264, no. 1, pp. 311-327.

Robb, L.J. & Meyer, F.M. 1995, "The Witwatersrand Basin, South Africa: geological framework and mineralization processes", *Ore Geology Reviews*, vol. 10, no. 2, pp. 67-94.

Rosner, T. (2000). *The environmental impact of seepage from gold mine tailings dams near Johannesburg, South Africa.* Pretoria: University of Pretoria(PhD Thesis). Retrieved 07 23, 2012, from < http://upetd.up.ac.za/thesis/available/etd-12202007-130236/ > 244pp.

Rösner, T. 2001, *A preliminary assessment of pollution contained in the unsaturated and saturated zone beneath reclaimed gold-mine residue deposits*, Water Research Commission.

Santos, R., Ribeiro, L. & Carvalho Dill, A. l. (2005): The use of multivariate statistical analysis to evaluate spatial and temporal water contamination in Germunde coal mine (Portugal). – In: Loredo, J. & Pendás, F.: Mine Water 2005 – Mine Closure. pp. 439-450, 7 fig., 3 tab.; Oviedo (University of Oviedo).

Saria, L., Shimaoka, T. & Miyawaki, K. 2006, "Leaching of heavy metals in acid mine drainage", *Waste management & research : the journal of the International Solid Wastes and Public Cleansing Association, ISWA*, vol. 24, no. 2, pp. 134-140.

Schneiderhan, E.A. 2008, *Neoarchaean clastic rocks on the Kaapvaal Craton: provenance analyses and geotectonic implications*, .

Setianto, A. & Triandini, T. "COMPARISON OF KRIGING AND INVERSE DISTANCE WEIGHTED (IDW) INTERPOLATION METHODS IN LINEAMENT EXTRACTION AND ANALYSIS", .

Simón, M., Martín, F., García, I., Bouza, P., Dorronsoro, C. & Aguilar, J. 2005, "Interaction of limestone grains and acidic solutions from the oxidation of pyrite tailings", *Environmental pollution*, vol. 135, no. 1, pp. 65-72.

Smedley, P. & Kinniburgh, D. 2002, "A review of the source, behaviour and distribution of arsenic in natural waters", *Applied Geochemistry*, vol. 17, no. 5, pp. 517-568.

TMH1 (1986), *Standard Methods of Testing Road Construction Materials - Technical Methods for Highways TMH1*, National Institute for Transport and Road Research of the Council for Scientific and Industrial Research (CSIR), Second edition.

Tutu, H., McCarthy, T. & Cukrowska, E. 2008, "The chemical characteristics of acid mine drainage with particular reference to sources, distribution and remediation: The Witwatersrand Basin, South Africa as a case study", *Applied Geochemistry*, vol. 23, no. 12, pp. 3666-3684.

USEPA, 1994. *Technical document: Acid Mine Drainage prediction*, Washington DC: US environmental protection agency.

USEPA, 1994. *TECHNICAL DOCUMENT; Acid Mine Drainage Prediction*, Washington, DC: U.S. Environmental Protection Agency. http://water.epa.gov/polwaste/nps/upload/amd.pdf.

USEPA, 2010. *Basic Information: Mercury*, *http://www.epa.gov/mercury/about.htm*

Van Biljon, M. 2007, "Geohydrological Review of the potential impact on the Sterkfontein dolomite during increased surface water runoff, April 2006–February 2007", *Report prepared for Johan Fourie & Associates for Harmony Gold Mining Limited*, .

Viljoen, M.J. 1999, "An introduction to South Africa's geological and mining heritage", Mintek, .

Vermeulen, N. (2001). *The composition and state of gold tailings.* Pretoria: University of Pretoria (PhD Thesis). Retrieved 09 06, 2013, from < http://upetd.up.ac.za/thesis/available/etd- 03102006-122937/ > 441pp.

Wade, P. & Coetzee, H. 2008, "Risk Assessment of Uranium in Selected Gold Mining Areas in South Africa" in *Uranium, Mining and Hydrogeology* Springer, , pp. 141-150.

Weltje, G.J. & Tjallingii, R. 2008, "Calibration of XRF core scanners for quantitative geochemical logging of sediment cores: theory and application", *Earth and Planetary Science Letters*, vol. 274, no. 3, pp. 423-438.

Winde, F., Wade, P. & Van der Walt, Izak Jacobus 2004, "Gold tailings as a source of water-borne uranium contamination of streams-the Koekemoerspruit (South Africa) as a case study-part III of III: fluctuations of stream chemistry and their impacts on uranium mobility", Water SA, vol. 30, no. 2, pp. 233-239.

Wright, D.A. & Welbourn, P. 2002, *Environmental toxicology*, Cambridge University Press.

Yang, Z., Lu, W., Long, Y., Bao, X. & Yang, Q. 2011, "Assessment of heavy metals contamination in urban topsoil from Changchun City, China", *Journal of Geochemical Exploration*, vol. 108, no. 1, pp. 27-38.

Zhang, C. & Selinus, O. 1998, "Statistics and GIS in environmental geochemistry—some problems and solutions", *Journal of Geochemical Exploration*, vol. 64, no. 1, pp. 339-354.

Zhang, X., Yang, L., Li, Y., Li, H., Wang, W. & Ye, B. 2012, "Impacts of lead/zinc mining and smelting on the environment and human health in China", *Environmental monitoring and assessment*, vol. 184, no. 4, pp. 2261-2273.

Appendix

Appendix A: The whole major elements dataset

Sample No	Sample ID	LOI	SiO_2	Al_2O_3	Fe_2O_3	CaO	MgO	Na_2O	K_2O	MnO	TiO_2	P_2O_5	Cr_2O_3	TOT/C	TOT/S
MT001	T008	2.02	90.3	4.63	1.42	0.28	0.41	0.03	0.28	<0.01	0.24	0.02	0.041	0.02	0.26
MT002	T008	1.72	90.2	4.56	0.86	0.3	0.29	0.02	0.26	<0.01	0.24	0.01	0.025	0.05	0.26
MT003	T008	5.54	83.4	5.33	3.4	0.24	0.54	0.03	0.25	<0.01	0.18	0.03	0.038	0.03	2
MT004	T008	3.6	85	5.96	2.69	0.27	0.59	0.03	0.25	0.02	0.26	0.02	0.035	0.03	1.25
MT005	T008	5.55	79.2	8.25	3.66	0.53	0.58	0.09	0.4	0.04	0.27	0.03	0.037	0.08	1.61
MT006	T008	5.38	78.5	7.82	3.73	0.85	0.81	0.16	0.39	0.3	0.29	0.04	0.04	0.13	1.53
MT007	T008	5.57	77	8.46	3.05	1.7	0.58	0.11	0.37	0.65	0.28	0.04	0.046	0.2	1.75
MT007-1	T008	4.62	70.7	9.08	8.77	1.64	0.6	0.14	0.55	0.45	0.28	0.04	0.049	0.22	1.78
MT008	T008	2.35	89	3.83	2.34	0.51	0.34	0.05	0.17	0.25	0.25	0.02	0.035	0.09	0.96
MT008-1	T008	2.71	85.9	5.11	4	0.19	0.3	0.04	0.19	0.11	0.28	0.02	0.038	0.03	2.19
MT008-2	T008	7.26	75.7	7.26	2.9	2.75	0.31	0.13	0.34	0.56	0.21	0.04	0.047	0.16	2.1
MT009	T008	2.59	88.6	4.69	2.1	0.4	0.31	0.03	0.21	0.08	0.23	0.02	0.034	0.04	0.96
MT010	T009	3.76	84.1	6.73	2.11	1.03	0.09	0.07	0.3	<0.01	0.22	0.03	0.038	0.07	0.67
MT011	T009	2.82	87.9	5.37	1.37	0.37	0.28	0.02	0.27	<0.01	0.23	0.02	0.029	0.04	0.64
MT012	T009	3.43	84.4	6.55	2.5	0.48	0.56	0.04	0.33	0.01	0.21	0.03	0.033	0.05	1.17
MT013	T009	2.23	87.1	6.05	2.21	0.27	0.31	0.05	0.24	<0.01	0.24	0.02	0.028	0.03	0.98
MT014	T009	3.59	82.1	8.45	2.59	0.54	0.64	0.12	0.35	0.02	0.29	0.03	0.036	0.05	1.28
MT015	T009	4.47	80.9	7.49	3.55	0.52	0.56	0.08	0.36	0.06	0.27	0.03	0.035	0.06	1.51
MT016	T009	4.49	81.6	7.21	3.52	0.55	0.49	0.11	0.35	0.05	0.29	0.03	0.035	0.04	1.58
MT017	T009	3.97	79	5.25	9.01	0.55	0.38	0.06	0.23	0.04	0.22	0.02	0.036	0.22	1.47
MT018	T009	3.18	85.3	5.71	3.51	0.48	0.39	0.05	0.22	0.02	0.27	0.03	0.037	0.04	1.94
MT018-1	T009	3.42	82.4	9.85	1.75	0.19	0.4	0.1	0.4	0.02	0.35	0.02	0.057	0.05	0.31
MT019	T009	3.23	82.6	7.78	3.21	0.4	0.46	0.15	0.35	0.02	0.26	0.03	0.035	0.09	1.63
MT020	T010	2.49	87.9	6.29	1.63	0.06	0.1	0.15	0.4	<0.01	0.23	0.01	0.044	<0.02	0.26
MT021	T010	2.78	86.4	7.04	1.83	0.31	0.13	0.17	0.44	<0.01	0.23	0.02	0.041	0.04	0.37

Appendix A: The whole major elements dataset

Sample No	Sample ID	LOI	SiO_2	Al_2O_3	Fe_2O_3	CaO	MgO	Na_2O	K_2O	MnO	TiO_2	P_2O_5	Cr_2O_3	TOT/C	TOT/S
MT021-1	T010	2.59	87.2	6.73	1.2	0.35	0.12	0.16	0.4	<0.01	0.28	0.02	0.045	0.02	0.34
MT023	T010	3.21	82.8	9.4	1.49	0.48	0.11	0.28	0.65	<0.01	0.29	0.03	0.044	0.05	0.39
MT024	T010	2.24	88.4	4.55	2.76	0.21	0.17	0.09	0.23	0.01	0.3	0.02	0.047	0.02	1.5
MT025	T010	3.14	83.9	9.21	1.61	0.36	0.23	0.22	0.55	0.01	0.24	0.05	0.062	0.04	0.86
MT026	T010	2.41	86.2	7.51	1.55	0.17	0.19	0.19	0.43	<0.01	0.22	0.05	0.048	<0.02	0.81
MT027-1	T010	4.43	76.5	6.97	9.31	0.54	0.48	0.11	0.39	0.04	0.24	0.03	0.044	0.08	1.53
MT028	T010	3.73	82.3	9.78	1.58	0.47	0.27	0.27	0.57	<0.01	0.26	0.04	0.055	0.06	1.04
MT029	T011	4.6	86.2	4.21	3.13	0.44	0.41	0.06	0.36	0.02	0.22	0.03	0.084	0.21	0.65
MT030	T011	2.1	90.1	3.06	2.59	0.28	0.66	0.04	0.24	0.02	0.26	0.01	0.045	0.03	1.03
MT031	T011	2.6	86.7	4.12	3.12	0.52	0.86	0.04	0.31	0.03	0.3	0.02	0.046	0.07	1.06
MT032	T011	2.81	87.6	4.96	2.39	0.7	0.23	0.05	0.35	0.02	0.24	0.02	0.042	0.14	0.94
MT033	T011	2.35	88.7	5.76	1.69	0.37	0.13	0.08	0.26	<0.01	0.26	0.02	0.037	0.03	0.83
MT034	T011	2.96	87.7	5.76	1.97	0.34	0.19	0.12	0.31	<0.01	0.24	0.02	0.046	<0.02	1.05
MT035	T011	2.49	86.7	6.28	2.44	0.32	0.48	0.02	0.35	0.01	0.2	0.02	0.045	0.04	1.09
MT036	T011	2.56	87	5.95	2.38	0.35	0.47	0.05	0.28	0.01	0.19	0.02	0.038	0.04	1.11
MT037	T011	2.41	87.2	5.68	2.48	0.3	0.58	0.03	0.25	0.02	0.21	0.02	0.038	0.04	1.17
MT038	T004	3.42	84.8	6.94	1.97	0.62	0.52	0.05	0.5	<0.01	0.2	0.02	0.04	0.08	0.44
MT039	T004	4.14	85.7	5.92	2.38	0.41	0.43	0.06	0.31	<0.01	0.19	0.03	0.041	0.04	1.03
MT040	T004	3.09	85.6	6.43	2.6	0.32	0.48	0.04	0.36	0.01	0.19	0.02	0.046	0.04	1.02
MT041	T004	3.65	83.6	8.25	2.31	0.4	0.43	0.07	0.38	0.01	0.23	0.03	0.049	0.11	1.08
MT042	T004	4.02	82.8	6.74	3.47	0.79	0.67	0.14	0.36	0.04	0.25	0.03	0.045	0.08	1.29
MT042-1	T004	4.93	80.6	7.64	3.68	0.7	0.56	0.1	0.41	0.05	0.24	0.03	0.034	0.08	1.49
MT043	T004	3.53	85.1	6.02	2.95	0.4	0.42	0.09	0.29	0.03	0.23	0.02	0.037	0.04	1.2
MT044	T004	3.15	79.7	5.56	9.05	0.63	0.39	0.07	0.25	0.02	0.23	0.02	0.047	0.03	1.34
MT045	T004	2.88	88.1	4.59	3.17	0.26	0.27	0.04	0.19	0.01	0.19	0.02	0.041	0.04	1.58
MT046	T004	3.25	85.1	6.14	3.37	0.47	0.4	0.07	0.27	0.02	0.22	0.03	0.043	0.07	1.72

Appendix B: The whole dataset for trace elements

Sample No	Sample ID	Co	Th	U	Mo	Cu	Pb	Zn	Ag	Ni	As	Au	Sb	Bi	Hg	pH	EC_µcm
MT001	T008	3.6	3.6	7	4.2	15.4	91.6	19	0.2	20	45.2	110.2	0.5	1.9	0.24	4.33	0.57
MT002	T008	2.9	3.7	7.4	1.4	11.7	74.1	15	0.1	11.2	23.3	271	0.4	1.8	0.18	3.49	0.74
MT003	T008	49.7	15.5	53.6	2.3	282.5	54.8	118	0.2	126.9	132.3	404.7	0.8	1.6	0.13	2.99	3.99
MT004	T008	36.9	8	100.9	3.2	42.6	43.1	124	0.1	123.3	85.3	204.6	0.5	1.3	0.08	3.45	2.17
MT005	T008	69.3	10.4	73	2.6	41.8	58.1	817	<0.1	256.1	102.9	134.9	0.7	1.4	0.15	2.91	2.83
MT006	T008	65.7	10.7	50.2	2.8	43.4	71.3	144	0.2	150.9	135.7	186.7	0.8	1.4	0.17	3.27	3.44
MT007	T008	57.1	35.8	68.9	2.5	57.9	143.9	260	0.4	149.4	331.9	103.5	0.7	2.7	0.18	6.66	0.61
MT007-1	T008	97.1	19.9	55.9	2.6	93.6	103.9	269	0.4	241.5	269.4	1417.5	2.3	3.6	0.23	6.82	1.67
MT008	T008	33.6	13.8	33.2	3.2	32.1	65.1	106	0.2	72.4	234.8	84	0.5	1.3	0.06	6.22	0.89
MT008-1	T008	51.7	8.3	30.1	4.4	53.2	23.5	80	0.1	119.9	165.6	105.3	0.8	1.2	0.15	4.96	1.05
MT008-2	T008	94.1	54.1	43.1	4.3	62.3	150.2	267	0.4	274.1	471.4	175.6	1	2.9	0.14	6.28	0.87
MT009	T008	25.2	9	30.5	4.5	30.1	62.9	95	0.2	65.4	119.6	144.1	0.7	1.5	0.14	5.29	1.03
MT010	T009	4.4	6.1	6.8	3.8	21	54.6	24	<0.1	9	192.7	396.7	0.8	2.1	1.32	3.52	1.19
MT011	T009	14.1	5.7	10.7	2.4	22.6	96.1	33	0.2	36	116.9	532.9	0.5	2.1	0.15	3.37	1.44
MT012	T009	21.4	10.8	13.8	2.6	33.3	69.6	64	0.1	62.1	146.6	270.7	0.8	2	0.12	3.88	1.22
MT013	T009	23.7	13.5	27.5	1.7	44.3	33.3	71	0.1	67.4	76.3	84.2	0.6	1.1	0.1	4.41	0.76
MT014	T009	44.4	9.6	655.5	1.6	46	49.5	177	<0.1	133.5	100.1	193	0.6	1.3	0.08	4.69	0.88
MT015	T009	69.6	10	65.5	1.9	41.9	43.3	538	0.1	229.4	128.2	323.5	0.7	1.2	0.1	3.63	2.1
MT016	T009	68.5	8.2	40.3	1.5	38.9	26.6	317	<0.1	218.9	92.6	191.8	0.7	0.9	0.16	3.01	1.7
MT017	T009	114	7.7	32.4	5.4	52.6	36.7	114	0.2	139.7	146.4	322	1.6	2.3	0.08	2.86	2.35
MT018	T009	41.1	8.3	31.3	3.4	55.5	24.8	102	0.1	115.7	170	120.6	1	1.3	0.15	4.43	1.1
MT018-1	T009	10.4	8.7	21.3	4.7	28.7	37.8	24	0.1	39.7	61.5	275.6	0.6	0.8	0.7	3.55	1.5
MT019	T009	45.3	8.8	36.5	1.2	50.4	36.4	163	0.1	112.9	141.4	237.3	1.3	1.3	0.24	7.92	1.18
MT020	T010	0.9	4.6	4.4	6.1	4.4	22.3	4	0.1	9.8	26	69.3	0.4	1	0.1	4.73	0.46
MT021	T010	1.3	4.9	4.3	4.8	4	21	18	0.1	8.1	116.6	66.1	0.5	0.7	0.06	3.12	0.63
MT021-1	T010	0.9	5.1	4	5.7	3.8	17.9	4	0.1	8.9	15.3	58.1	0.4	0.8	0.1	3.73	0.43

Continued from page 162

Appendix B: The whole dataset for trace elements

Sample No	Sample ID	Co	Th	U	Mo	Cu	Pb	Zn	Ag	Ni	As	Au	Sb	Bi	Hg	pH	EC(µS/cm)
MT023	T010	1.3	5.4	5.2	3.3	7	25.1	6	0.2	3.8	137.3	126	0.6	1	0.68	4.1	0.7
MT024	T010	27.6	6.2	7.6	6.4	8.6	21	6	0.2	36.5	110.1	390.9	0.8	0.9	2.51	3.97	0.78
MT025	T010	26.2	16.2	25.7	5.3	308.8	27.4	70	0.1	65.2	113	73.4	0.6	0.9	0.83	4.4	0.95
MT026	T010	24.5	14.2	22	4	218.5	24.3	73	0.1	65.4	185.1	106	0.6	1	0.46	3.57	0.71
MT027-1	T010	125.9	9.1	35.6	5.5	69.8	51.9	136	0.2	154.7	161.3	831.5	1.8	2.4	0.19	2.88	2.34
MT028	T010	30.7	13.6	40	3.7	64	34.5	98	0.1	91.1	108.5	127	0.6	1.1	0.51	4.74	1.13
MT029	T011	10.5	4.2	7.5	4.2	32.5	46.6	63	0.1	41.1	77.1	285.9	1.1	0.7	1.51	2.99	3.24
MT030	T011	29.2	4	10.9	4.8	37.3	31.6	94	<0.1	116.3	47.8	86.9	0.5	0.7	0.29	6.31	0.91
MT031	T011	37.9	5.8	33.8	3.8	50.6	60.2	169	0.1	153.8	74.1	408.8	0.5	1.5	0.41	7.48	0.84
MT032	T011	31.1	7.6	35.6	4.5	39.9	38.4	145	<0.1	77.6	89.7	440.3	0.6	1.7	0.5	8.02	0.61
MT033	T011	18.6	12	33.9	3.9	39	37.2	57	0.1	51.8	118.4	70.5	0.7	2.2	1.37	5.68	0.6
MT034	T011	19.3	6.8	9.6	5.9	51	16.2	8	<0.1	35.7	80.9	94.7	0.7	1.1	0.36	2.61	1.07
MT035	T011	36.2	9.4	75.9	5.2	37.8	72.5	144	0.2	109.1	105.9	128.5	0.7	2.5	0.07	6.35	0.6
MT036	T011	34.6	8.5	63	3.6	38.3	57.5	147	0.2	105.5	97	63.5	0.8	2	0.11	6.02	0.59
MT037	T011	36.7	8.8	106.5	4	46.6	62.9	148	0.1	113.3	88.4	576.5	0.7	2.1	0.21	8.69	0.57
MT038	T004	7	5.9	7.3	2.7	16.9	83.2	14	0.2	16.6	92.2	229.5	0.6	1.8	1.23	4.41	0.84
MT039	T004	17.3	7.3	9.6	4.1	18.1	63	32	0.1	46.3	130.2	125.9	0.7	1.9	0.05	3.32	1.71
MT040	T004	17.8	9.1	10	4.9	32.9	51.1	42	0.1	51.5	82.5	250.5	0.7	1.7	0.11	3.84	0.87
MT041	T004	39.4	9.3	57.6	5.1	37.4	43.8	175	0.1	94.9	87.8	290.6	0.9	1.5	0.17	3.9	1.02
MT042	T004	49.9	7.4	39.5	4.6	36.4	26.8	346	0.1	198.8	81.2	130.1	0.6	1.3	0.12	3.61	1.23
MT042-1	T004	65.1	8	41.6	1.7	36.6	35.4	299	<0.1	246.3	89.8	270	0.8	1.3	0.14	2.96	1.63
MT043	T004	44.7	7.4	42.4	4.5	37.8	27.5	91	<0.1	98.6	96.4	168.7	0.7	1	0.12	3.64	1.53
MT044	T004	89.7	8.5	34.5	5.1	52.1	38.9	99	0.1	141.6	123.4	403.9	1.8	2.5	0.09	3.79	1.13
MT045	T004	34.7	7.1	25.7	6.3	39.4	15.4	67	<0.1	78.6	137.1	174.8	0.8	1.1	0.12	3.93	1.2
MT046	T004	38.5	7.6	30.3	4.8	44.5	28	99	<0.1	92.9	115.9	331.8	1.3	1.4	0.31	4.63	0.95

Appendix C: The average, maximum and minimum concentration of trace elements in each drilled hole.

T008	Co	Th	U	Zr	Mo	Cu	Pb	Zn	Ni	As	Au	Sb	Bi	Hg
Mean	48.91	16.07	46.15	128.97	3.17	63.88	78.54	192.83	134.26	176.45	278.51	2.30	1.88	0.15
Max	97.10	54.10	100.90	204.70	4.50	282.50	150.20	817.00	274.10	471.40	1417.50	0.40	3.60	0.24
Min	2.90	3.60	7.00	98.40	1.40	11.70	23.50	15.00	11.20	23.30	84.00	0.81	1.20	0.06
T009	Co	Th	U	Zr	Mo	Cu	Pb	Zn	Ni	As	Au	Sb	Bi	Hg
Mean	41.54	8.85	85.60	124.78	2.75	39.56	46.25	147.91	105.85	124.79	268.03	0.84	1.49	0.29
Max	114.00	13.50	655.50	160.00	5.40	55.50	96.10	538.00	229.40	192.70	532.90	1.60	2.30	1.32
Min	4.40	5.70	6.80	99.80	1.20	21.00	24.80	24.00	9.00	61.50	84.20	0.50	0.80	0.08
T010	Co	Th	U	Zr	Mo	Cu	Pb	Zn	Ni	As	Au	Sb	Bi	Hg
Mean	26.59	8.81	16.53	133.40	4.98	76.54	27.27	46.11	49.28	108.13	205.37	0.70	1.09	0.60
Max	125.90	16.20	40.00	233.80	6.40	308.80	51.90	136.00	154.70	185.10	831.50	1.80	2.40	2.51
Min	0.90	4.60	4.00	105.60	3.30	3.80	17.90	4.00	3.80	15.30	58.10	0.40	0.70	0.06
T011	Co	Th	U	Zr	Mo	Cu	Pb	Zn	Ni	As	Au	Sb	Bi	Hg
Mean	28.23	7.46	41.86	120.28	4.43	41.44	47.01	108.33	89.36	86.59	239.51	0.70	1.61	0.54
Max	37.90	12.00	106.50	155.20	5.90	51.00	72.50	169.00	153.80	118.40	576.50	1.10	2.50	1.51
Min	10.50	4.00	7.50	92.70	3.60	32.50	16.20	8.00	35.70	47.80	63.50	0.50	0.70	0.07
T004	Co	Th	U	Zr	Mo	Cu	Pb	Zn	Ni	As	Au	Sb	Bi	Hg
Mean	40.41	7.76	29.85	117.86	4.38	35.21	41.31	126.40	106.61	103.65	237.58	0.89	1.55	0.25
Max	89.70	9.30	57.60	172.10	6.30	52.10	83.20	346.00	246.30	137.10	403.90	1.80	2.50	1.23
Min	7.00	5.90	7.30	95.10	1.70	16.90	15.40	14.00	16.60	81.20	125.90	0.60	1.00	0.05

Appendix D: The percentage (%) accuracy results for all major and trace elements and standard used

Analyte	**%Accuracy**
	STD SO-18
Ba	-3.31
Be	
Co	-2.43
U	-1.52
V	-4.13
W	-4.65
Zr	0.14
Y	-2.58

	STD SY-4(D)	**STD OREAS72A**
Analyte	%Accuracy	%Accuracy
LOI	0.00	1.48
SiO_2	0.33	0.34
Al_2O_3	0.02	-0.61
Fe_2O_3	-1.45	-1.80
CaO	-2.03	-1.85
MgO	-3.09	-0.90
Na_2O	-0.61	1.26
K_2O	-4.42	0.93
MnO	1.85	0.00
TiO_2	-2.44	-0.78
P_2O_5	-0.84	-4.28

The percentage (%) accuracy results for all major and trace elements and standard used contd.

Analyte	%Accuracy	%Accuracy
	STD OREAS45EA	STD DS9
Mo	-15.73	-2.13
Cu	-3.02	0.74
Pb	-3.03	2.67
Zn	-1.96	-2.10
Ag	-14.26	0.18
Ni	5.31	0.58
As	-9.94	6.27
Au	28.74	12.94
Cd		0.00
Sb	-68.75	1.21
Bi	-10.26	-6.12
Hg	-93.14	13.33
Tl		5.03
Se	-52.15	1.92

	STD SY-4(D)	**STD OREAS72A**
Analyte	%Accuracy	%Accuracy
LOI	0.00	1.48
SiO2	0.33	0.34
Al2O3	0.02	-0.61
Fe2O3	-1.45	-1.80
CaO	-2.03	-1.85
MgO	-3.09	-0.90
Na2O	-0.61	1.26
K2O	-4.42	0.93
MnO	1.85	0.00
TiO2	-2.44	-0.78
P2O5	-0.84	-4.28

APPENDIX E: The precision control scatterplot for major and trace elements

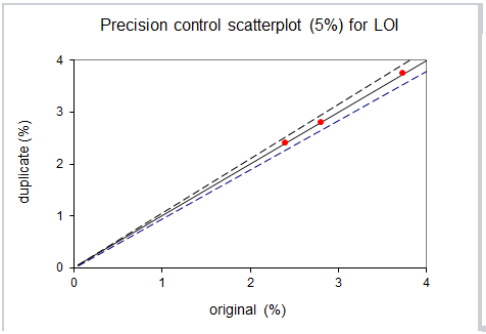

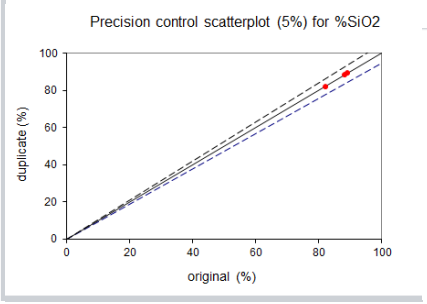

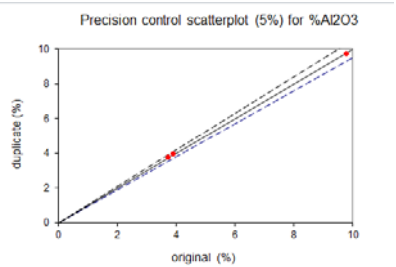

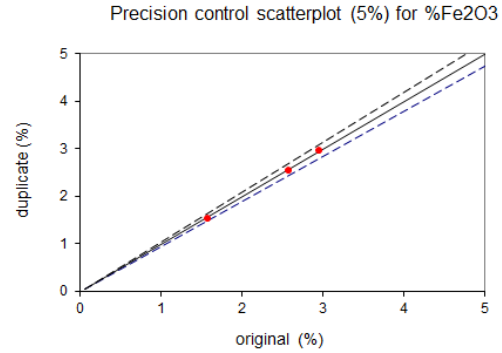

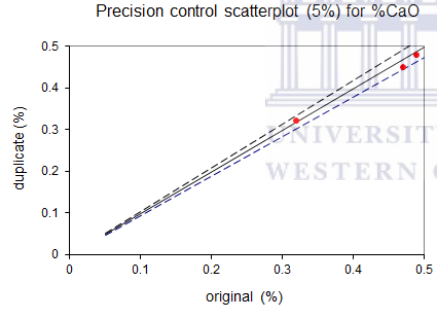

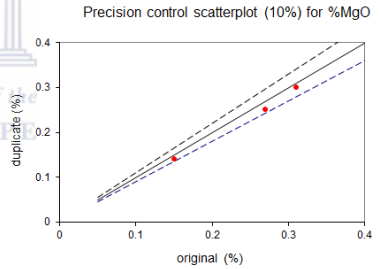

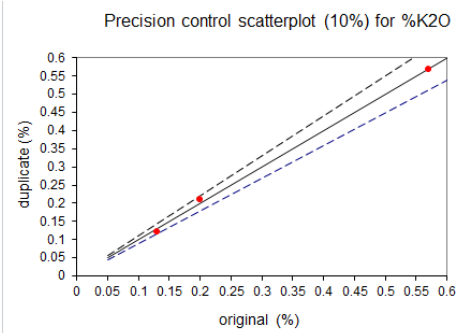

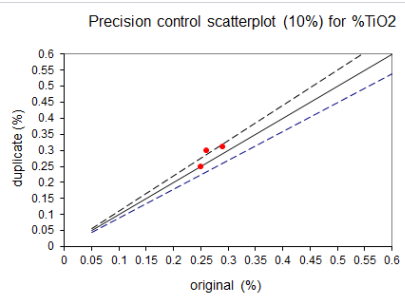

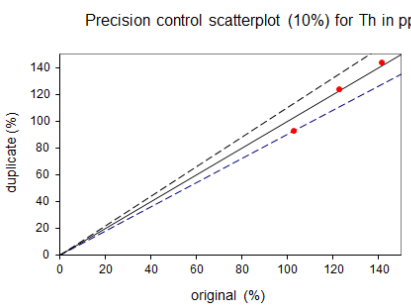

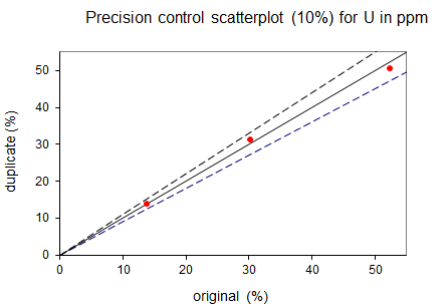

The precision control scatterplot for major and trace elements

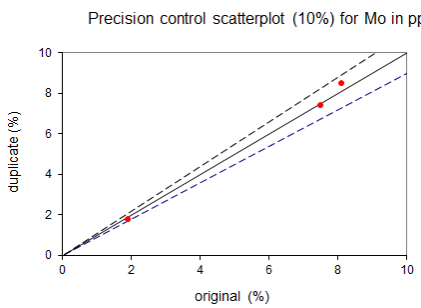

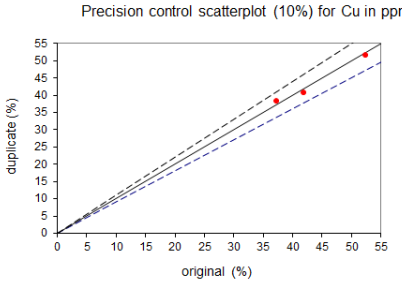

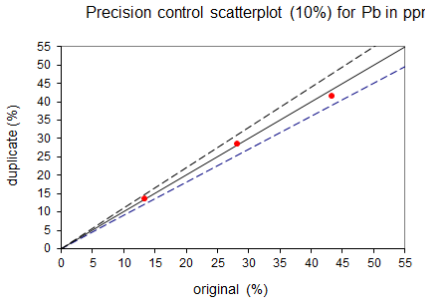

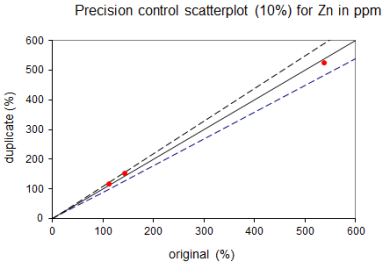

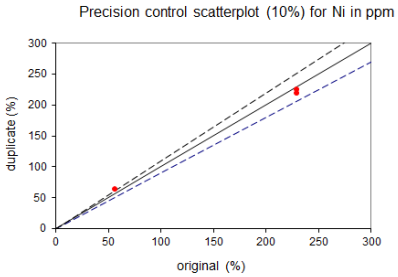

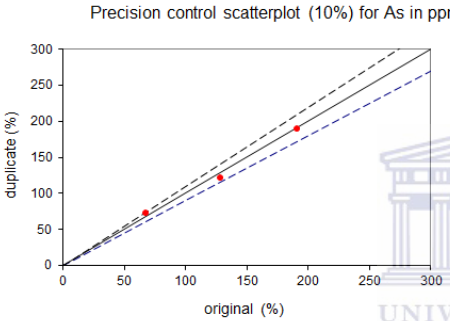

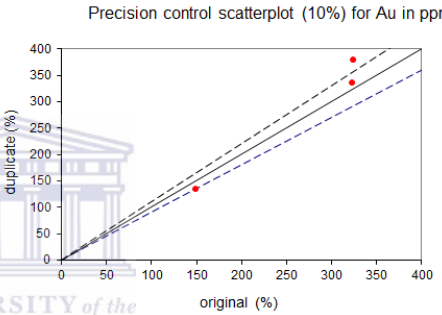

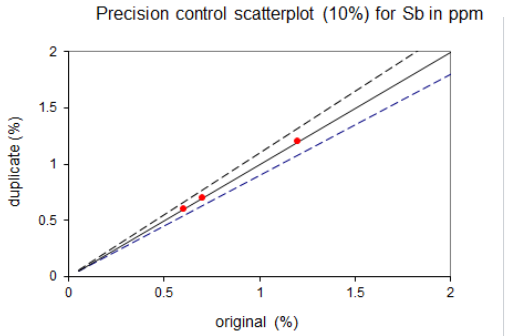

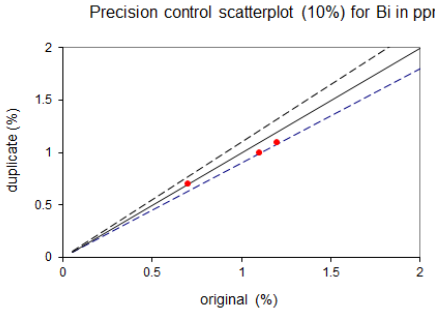

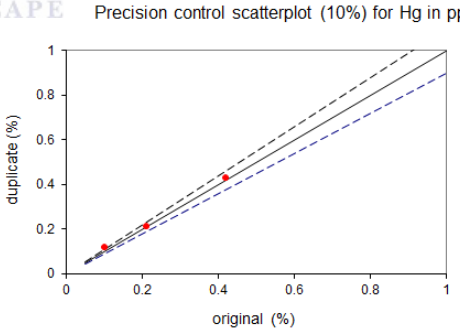

Appendix F: Geochemical mass balance results of layers for major and trace elements

ISOCON

			Overall volume change (%)	0.60
			Overall mass change (%)	0.60
Table 1 Results			Slope	0.99
	Unaltered	Altered	Gain/Loss relative to C_i^0	Gain/Loss in wt.%
Sample	B. samples	Layer 1	$\Delta C_i/C_i^0$	ΔC_i
LOI	3.04	2.99	-0.01	-0.04
SiO_2	85.16	87.36	0.03	2.72
Al_2O_3	6.81	5.48	-0.19	-1.31
Fe_2O_3	2.55	1.93	-0.24	-0.61
CaO	0.41	0.41	0.01	0.00
MgO	0.40	0.33	-0.17	-0.07
Na_2O	0.11	0.07	-0.39	-0.04
K_2O	0.33	0.34	0.02	0.01
MnO	0.03	0.01	-0.72	-0.02
TiO_2	0.24	0.23	-0.04	-0.01
P_2O_5	0.03	0.02	-0.28	-0.01
S	1.30	0.56	-0.57	-0.74
Cr_2O_3	0.04	0.04	0.05	0.00
C	0.06	0.06	-0.01	0.00

Geochemical mass balance results of layers for major and trace elements

ISOCON

			Overall volume change (%)	-0.18
			Overall mass change (%)	-0.18
Table 1 Results			Slope	1.00
	Unaltered	Altered	Gain/Loss relative to C_i^0	Gain/Loss in wt.%
Sample	B. samples	Layer 2	$\Delta C_i/C_i^0$	ΔC_i
LOI	3.04	3.28	0.07	0.23
SiO_2	85.16	85.34	0.00	0.03
Al_2O_3	6.81	6.38	-0.07	-0.45
Fe_2O_3	2.55	2.39	-0.06	-0.16
CaO	0.41	0.40	-0.01	-0.01
MgO	0.40	0.42	0.05	0.02
Na_2O	0.11	0.08	-0.28	-0.03
K_2O	0.33	0.35	0.06	0.02
MnO	0.03	0.01	-0.59	-0.02
TiO_2	0.24	0.24	0.02	0.01
P_2O_5	0.03	0.02	-0.14	0.00
S	1.30	1.02	-0.22	-0.28
Cr_2O_3	0.04	0.04	-0.01	0.00
C	0.06	0.06	-0.05	0.00

Geochemical mass balance results of layers for major and trace elements

ISOCON

			Overall volume change (%)	0.43
			Overall mass change (%)	0.43
Table 1 Results			Slope	1.00
	Unaltered	Altered	Gain/Loss relative to C_i^0	Gain/Loss in wt.%
Sample	B. samples	Layer 3	$\Delta C_i/C_i^0$	ΔC_i
LOI	3.04	4.04	0.33	1.02
SiO_2	85.16	76.48	-0.10	-8.35
Al_2O_3	6.81	6.72	-0.01	-0.07
Fe_2O_3	2.55	9.04	2.56	6.53
CaO	0.41	0.84	1.07	0.44
MgO	0.40	0.46	0.15	0.06
Na_2O	0.11	0.10	-0.13	-0.01
K_2O	0.33	0.36	0.08	0.03
MnO	0.03	0.14	3.76	0.11
TiO_2	0.24	0.24	0.03	0.01
P_2O_5	0.03	0.03	-0.01	0.00
S	1.30	1.53	0.18	0.23
Cr_2O_3	0.04	0.04	0.08	0.00
C	0.06	0.14	1.30	0.08

Geochemical mass balance results of layers for major and trace elements

ISOCON

			Overall volume change (%)	0.07
			Overall mass change (%)	0.07
Table 1 Results			Slope	1.00
	Unaltered	Altered	Gain/Loss relative to C_i^0	Gain/Loss in wt.% or ppm
Sample	B. samples	layer 4	$\Delta C_i/C_i^0$	ΔC_i
LOI	3.04	3.04	0.00	0.00
SiO2	85.16	85.85	0.01	0.75
Al2O3	6.81	6.19	-0.09	-0.62
Fe2O3	2.55	2.67	0.05	0.12
CaO	0.41	0.37	-0.09	-0.04
MgO	0.40	0.34	-0.15	-0.06
Na2O	0.11	0.09	-0.20	-0.02
K2O	0.33	0.30	-0.08	-0.03
MnO	0.03	0.04	0.53	0.02
TiO2	0.24	0.24	0.02	0.00
P2O5	0.03	0.03	-0.04	0.00
S	1.30	1.29	-0.01	-0.02
Cr2O3	0.04	0.04	0.00	0.00

: Geochemical mass balance results of layers for major and trace elements

ISOCON

			Overall volume change (%)	0.60
			Overall mass change (%)	0.60
Table 1 Results			Slope	0.99
	Unaltered	Altered	Gain/Loss relative to C_i^0	Gain/Loss in ppm(Au in ppb)
Sample	B. samples	Layer 1	$\Delta C_i/C_i^0$	ΔC_i
Ba	55.40	52.00	-0.06	-3.09
Co	35.28	9.12	-0.74	-26.11
Cs	1.04	0.90	-0.13	-0.13
Ga	6.88	6.00	-0.12	-0.84
Hf	2.90	2.94	0.02	0.06
Nb	3.80	3.89	0.03	0.11
Rb	10.32	9.31	-0.09	-0.95
Sr	30.80	24.08	-0.21	-6.58
Ta	0.98	1.10	0.13	0.13
Th	9.56	5.00	-0.47	-4.53
U	48.76	7.59	-0.84	-41.12
V	36.60	35.90	-0.01	-0.49
W	1.16	0.84	-0.27	-0.31
Zr	114.70	110.09	-0.03	-3.95
Y	10.82	7.42	-0.31	-3.36
Mo	3.64	3.85	0.06	0.23
Cu	47.12	18.39	-0.61	-28.62
Pb	44.94	58.41	0.31	13.82
Zn	120.60	31.60	-0.74	-88.81
Ni	95.12	31.44	-0.67	-63.49
As	114.76	86.80	-0.24	-27.44
Au	283.34	217.44	-0.23	-64.60
Sb	0.92	0.60	-0.34	-0.32
Bi	1.48	1.47	0.00	0.00
Hg	0.28	0.51	0.83	0.23

Geochemical mass balance results of layers for major and trace elements

ISOCON

			Overall volume change (%)	-0.18
			Overall mass change (%)	-0.18
Table 1 Results			Slope	1.00
	Unaltered	Altered	Gain/Loss relative to C_i^0	Gain/Loss in ppm(Au in ppb)
Sample	B. samples	Layer 2	$\Delta C_i/C_i^0$	ΔC_i
Ba	55.40	55.50	0.00	0.00
Co	35.28	26.01	-0.26	-9.32
Cs	1.04	1.04	0.00	0.00
Ga	6.88	6.71	-0.03	-0.18
Hf	2.90	3.18	0.09	0.27
Nb	3.80	3.75	-0.01	-0.06
Rb	10.32	10.79	0.04	0.45
Sr	30.80	28.01	-0.09	-2.84
Ta	0.98	0.89	-0.09	-0.09
Th	9.56	9.01	-0.06	-0.57
U	48.76	34.20	-0.30	-14.62
V	36.60	38.70	0.06	2.03
W	1.16			
Zr	114.70	117.89	0.03	2.98
Y	10.82	9.84	-0.09	-1.00
Mo	3.64	3.71	0.02	0.06
Cu	47.12	57.43	0.22	10.21
Pb	44.94	43.73	-0.03	-1.29
Zn	120.60	91.80	-0.24	-28.97
Ni	95.12	77.02	-0.19	-18.24
As	114.76	92.72	-0.19	-22.21
Au	283.34	253.85	-0.11	-29.95
Sb	0.92	0.64	-0.31	-0.28
Bi	1.48	1.42	-0.04	-0.06
Hg	0.28	0.24	-0.15	-0.04

Geochemical mass balance results of layers for major and trace elements

ISOCON

			Overall volume change (%)	0.43
			Overall mass change (%)	0.43
Table 1 Results			Slope	1.00
	Unaltered	Altered	Gain/Loss relative to C_i^0	Gain/Loss in ppm(Au in ppb)
Sample	B. samples	Layer 3	$\Delta C_i/C_i^0$	ΔC_i
Ba	55.40	85.50	0.55	30.47
Co	35.28	106.68	2.04	71.86
Cs	1.04	1.55	0.50	0.52
Ga	6.88	6.85	0.00	0.00
Hf	2.90	3.68	0.27	0.79
Nb	3.80	4.23	0.12	0.44
Rb	10.32	11.53	0.12	1.26
Sr	30.80	36.30	0.18	5.66
Ta	0.98	0.98	0.00	0.00
Th	9.56	11.30	0.19	1.79
U	48.76	39.60	-0.18	-8.99
V	36.60	39.25	0.08	2.82
W	1.16	1.80	0.56	0.65
Zr	114.70	153.40	0.34	39.37
Y	10.82	12.80	0.19	2.04
Mo	3.64	4.65	0.28	1.03
Cu	47.12	67.03	0.43	20.20
Pb	44.94	57.85	0.29	13.16
Zn	120.60	154.50	0.29	34.57
Ni	95.12	169.38	0.79	74.99
As	114.76	175.13	0.53	61.13
Au	283.34	743.73	1.64	463.61
Sb	0.92	1.88	1.05	0.96
Bi	1.48	2.70	0.83	1.23
Hg	0.28	0.15	-0.47	-0.13

Geochemical mass balance results of layers for major and trace elements

			Overall volume change (%)	0.07
			Overall mass change (%)	0.07
Table 1 Results			Slope	1.00
	Unaltered	Altered	Gain/Loss relative to C_i^0	Gain/Loss in wt.% or ppm
Sample	B. samples	layer 4	$\Delta C_i/C_i^0$	ΔC_i
C	0.06	0.04	-0.35	-0.02
S	1.30	1.29	-0.01	-0.02
Ba	55.40	55.62	0.00	0.25
Co	35.28	38.72	0.10	3.46
Cs	1.04	1.01	-0.03	-0.03
Ga	6.88	6.53	-0.05	-0.34
Hf	2.90	3.39	0.17	0.49
Nb	3.80	4.12	0.09	0.33
Rb	10.32	9.65	-0.06	-0.67
Sr	30.80	29.22	-0.05	-1.57
Ta	0.98	1.00	0.02	0.02
Th	9.56	10.02	0.05	0.46
U	48.76	38.35	-0.21	-10.38
V	36.60	41.54	0.14	4.97
W	1.16	1.07	-0.08	-0.09
Zr	114.70	132.25	0.15	17.63
Y	10.82	11.02	0.02	0.20
Mo	3.64	4.08	0.12	0.45
Cu	47.12	76.32	0.62	29.25
Pb	44.94	35.48	-0.21	-9.43
Zn	120.60	138.46	0.15	17.95
Ni	95.12	105.09	0.11	10.04
As	114.76	132.69	0.16	18.02
Au	283.34	131.18	-0.54	-152.08
Sb	0.92	0.72	-0.22	-0.20
Bi	1.48	1.36	-0.08	-0.12
Hg	0.28	0.31	0.11	0.03